ADVANCED MATERIALS
www.advmat.de

Smart Textile-Integrated Microelectronic Systems for Wearable Applications

Jidong Shi, Su Liu, Lisha Zhang, Bao Yang, Lin Shu, Ying Yang, Ming Ren, Yang Wang, Jiewei Chen, Wei Chen, Yang Chai,* and Xiaoming Tao**

The programmable nature of smart textiles makes them an indispensable part of an emerging new technology field. Smart textile-integrated microelectronic systems (STIMES), which combine microelectronics and technology such as artificial intelligence and augmented or virtual reality, have been intensively explored. A vast range of research activities have been reported. Many promising applications in healthcare, the internet of things (IoT), smart city management, robotics, etc., have been demonstrated around the world. A timely overview and comprehensive review of progress of this field in the last five years are provided. Several main aspects are covered: functional materials, major fabrication processes of smart textile components, functional devices, system architectures and heterogeneous integration, wearable applications in human and nonhuman-related areas, and the safety and security of STIMES. The major types of textile-integrated nonconventional functional devices are discussed in detail: sensors, actuators, displays, antennas, energy harvesters and their hybrids, batteries and supercapacitors, circuit boards, and memory devices.

1. Introduction

Smart textile integrated microelectronic systems (STIMES) are fibers or fiber assemblies that have capacity of sensing, actuating, adopting, communicating, self-healing, self-powering, memorizing, learning, etc. The smart textiles respond to external stimuli in a manual or preprogrammed manner.[1] These intelligent functions are rendered by sub-micron-or nanometer structures on the surface or inside the fibers or embedded microelectronic components. The programmable feature has resulted in a wide exploration because of their communication capacities with modern communication networks, such as internet, mobile network, IoT and aeronautical network, etc., as envisaged some twenty years ago.[1,2] Indeed, during the past two decades, textiles have become an indispensable part of STIMES in emerging disruptive smart wearable technology that combines with microelectronics and information technology like artificial intelligence and augmented or virtual reality.

STIMES are worn on the bodies of humans, animals, machines or even buildings, etc. They may be just like, or more than, a second skin covering the bodies. As shown in **Figure 1**, they should be easily attached to and detached from the bodies and replaced. Headgears, clothing, footwear, watches, glasses, jewelry are typical examples of wearable items. For human consumption, they should be fashionable, ubiquitous, comfortable, cleanable and convenient in use in addition to the smart functions.

Remarkably, another important type of wearable electronic devices besides STIMES is electronic skin (e-skin), which is also rapidly developed in recent years.[3] Except for excellent sensing and feedback behavior, e-skins could also be endowed with self-healing capability, which resembles the property of natural skins.[3b,c] However, most e-skins are continuous film-like structure, which can be stretched, and bent in one direction only, while do not allow significant amount of double-curvature bending and in-plane shear. In comparison, being fibrous structured devices and systems, STIMES has some unique features, apart from above mentioned requirements for wearables. Flexibility is the most visible and unique one as they can accommodate large extension (stretch), double-curvature bending and in-plane shear simultaneously. Thus, fibrous devices and systems can drape well on a 3D curvilinear surface like human bodies. Another unique feature is the structural transformation of textiles that may result in very low fiber strain in a large deformed fabric. The fiber assembly is excellent in arresting

Dr. J. Shi, S. Liu, L. Zhang, Dr. B. Yang, Prof. W. Chen, Prof. Y. Chai, Prof. X. Tao
Research Centre for Smart Wearable Technology
Institute of Textiles and Clothing
Hong Kong Polytechnic University
Hong Kong 999077, China
E-mail: weii.chen@polyu.edu.hk; ychai@polyu.edu.hk; xiao-ming.tao@polyu.edu.hk
Dr. L. Shu
School of Electronic and Information Engineering
Southern China University of Technology
Guangzhou 510640, Guangdong, China
Dr. Y. Yang, M. Ren
i-Lab
Suzhou Institute of Nano-Tech and Nano-Bionics
Chinese Academy of Sciences
Suzhou 215123, China
Y. Wang, J. Chen, Prof. Y. Chai
Department of Applied Physics
Hong Kong Polytechnic University
Hong Kong 999077, China
The ORCID identification number(s) for the author(s) of this article can be found under https://doi.org/10.1002/adma.201901958.

DOI: 10.1002/adma.201901958

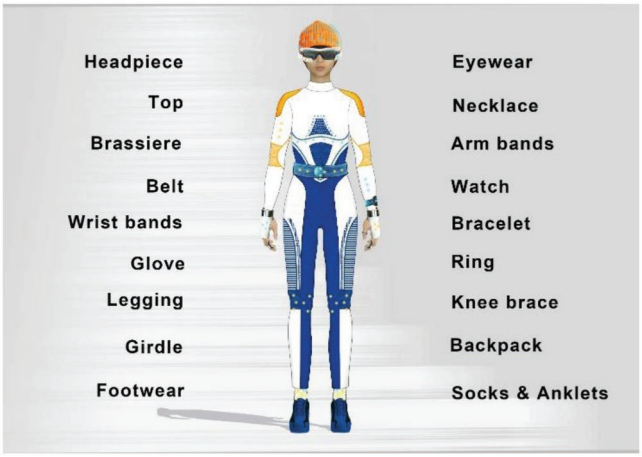

Figure 1. Types of STIMES for human.

crack propagation with a high damage tolerance. As a consequence, the textile-based devices render an outstanding service life of multiple million loading cycles, much longer than flexible thin-film based counterparts. Considering all the favorable properties and characteristics, cost-effectiveness in mass manufacturing, smart textiles provide an ideal platform for wearable technology development.

Nowadays, most wearable microelectronic devices are rigid although some of them are embedded in flexible textiles. The real applications of textile-based wearable systems are only at the early stage. The related research is extremely inspiring but, at the same time, very challenging. It involves flexible functional materials, fabrication technologies, functional and human factor design, evaluation instruments, testing methods and standards, application domain knowledge and business models for wearable technology. In addition, there are few established works on the multiscale and multimaterials science and engineering tools that guide the design, fabrication and evaluation of such smart textile devices and systems.

This review provides a comprehensive overview of the published work reported in the recent five years since our first review in 2014.[4] It covers the materials, structures, fabrication of devices and components of STIMES, system integration, and human and nonhuman application as well as important issues of safety and security.

Wei Chen received his Ph.D. degree in condensed matter physics from the Chinese Academy of Sciences in 2001. He is now a professor at the Hong Kong Polytechnic University. His research interests currently focus on nanotechnology-based soft intelligent materials and devices for wearable applications.

Yang Chai received his Ph.D. degree from the Hong Kong University of Science and Technology in 2009. He joined the Department of Applied Physics of the Hong Kong Polytechnic University in 2012. His current research interests focus on micro/nanoelectronic devices and 2D materials.

Xiaoming Tao is the Chair Professor of Textile Technology, founding director of the Research Centre of Smart Wearable Technology, at the Hong Kong Polytechnic University. Prof. Tao is a former World President of the Textile Institute International, and the recipient of an Honorary Fellowship of the Textile Institute and the Founder's Award by the Fiber Society of the USA.

2. Fabrication Processes of Components for STIMES

Most textiles are made of dielectric fibers that lack the required functionality. Hence there are three major routes to impart electronic functions in wearables. The first is to build nanostructures on the surface or inside fibers, which leads to high level of ubiquitous-ness. Generally, the first route enables a more homogeneous modification amongst the whole electronic textile system, as well as a more delicate design of the internal structures. To build nano- or sub-micrometer structures inside a fiber has been demonstrated via preform-drawing, normally for those fibers with a large diameter. The high rigidity of such coarse fibers is a direct reason for their low durability in repeated deformation and unaccepted harsh handle of resultant fabrics for clothing. It is a great challenge to make complex internal structures in finer textile-grade fiber with a diameter of several microns and high durability even in laboratories, not to mention scaling up in mass production. The second route is to impart electronic functions by surface coating or printing by modification at both fiber and textile level. This route is simple and scalable, and benefits a higher yield in mass production by existing production processes and machinery. It is applicable for normal textile grade fibers and fabrics with satisfactory durability and handle. The third route is to embed microelectronic devices into wearable products or their building elements like fibers, yarns or fabrics, which has the advantage of utilization

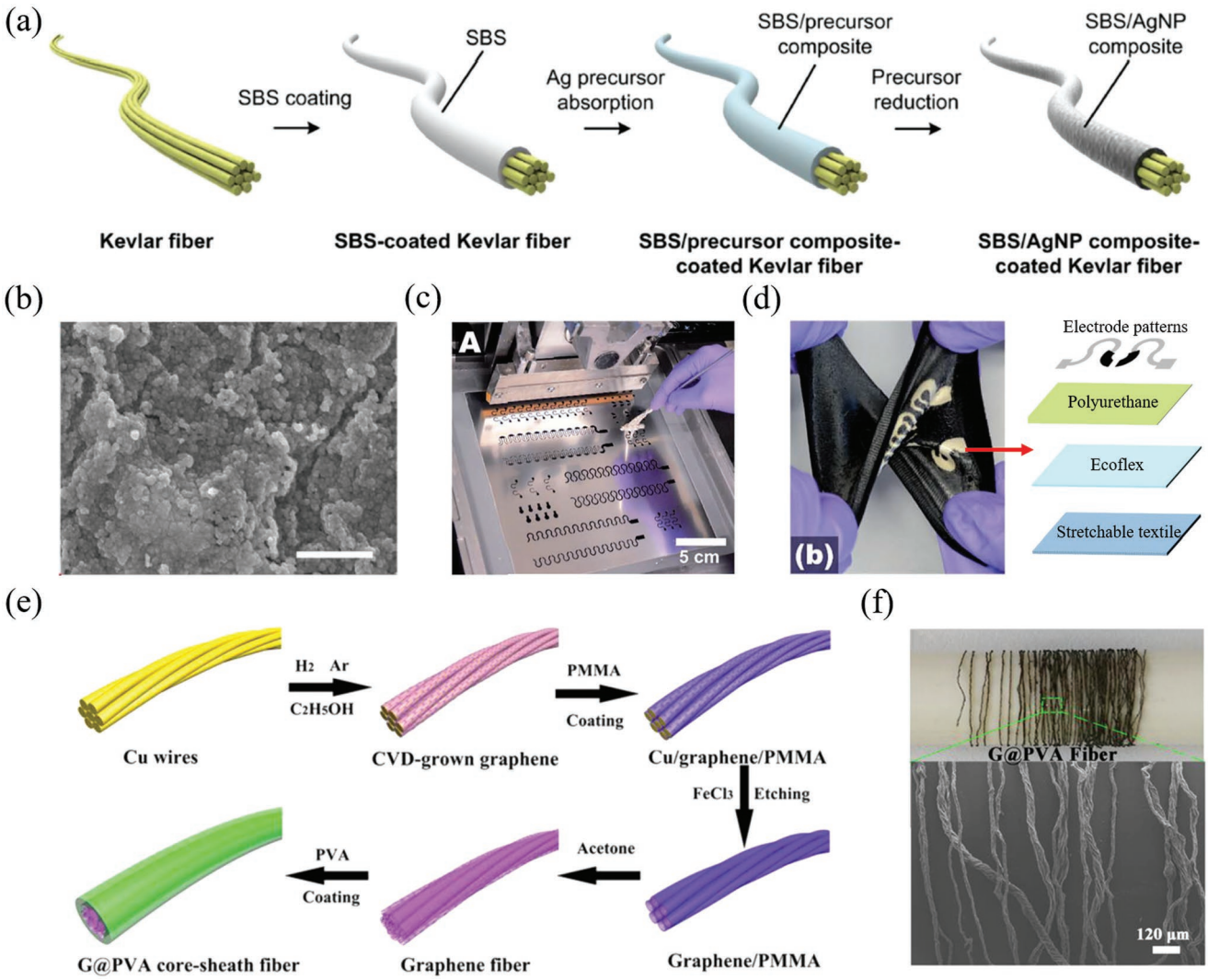

Figure 2. Preparation of e-fiber/e-textile by surface mounting and printing. a) The process flow for coating a Kevlar fiber with SBS/AgNP composite. b) An SEM image of the SNS/AgNP coating. Reproduced with permission.[8c] Copyright 2015, WILEY-VCH. c) Photograph of the stencil used for screen printing conductive circuits on a fabric. d) Left: a piece of fabric incorporating a printed circuit that could be dramatically twisted. Right: a structural schematic of the printed e-textile. Reproduced with permission.[21] Copyright 2015, ACS. e) The process flow of the fabrication of CVD-derived graphene@PVA fibers. f) A photo (top) and SEM image (bottom) of the graphene@PVA fibers. Reproduced with permission.[24] Copyright 2015, ACS.

of the existing strength of several industries, including textile and apparel, footwear, jewelry and electronics, with the combined global markets well beyond trillion dollars.

2.1. Coating and Printing

To form an electrically conductive layer on the surface of fiber, yarn or textile is a scalable electrical functionalization method without losing much of the intrinsic flexibility of the fibers/textiles. Solution-based and low- or room-temperature fabrication methods include dip coating, stencil printing, screen printing, inkjet printing, etc. After the evaporation of solvent, the solute could precipitate on the surface of the fiber/textile and form a conductive layer. For instance, the dispersion of graphene oxide (GO) could be scalably prepared by Hummers' method.[5] A hydrophilic fiber could be infiltrated by GO aqueous dispersion through a dip coating process. After the vaporization of the solvent, the GO coating could be treated with reducing agents, resulting in a conductive reduced GO (rGO) coating surrounding the fiber.[6] Karim et al. found that the adhesion and continuity of rGO coatings could be enhanced by a predeposition of polymer interlayer.[7] On the other hand, inks based on metal precursors endows a metallic coating with higher conductivity than rGO (**Figure 2**a,b),[8] while the tendency for oxidation and high cost might restrain their use. Since rGO and metal coatings are continuous film-like structure, it could generate cracks upon mechanical stretch. The immersion of carbon nanotubes (CNTs)[9] and silver nanowires (AgNWs)[10] inks renders a coating of conductive network structure after solvent evaporation, which has a much higher strain tolerance than a film structure. However, due to the high surface area

of 1D nanostructures, CNTs and AgNWs are prone to agglomerate in dispersions.[11] In order to obtain a homogeneous dispersion of CNTs and AgNWs, surface functionalization[12] and addition of surfactants could be adopted,[13] while the electrical conductivity could be sacrificed to some extent.[11a,14] The wet-coated layer could also serve as intermediate coatings, which further self-assembled into coatings of the final product, such as metal-organic framework (MOF).[15] In solution processing, the quality of obtained conductive coatings is closely related to the solvents of conductive inks. For example, in dip coating and spin coating process, the solvents should be capable to wet the fiber/textile to ensure the continuity of the coating after solvent evaporation. On the other hand, the viscosity and boiling point of solvents should be minimized for easier manipulation of the conductive inks.[16] Despite the scalability of the method, the uniformity of the coating might be sacrificed due to the non-uniform evaporation of the solvent. The thickness of coatings could be hardly controlled.

Printing is applicable to achieve a site-selective deposition of electrical components. Screen printing has been used successfully in industrial production of textile strain sensors since 2008.[17] The method is cost-effective for production of electronic fabrics with spatial resolution in mm. In stencil printing, target materials are coated on a stencil covered substrate with a higher spatial resolution in dozens of microns. Guo et al. printed a poly(3,4-ethylenedioxythiophene): poly(styrene sulfonate) (PEDOT: PSS) conductive "wire" on a nonwoven polyethylene terephthalate (PET) fabric, which has tunable sheet resistance from 1.6 $\Omega\,\square^{-1}$ to a few k$\Omega\,\square^{-1}$ by controlling the thickness of the coating. There was little electrical degradation after 3 washing cycles.[18] In the work by Frutiger et al., a coaxial 4-layer fiber-based capacitor was prepared by sequential printing of conductive and dielectric materials.[19] On the other hand, inkjet printing is achieved by programmably coating the target materials on defined sites, which is material saving and has higher spatial resolution.[20] While the rough surface of fibers and textiles leads to low spatial resolution and poor surface adhesion between the electrical components and the fiber/textile surface. A variety of methods have been proposed in designing and optimizing the conductive inks for printing. Jeerapan et al. mixed Ag ink with 10% Ecoflex, which could be screen printed onto socks as mechanically resilient circuits (Figure 2c,d).[21] Matsuhisa et al. added fluorine rubber and surfactant into Ag inks, which could be printed onto a textile garment and maintains a conductivity of 182 S cm^{-1} even at a strain of 215%.[22]

Dry fabrication methods include sputtering, physical vapor deposition (PVD), and chemical vapor deposition (CVD) of conductive materials.[23] Sputtering of metal nanoparticles is a common method for electrode fabrication of electronic devices. The thickness of sputtered metal film is more precisely controlled compared with solution-based coatings. Besides, the sputtering method could be combined with stencil printing and lithography for surface patterning on textiles.[23c] CVD derived coatings are usually of high crystalline quality, homogeneous and adhere strongly to the underlying substrates. Our group coated conductive polypyrrole (PPy) on plasma treated DOW XLATM elastic fibers by CVD.[23d] Large-range stretchability is achieved despite the fragility of PPy, which is attributed to the restraint of crack propagation due to the strong interfacial stress. Wang et al. prepared CVD derived graphene nanofibers on Cu wire substrate (Figure 2e,f),[24] demonstrating a stretchability of 16% and a conductivity of 96 S cm^{-1}, which surpasses most solution-based rGO fibers. However, the dry methods usually necessitate vacuum operation and high temperature, which restricts its application scenario and increases the equipment and energy cost.

2.2. Fiber Making

Electrically functional materials could be added into the precursors for spinning, which thus results in the as-prepared fibers with electrical conductivity. Up till now, the most frequently used method is wet-spinning and electrospinning. Wet-spinned GO fibers could be blended with Ag nanoparticles to increase the electrical conductivity,[25] or with CuI particles for improved humidity sensitivity[26] through a scalable prespinning blending process. Choi et al. prepared nitrogen doped rGO fibers through a postspinning thermal annealing in H_2/N_2 atmosphere (**Figure 3**a–c).[27] Sun et al. prepared crumpled rGO fibers by collecting the wet-spun fibers in a stirred viscous chitosan solution,[28] as a result of the shear stress in the spinning process. On the other hand, in electrospinning process, a high voltage (several kV) is applied to the extruded liquid drops, which could further "stretch" the liquid drop due to the electrostatic repulsion within the dispersion and render a longer and thinner fiber after deposited onto the collection substrate. Ling et al. prepared electrospun graphene reinforced silk fibers out of well-dispersed graphene/silk fibroin suspensions, which could be further processed into different formats with outstanding electrical conductivity and mechanical strength.[29] Yun et al. blended polyacrylonitrile (PAN) solutions with TiO_2 and multiwalled CNT (MWCNT), which were processed into a doped carbon fiber after electrospinning and carbonization. The addition of TiO_2 and MWCNT greatly improves the sensitivity of the carbon fibers as gas sensors.[30] Furthermore, during the electrospinning process, the fibers could be polarized along the electric field, which is significant for building the triboelectric systems. Electrospun poly(vinylidene fluoride) (PVDF) fibers are widely applied in building triboelectric nanogenerators.[31] Notably, Persano et al. prepared a highly aligned electrospun PVDF array through rotating the collection substrate at high speed.[32] Lin et al. obtained a core–shell fiber mat by coaxially electrospinning polydimethylsiloxane (PDMS) ion gel core and PVDF coatings at the same time, which enables the detection of both static and dynamic pressures (Figure 3d–f).[33] Further development of the spinning technique lies in a better control of the morphology and homogeneity of the as-prepared fibers. This route is limited for complex structures as required by electronic devices.

Multicomponent and multifunctional electronic fibers have been investigated by several groups via preform-drawing processes (Figure 3g). The lateral size of fibers in textile industry are generally from tens to hundreds of micrometers, which brings much difficulty in the fabrication of complex architectures within the fiber by conventional fiber spinning processes. Fink et al. developed a preform drawing technique for the scalable preparation of multicomponent and multifunctional

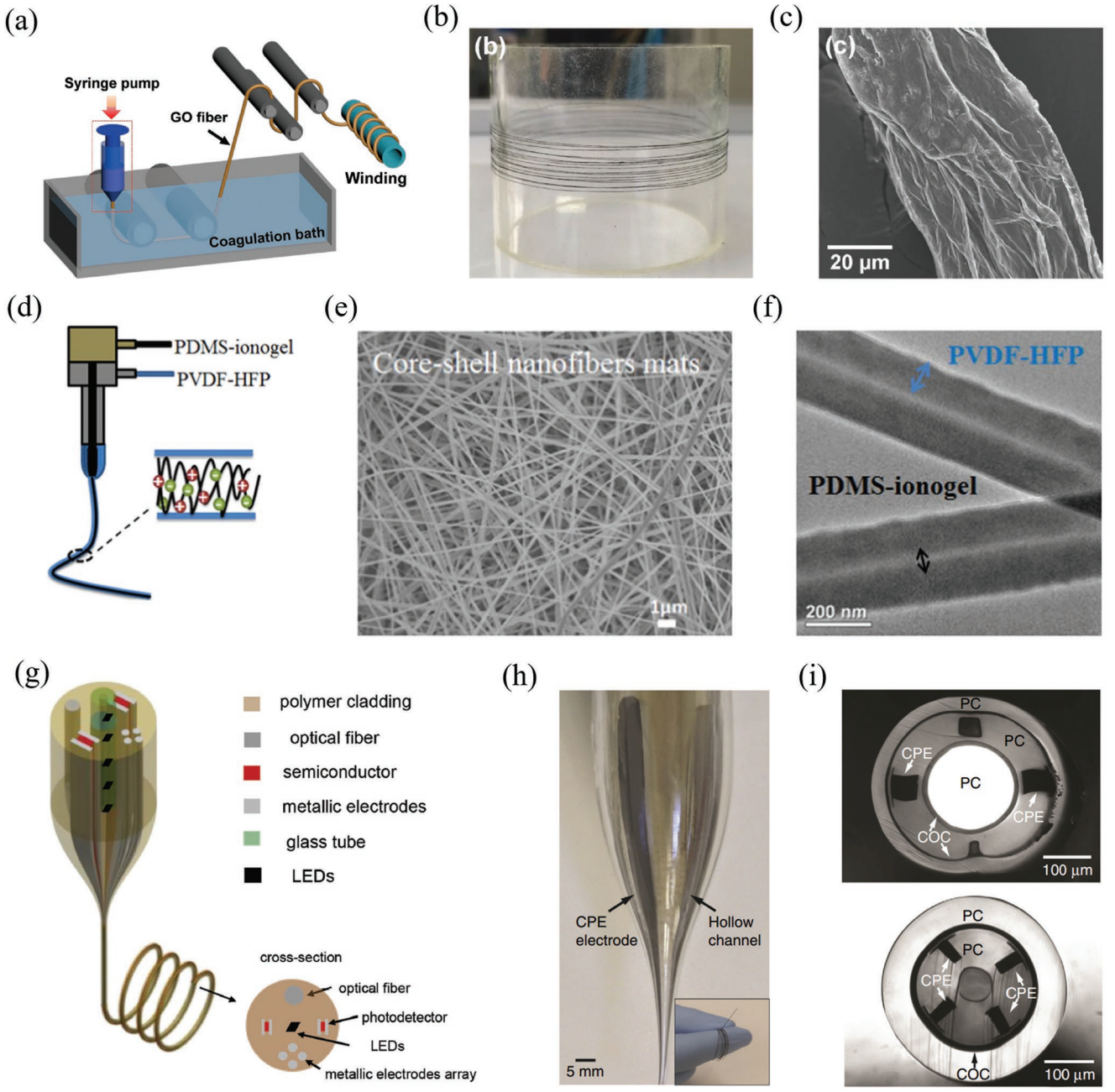

Figure 3. Methods of fiber making. a) A schematic for the preparation of GO fibers by wet spinning. b) A photo of wet-spun GO fibers wound on a bobbin. c) An SEM image of a wet-spun GO fiber. Reproduced with permission.[27] Copyright 2018, WILEY-VCH. d) A schematic for the preparation of core–shell PDMS ion gel/PVDF-HFP nanofibers through electrospinning. e) An SEM image of electrospun core–shell PDMS ion gel/PVDF-HFP nanofibers. f) A TEM image of electrospun core–shell PDMS ion gel/PVDF-HFP nanofibers. Reproduced with permission.[33] Copyright 2018, Elsevier. g) A Schematic of the thermal drawing of multimaterial fibers with different components. Reproduced with permission.[34] Copyright 2019, WILEY-VCH. h) A photo of a macroscopic preform partially drawn into a neural-fiber probe. i) Cross-sectional view of as-drawn multifunctional neural fiber probes. Reproduced with permission.[40b] Copyright 2017, Springer Nature.

fibers. The architectures are first assembled in a macroscopic preform containing polymer, low-melting-temperature metal and microchips. Then the preform is heated above the melting temperature (softening temperature for noncrystalline materials) of metal and polymer, followed by a mechanical drawing process. The methodology removes expensive micro/nanofabrication procedures in preparing the multifunctional fibers, but requires precision control of the melt flow. Comparable melting temperature (or softening temperature), viscosity and thermal expansion coefficient, for the maintenance of a stable architecture during drawing process, hinder the selection of constituent materials and components in the fiber.[34]

The attempt for preparing micro/nanofibers by thermal drawing started in 2004. An amorphous semiconductor core

coated with metallic microwires and optically responsive polymers, was drawn into a fiber with feature size below 100 nm.[35] After the thermal drawing process, an intimate contact was built amongst these components. The as-prepared fibers demonstrated a strong photocurrent within near-infrared range, which could be further woven into an optoelectronic fabric to manipulate the spatial distribution of illuminated light. Thermally drawn piezoelectric fibers were reported in 2010, by both infusing and cladding the piezoelectric poly(vinylidenefluoride-*co*-trifluoroethylene) [P(VDF-TrFE)] shell with carbon loaded polycarbonate (CPC) electrodes, which have adequate viscosity to confine the P(VDF-TrFE) shell during the drawing process.[36] The piezoelectric fiber demonstrated an acoustic transduction from kilohertz to megahertz frequencies, which could also be contacted with a Fabry-Perot optical layer for the modulation of its resonant properties. Besides, thermally drawn fibers for logic device[37] and supercapacitors[38] were also be achieved in subsequent years.

Neural probes for the monitoring and interrogation of brain activities have drawn great attention in recent years. To reduce the insertion trauma of the probes, micro/nanoscale fibers are preferred in the construction of neural probes due to their small footprints.[39] The introduction of multifunctional components within a single fiber is enticing, while the assembly of these components is usually costly and labor-consuming with traditional micro/nanofabrication techniques. Through macroscopic assembly followed by thermal drawing, fiber electrodes with waveguides and microfluidic channels could be prepared (Figure 3h,i), which could not only conduct electrical recording and stimulation, but also achieve optogenetic stimulation as well as drug delivery.[40] Besides, the multifunctional fiber could interface stably with neural tissues for more than 2 months.

2.3. Embedding Electronic Functions into Textile Fabrics

Conventional textile processes have been explored including weaving, knitting, embroidery and stitching processes, by which the electrical properties of electronic fibers are not sacrificed, and the interlaced network structure has superior flexibility and stretchability than individual fibers. Apart from these, another method is lamination of circuit board assemblies onto fabrics.

Weaving of two groups of orthogonally perpendicular yarns has been explored to connect various electronic components, such as discrete strain or temperature sensors. A fabric-based temperature sensing network was integrated on a flexible woven fabric circuit board (FCB) in our group.[41] For the fabrication of FCB, polyurethane (PU) yarns coated with silver nanoparticles were woven into conductive tracks which is highly stretchable. Discrete temperature sensors were then mounted at predesigned locations of the woven FCB in an island-bridge manner. The as-prepared temperature sensing network demonstrates a high stretchability up to 40% for the applied strain could mainly be undertaken by the flexible and stretchable FCB, rather than the rigid temperature sensors. For reading the temperature sensing results, the conductive tracks in FCB were linked to the electrical instrument through bonding interposers at the ends of the circuits.

Knitting could produce a mostly 2D fabric through interlacing consecutive rows of loops, thus the fabric is more stretchable than woven ones. Knitted fabrics have been studied to develop kinds of electronic textiles such as stain sensors,[42] stretchable interconnect,[43] fabric electrodes.[44] Li and Tao demonstrated a three-dimensionally stretchable FCB through incorporating PU-coated copper fibers and elastic filament yarns into a knitted fabric assembly.[43] Discrete strain sensors were mechanically and electrically linked with conductive tracks on the knitted FCB fabric. The first step is to produce an intarsia pattern by a computerized knitting machine to design conductive wiring layout of FCB. Next, sensors with two soft electrodes are fixed on the corresponding positions of knitted FCB. The third step involves adopting a rigid needle to assist electrodes of sensor go through micropores of the FCB, and the electrodes are physically and electrically connected with the looped conductive fibers.

Post et al. first reported to use embroidery of conductive yarns to route circuits and directly embed electrodes on textiles.[45] Different kinds of conductive yarns were discussed, while the resistance of them was high ($\approx 10\ \Omega\ m^{-1}$). Irwin and his colleagues fabricated conductive polymer coated silk fibers, and stitch them successfully into fabric as a functional timer circuits.[46] This study took advantage of conductive threads, which resulted in flexible electrical connection compared with rigid metal coated yarns. In 2017, Roh et al. developed an all-fabric interconnection using embroidery technique for routing connections between different layers.[47] Within the multilayer textile touch sensor, a resistive yarn stitch is adopted to link conductive fabric (upper layer) to the sensing pattern and circuit patterns (base layer) through embroidery, which forms a robust electrical contact between upper layer and the end of the circuit pattern on the base layer through a via hole. In this work, an embroidery machine controlled by computer made it possible to implement fabric interconnection for electronic sensors in an industrial scale. Even routing electronic circuits through embroidery is simpler than weaving and knitting, while the conductive traces embedding on the surface of fabric may cause electrical shorts.

3. Functional Components of STIMES

3.1. Sensors

Mechanical Sensors: Textiles could be generally regarded as a 3D network structure of weaved/knitted fibers. Such structural characteristic of textiles brings about great priority in designing mechanical sensors, including large strain sensors and haptic sensors. For textile-based strain sensors, the applied tensile strain could induce a macroscopic deformation of the network structure, instead of individual fibers. In this way, the textiles could withstand large strain without fracture, compared to a film or a single fiber. Textile based resistive strain sensors are the most widely applied, which could be weaved/knitted from conductive fibers or come from commercial textiles with conductive coatings. Upon tensile stretch, the deformation of the textile network undertakes the majority of strain.[48] Commercial fabric strain sensors made from coated conductive

knitted fabric have been available since 2013.[49] The wide range strain sensors were prepared by screen printing a composite of carbon black and silicone elastomer onto a fabric and connecting conductive yarns. They have extraordinary cyclic stability of over 100 000 tensile cycles at 50% strain. The washable sensors have a tunable gauge factor from 1 to 100. When used for monitoring of upper limb muscle contraction, the measurement accuracy reaches 93%. Seyedin et al. knitted wet-spun PU/PEDOT: PSS fibers into various textile structures, which demonstrate a moderate sensitivity with gauge factor (GF) up to –1 within 100% strain.[50] The fibers could even be knitted into commercial Spandex yarn which further improve the stretchability to 160%. In another work by Zhou et al, thermoplastic elastomer (TPE) wrapped CNT fibers with gauge factor of 425 within 100% strain could be stitched onto a jacket sleeve for the detection of arm motions.[51] Besides, carbonization process could scalably endow the wearable textile with electrical conductivity and electromechanical sensitivity, with maximum GF of 37.5 (to 500% strain) for carbonized silk fabric[52] and maximum GF of 64 (to 140% strain) for carbonized cotton fabric.[53] Except for resistive strain sensors, capacitive and triboelectric strain sensors[54] are also reported. For resistive and capacitive pressure sensing application, the porous structure endows e-textiles with high compressibility, thereafter high operational range could be achieved. A resistive pressure sensor with an operational range of more than 100 kPa could be prepared by impregnating silk fabric with rGO, although the sensitivity is low (maximum 0.4 kPa^{-1}).[55] In another report, Liu et al. face-to-face contacted a Ni-coated polyester textile with a CNT coated cotton fabric (**Figure 4**a,b), the as-prepared pressure sensor demonstrates a high sensitivity of 7.8 kPa^{-1} at a pressure of 15 kPa (Figure 4c), as well as low detection limit of 2 Pa, which enables the detection of both ultrasmall pressures from pulses and sounds, as well as accurately record large pressures from finger pressings.[56] On the other hand, the textile based capacitive pressure sensing system could not only built on textile level,[57] but on fiber level as well,[8c,58] which facilitates the building of orthogonal textile arrays.[59] Besides, textile-based triboelectric pressure sensors provide a self-powered system for sensitive detection of dynamic pressures.[60] Since the working principle of triboelectric pressure sensors is the contact-induced charge transfer, the hysteresis due to the viscoelasticity of flexible textile substrate could be largely avoided. For example, a core–sheath triboelectric fiber demonstrates repeatable electrical response under dynamic pressures with a frequency of 5 Hz.[60] The high surface area of textiles and fibers also favors an increased charge generation upon applied pressures, thus increases the sensitivity.

Humidity Sensors: Usually, water-sensitive materials should be added into the textile-based humidity sensing system for improved sensitivity.[11b,61] Zhou et al. prepared wet-spun SWCNT-polyvinyl alcohol (PVA) filaments, which was stitched onto a cloth substrate. Combination of water molecules swells the fiber (Figure 4d), which enables the detection of humidity change within relative humidity (RH) 60% to 100%.[62] Cotton fabric coated by oxidized MWCNT was demonstrated to perform humidity sensing from RH 60%.[63] A CNT-chitosan based fiber network synthesized by 3D printing could not only sense the environmental humidity from RH 35% to 85%, but also demonstrate self-healing behavior under the exposure of water vapor, which guarantees dramatically improved stability in everyday use.[64] In general, the state-of-art textile-based humidity sensors have relatively long response time, as well as limited detection range. Further structural optimization is needed for improved performance.

Temperature Sensors: Textile-based temperature sensors also show great importance in monitoring the physiological condition of the wearers.[65] The simplest design of textile-based temperature sensors is through embedding intrinsically thermoresistive metal wires into textile substrates.[41,66] Usually, metal wires demonstrate a linear response within a large temperature range, with high stability and resistance to other environmental disturbance, while the high rigidity of metal wires restricts the flexibility of the whole e-textile system, and the sensitivity is usually low (around 0.39% K^{-1} for Pt wire[41]). On the other hand, textile-based temperature sensors based on a coiled organic semiconducting polypyrrole fiber (Figure 4e,f)[67] and a MWCNT-polyacrylic resin nanocomposite coating[63] demonstrate improved sensitivity (around 0.54% K^{-1} for polypyrrole fiber[67] and 8% K^{-1} for the nanocomposites[63]) and flexibility, while the performance of these systems could be affected by other environmental factors such as humidity.

Chemical Sensors: Textile-integrated chemical sensors play a vital role in monitoring the physiological conditions of the wearers and alerting the wearer to the dangerous chemicals in nearby environment.[68] There are basically three principles for these sensors: The resistive chemical sensors are usually prepared through integrating chemically sensitive materials and electrical components.[6b,11a,30,69] Despite a simple design and high sensitivity, the adsorption of the analyte molecules is usually irreversible, which leads to a poor cyclic performance. Semiconductor-based chemical sensors utilize the doping effect of target molecules, which is more reversible,[70] while the fabrication of gate electrodes is somehow complex. Electrochemical sensors are widely applied for the detection of ions, which facilitates the analysis of sweat (Figure 4g,h).[20a,21,71] In general, selectivity is a key issue in the design of chemical sensors. For improving the selectivity, chemical sensors are modified for a specific bonding with certain analytes, at the expense of their durability.

The integration of multiple sensors has been adopted in e-textile system[26,72] for comprehensiveness. Efforts should be devoted to avoiding the interference of irrespective parameters and cross-talking of the various sensors. Wireless communication module may be introduced in electronic textiles,[20,21] by which the tethering force of electrical wires could be eliminated in data collection. Its added bulkiness and rigidity to the textile system should be considered.

3.2. Shape Actuators

Shape actuating devices are kinds of devices that convert external energy into mechanical energy, making a mechanical (shape) response under external stimulus. Traditional shape actuators (such as motor, pneumatic actuator, hydraulic actuator), due to their bulkiness, noise, and hardness, are not suitable for fabric integration. In the past, flexible actuators

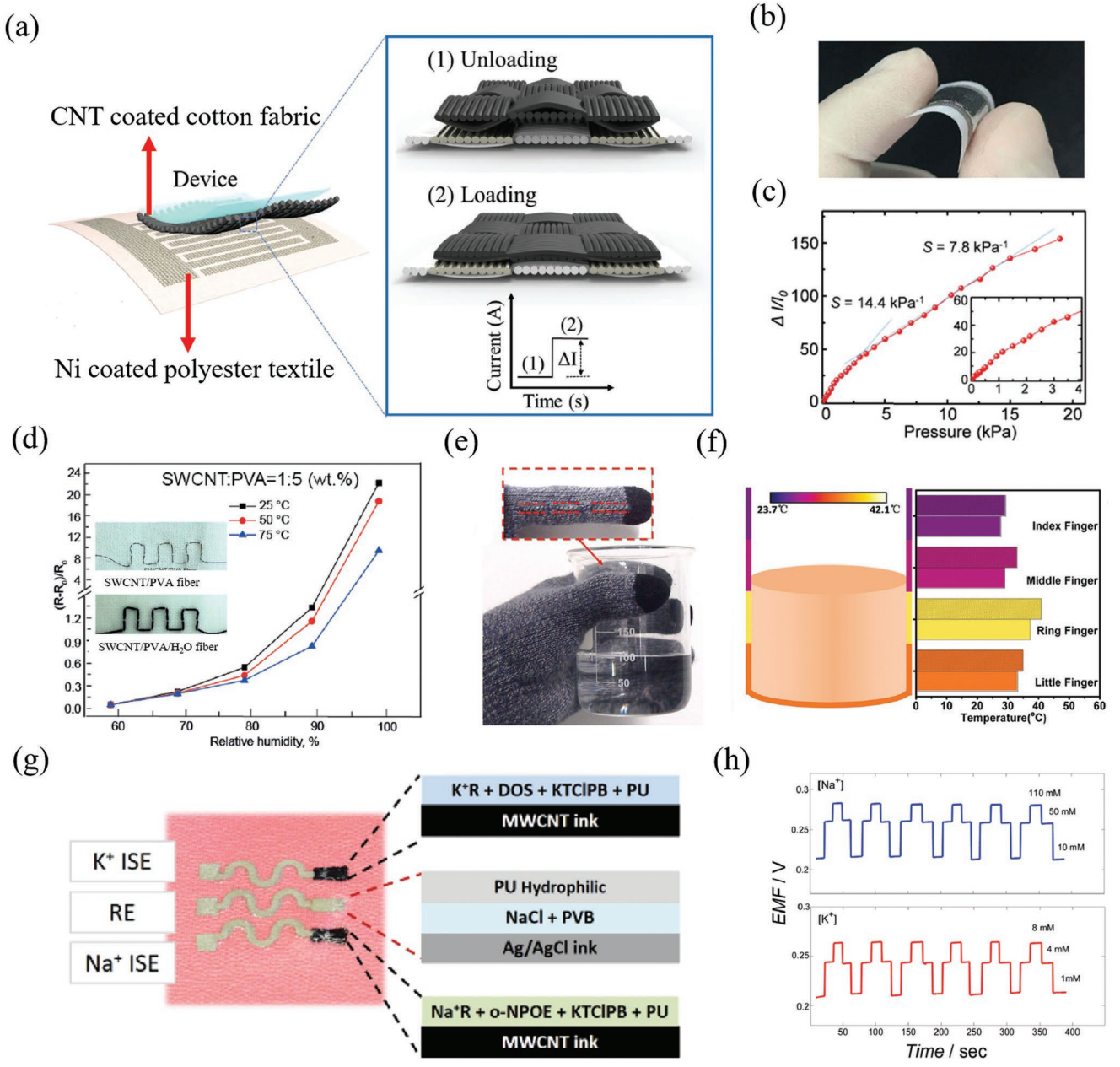

Figure 4. Textile-based sensors. a) A schematic of the design of a resistive pressure sensor by interfacing CNT-coated cotton fabric and Ni-coated polyester textile. b) A photo of the pressure sensor. c) The pressure sensing performance of the pressure sensor. Reproduced with permission.[56] Copyright 2017, WILEY-VCH. d) The pressure-sensing performance of a humidity sensor based on SWCNT/PVA fibers. Inset: photos of the SWCNT/PVA fiber embedded in a cloth before (top) and after (bottom) water adsorption. Reproduced with permission.[62] Copyright 2017, ACS. e) A fiber-based temperature sensor embedded in a glove. f) The temperature-sensing performance when a hand is holding a beaker with hot water. Reproduced with permission.[67] Copyright 2016, WILEY-VCH. g) An image of a textile-based chemical sensor for ion detection. h) Cyclic tests with concentrations of Na^+ and K^+ within physiological range. Reproduced with permission.[20a] Copyright 2016, WILEY-VCH.

have developed rapidly[73] and been widely used in soft robots,[74] intelligent sensing,[75] assistance medical treatment,[76] energy harvesting and conversion,[77] etc. The flexible shape actuators have the advantages of flexibility, light weight and high safety compared to rigid traditional shape actuators, so they can be easily integrated with fabric by weaving, sewing or direct coating active materials on fabrics. According to the type of external stimulus, flexible shape actuators can be divided into: thermal actuators,[78,79] electrochemical actuators,[80] humidity actuators,[81] optical actuators,[82] etc.

Thermal Actuators: The source of stimulus for thermal actuator is heat, that is, volume or shape change of the actuator occurs when the temperature changes. The required heat can be obtained by direct heating,[78] electrical heating,[83] or photothermal heating.[84] A semicrystalline polymer could demonstrate anisotropic thermal expansion behavior. To be specific,

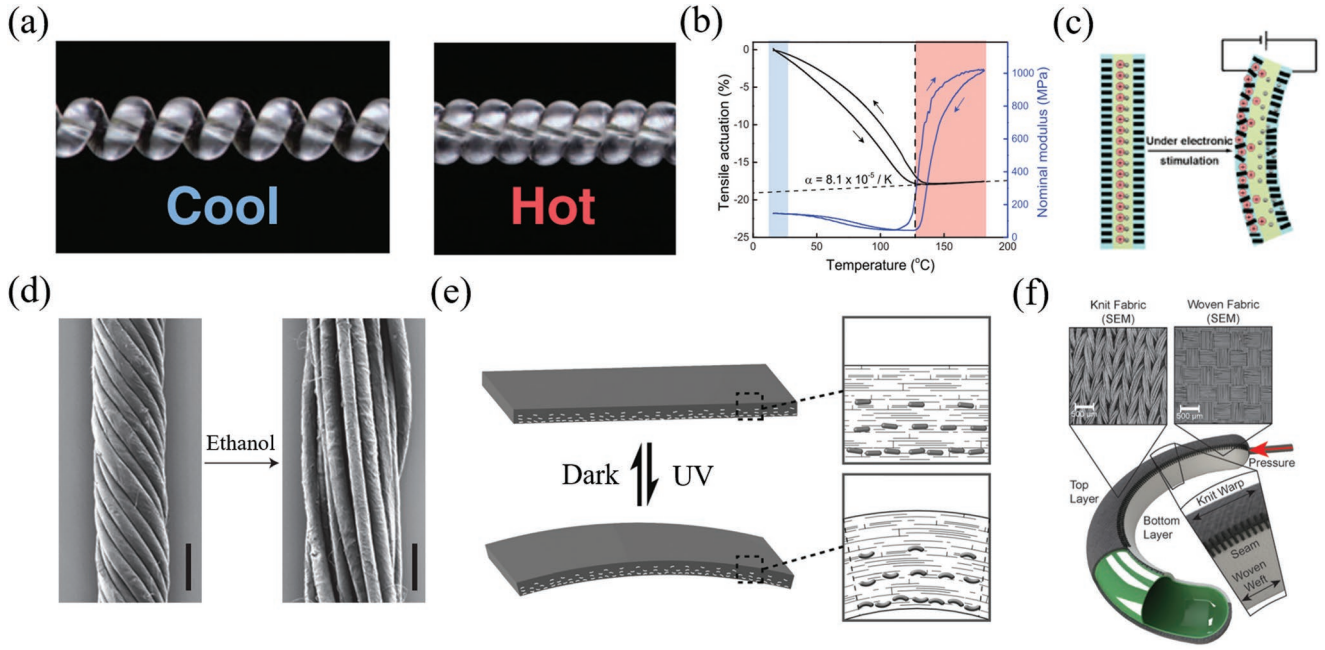

Figure 5. Fiber-based shape actuators. a) Optical images of a coil before (left) and after (right) heat-induced contact. b) The contraction strain versus temperature of braided polyethylene, nylon 6 monofilament, nylon 6,6 monofilament, and silver-coated nylon 6,6 multifilament fibers before twisting (inset) and after coiling by twist insertion. Reproduced with permission.[78] Copyright 2014, The American Association for the Advancement of Science. c) Schematic of an electrochemical actuator. Reproduced with permission.[73c] Copyright 2014, WILEY-VCH. d) SEM images of a twisted MWCNT fiber before (left) and after (right) ethanol treatment. Reproduced with permission.[81a] Copyright 2015, Springer Nature. e) Reversible bending mechanism of HNNA nanorods under UV irradiation. Reproduced with permission.[113] Copyright 2013, WILEY-VCH. f) Operating principle of a textile-based pneumatic actuator.[117] Reproduced with permission. Copyright 2018, Mary Ann Liebert, Inc.

volume expansion occurs in the crystallization zone upon heating. While in the amorphous region, the resistance of polymer chain is small, so that the chain length is shortened and a large shrinkage phenomenon occurs.[73a] Haines et al. prepared high performance actuators using polyethylene and nylon 6,6 twisted fibers, as shown in **Figure 5**a.[78] This type of actuator has the advantages of fast response speed and long cycle life. The reversible heat shrinkage of nylon 6,6 fibers between 20 and 240 °C was increased significantly from 4% to 34% (Figure 5b), and the twisted fibers produced by extreme distortion could shrink by 49%. Mirvakili et al. prepared a kind of thermal actuator by applying a conductive coating on a nylon beam.[85] Upon differentially heating, the actuator achieved a 125% displacement-to-length ratio and less than 5% deterioration in amplitude response over 100 000 cycles. Kim et al. prepared a thermal actuator by distorting composite fibers made from liquid crystal (LC) GO solution and penetrating nylon-6,6 polymer.[79b] The actuation behavior of twisted and coiled LCGO/nylon fibers showed a reversibility of ≈80% without hysteresis during cyclic heating and cooling. These thermal actuators are capable of lifting more than 100 times their own weight. Composite yarns based on spandex (SPX)/CNT are also used in textiles with spandex as thermal expansion material and CNT as conductive material.[86] The stretched textile produces a large stretch shrinkage of up to 33% and produces a weight mechanical work capacity up to 0.64 kJ kg^{-1} during shrinkage and a maximum specific power output of 1.28 kW kg^{-1}. The energy conversion efficiencies were in the range of 0.6% to 3.2% based on the ratio of input electrical energy and output mechanical energy during the contractile cycle. The highest efficiency for the SPX/CNT operated at 2 Hz was higher than the best efficiency reported for the coiled polymer fibers, that is, 1.08 and 1.32% for the coiled nylon and polyethylene fibers respectively.[78] These are similar to those of commercial shape-memory metals, which can reach 1 or 2%.[87] In addition, the electrochemically powered CNT yarn made from CNT forest can delivered a much higher contractile energy conversion efficiency of 5.4%.[88]

Besides semicrystalline polymers, thermal actuators could also be operated through phase change. Paraffin is a commonly used phase change material based on melting/crystallization,[73b] which was impregnated into vertically aligned carbon nanotube films to make an actuator by Copic et al.[89] In order to restrain the mechanical oscillations and reduce the response time of the actuator, a high loss viscoelastic material comprising paraffin and polystyrene-poly(ethylene-butylene)-polystyrene copolymer was used as the yarn guest to produce an overdamped dynamic response, which showed a tenfold decrease of stabilization time compared with pure CNT yarn based actuators.[90] Janus polymer fiber actuators have also been reported,[91] with fusible polycaprolactone (PCL) on one side and a polymer with a high softening point (such as acrylonitrile butadiene styrene (ABS) or polylactide (PLA)) on the other side. Upon melting and crystallization, the length of the PCL side of the fiber changes by 3%, which results in reversible bending of the Janus fiber.

In addition, composites with each component having different coefficients of thermal expansion (CTE) are also applied for actuation. Thermal stimulation leads to heterogeneous

thermal expansion within the composite, thus motions could be caused. PDMS is biocompatible, stable and have large CTE, which is suitable for building an actuator. The double-layer composites based on PDMS and low CTE carbon nanomaterials (such as CNT,[84] rGO,[83a] and GO,[92]) could generate internal stress at the interface, resulting in the deformation of the composite.

Electrochemical Actuators: Electrochemical actuators, also known as ion actuators, are operated based on ion motion. Electrochemical actuators show great potential in wearable devices due to their low actuation voltage, flexibility, and large deformability in the air. At present, electrochemical actuators mostly include a sandwich structure, that is, an electrolyte layer sandwiched between two electrodes, as shown in Figure 5c.[73c] Electrochemical actuators generally have two working principles, one based on the pseudocapacitance effect of a conductive polymer and the other based on the double layer effect of an ionic gel or ionic polymer/metal composite (IPMC). For the former mechanism, some conductive polymers (such as polypyrrole and its derivatives) could lose/obtain electrons in electrochemical reaction, thus the polymer chains are charged. In order to maintain the electrical neutrality of the chain structure, the anions/cations in the electrolyte will migrate and become embedded in the polymer, which causes the volumetric change of the polymers.[73a,c] For the latter mechanism, the positive and negative ions migrate to the two electrodes upon the applied voltage, and are adsorbed in the pores of the electrode materials to form an electric double layer, which causes the electrode material to expand. Due to the volumetric difference of positive and negative ions, the two electrodes expand in different extent, which causes the actuators to bend.[93]

The materials for building electrochemical actuators mainly include ionic gels,[80b] conductive polymers,[94] and IPMCs.[80a,83a,95] These materials have advantages such as light weight, good flexibility, low actuation voltage, as well as stable and large deformability in the air. Besides, metal foils,[96] conductive polymers,[97] and carbon nanomaterials[80a,95] are commonly used as electrode materials. In order to increase ion storage density and actuation strain, as well as reduce actuation response time, electrodes based on nanocomposites or with nanostructural design have also been adopted. Our research group has done a lot of research on this.

Graphene flakes have been widely applied as the filler to improve the dielectric constant of the matrix. However, due to the high surface area and abundant in-plane free carriers, the graphene flakes easily stack with each other rather than form a large scale ordered structure, which reduces the efficiency for carrier transportation. The alignment of the graphene flakes is extremely advantageous for the driving characteristics of the electrochemical actuator. Chen et al. designed and fabricated a graphene electrode oriented parallel to the direction of the electric field.[98] This structure shortens the path of ion migration by which a deformability of 98% is achieved, an order higher than CNT-based actuator. The hybrid structure of CNT and graphene has unique structural stability with CNT as the basic framework and graphene as the reinforcement.[99] A 3D porous graphene/CNT hybrid is applied as electrodes of actuators. Improved stability of the actuator is achieved, with 90% of the original deformability maintained after millions of actuation cycles.[100] However, the conductivity of the electrode was still not comparable to that of the metal material. Chen et al. further prepared the graphene/silver hybrid electrode with improved conductivity of 900 S cm^{-1}.[101] Furthermore, in order to increase the electrochemical activity of the electrode material, they prepared a CNT/carbon nitrogen(g-CN) 2D nanosheet composite electrode material.[95] The nitrogen active sites increase the tantalum effect and promotes the charge in the electrode, resulting in an actuation strain of up to 0.5% in 300 ms, a strain of 0.9% at equilibrium, 100 000 cycles stability, and a strain rate of 13.8% s^{-1}. To further improve the high frequency response, they designed a polyaniline/vertical ordered carbon nanotube array composite electrode material,[93a] and constructed an interface ion channel, which realized the rapid migration and removal of ions under low voltage electric field, thus increases the strain rates up to 42.5% s^{-1} at 50 Hz AC voltage. In addition, they proposed and experimentally verified a new molecular actuation mechanism: alkene–alkyne complex transition effect in an electrochemical actuator based on graphdiyne.[80a] The molecular-scale active graphdiyne-based electrochemical actuator was successfully prepared with a high electromechanical transduction efficiency of up to 6.03%, which surpasses the performance of the actuators based on piezoelectric ceramics, shape memory alloys and electroactive polymers. Besides, the energy density (11.5 kJ m^{-3}) of the actuator is comparable to that of mammalian skeletal muscle (≈8 kJ m^{-3}). Meanwhile, the actuator could work over a wide frequency range from 0.1 to 40 Hz with excellent fatigue resistance over 100 000 cycles.

Humidity Actuators: Humidity actuators produce actuation behavior when humidity changes. Some materials contain hydrophilic groups,[81b] which form hydrogen bonds with water molecules. These materials are capable of absorbing water molecules from the air, causing the material to expand.

Actuators based on twisted yarn coils exhibit much greater output force than the skeletal muscles.[84,102] Humidity induced actuation behavior of twisting yarn coil has been extensively studied. Graded torsion CNT fibers treated by oxygen plasma provide rapid and large shrinkage and rotation with high reversibility in response to water and moisture.[103] The addition of water-absorbing guest materials to twisted hydrophobic CNT yarns is also a commonly used mode of actuation. Kim et al. prepared a crimped and creped structure using a highly twisted CNT sheet stack and a hydrophilic poly(diallyldimethylammonium chloride) (PDDA) guest.[104] PDDA/CNT can be actuated by changes in water absorption or ambient RH. It offers a large stretch stroke (up to 78%), a large weight working capacity (2.17 kJ kg^{-1}) and a high volume working capacity (1.8 MJ m^{-3}). Natural fibers contain hydroxyl (-OH) or amide groups (-NH-), which form hydrogen bonds with water molecules. Natural fiber-based humidity actuated actuators have been reported,[83b] which provide output strain, pressure, and work capacity that are orders of magnitude higher than animal skeletal muscle and many actuators made of synthetic materials. Besides, the performance of natural fiber-based actuators can be further improved by the nonionic surfactant or alkali washing treatment. In addition to absorbing molecules, wetting the gap between fibers by capillary force can also actuate twisted carbon nanotube yarns.[81a] The hierarchically arranged helical fibers (HHFs) that respond to humidity

are produced by spirally assembling MWCNTs into primary fibers and then twisting the primary fibers together (Figure 5d). A large number of nanoscale gaps in the MWCNT and micrometer-scale gaps between the primary fibers are produced by the graded spiral arrangement. The solvent and vapor first diffuse through the micrometer-scale gap and then through the nanoscale gap, which results in a fast response and large actuation stroke.

As well as fiber-based actuators, GO is also a good candidate for building humidity actuators due to its abundance of oxygen-containing groups.[105] A typically layout of GO-based humidity actuator is a GO/rGO bilayer film. Thanks to the different water absorbance ability of GO and rGO, the swelling degree of the two layers is different under humidity stimulation, and this asymmetric expansion can cause the bilayer film to exhibit an actuating behavior. Besides, some polymers with good water absorption ability, such as PEDOT:PSS,[106] PPy,[107] poly(3-sulfopropyl methacrylate potassium salt) (PSPMA),[108] a π-stacked carbon nitride polymer (CNP),[75] could also be used to prepare humidity actuators.

Optical Actuators: Optical actuators are widely studied for their unique advantages, such as noncontact actuation and remote control. In addition, light is a clean and safe source of energy. Accurate light manipulation can be achieved by controlling parameters such as light intensity, wavelength, exposure duration, and polarization direction.[109] Generally, optical actuators have different categories depending on their actuation principle. Photochemical actuators and photothermal actuators are widely used.[82b,109b,110]

Photochemical actuators mainly refer to the actuating behavior of some photosensitive polymers that undergo molecular structure changes under light stimulation. Azobenzene and its derivatives are commonly used photosensitive materials.[75,82a,111] Under the irradiation of ultraviolet light, the azobenzene is transformed from a rod-shaped trans structure to a curved cis structure. Since the trans structure facilitates the ordered alignment of the polymer mesogens, while the cis structure facilitates the formation of the disordered state of the mesogens; the volume and shape of azobenzene could change upon light stimulation.[110,112] Compared to the azobenzene-based liquid crystal elastomers (LCEs) actuation described above, organic molecular crystals (OMCs) can be directly driven by photoisomerization and subsequent molecular lattice deformation, resulting in better repeatability, fatigue resistance and faster response rate. However, molecular crystal actuators are fragile and are highly limited in performance due to crystal size and shape. Our group prepared the assembly of 2hydroxynaphthylidene-1'-naphthylamine (HNAN) nanocrystals in polymers.[113] Under ultraviolet light, horizontally placed nanorods are curved into arches; these curved rods occupy more vertical space and less horizontal space than unbent nanorods (Figure 5e). Therefore, this deformation will drive the surrounding polymer unit to contract in the horizontal direction and expand in the vertical direction.

Photothermal actuation is also a commonly used photoactuation mechanism that converts light energy into thermal energy and then produces a shape or volume change through thermal expansion/contraction, similar to the working mechanism of thermal actuators. Although significant advances have been made in the study of photochemical actuators based on LCEs and OMCs, they are difficult to perform molecular design, synthesis, and assembly, and one-to-one corresponding wavelength selectivity cannot be achieved. Our group produced a wavelength selective bimorph optical actuator based on selective light absorption of Au nanocrystals (AuNCs).[114] The wavelength dependent energy conversion is provided by Au nanocrystals due to longitudinal surface plasmon resonance (SPR). Recently, Han et al. prepared an rGO-AuNRs/PMMA bilayer structure by compounding gold nanorods (AuNRs) in rGO.[115] By coupling the plasma near-field enhancement effect, the energy conversion efficiency of the device is greatly improved.

Sunlight driven actuators are more attractive than infrared and ultraviolet driven actuators because they are more suitable for wearable textiles. Carbon nanomaterials have excellent photothermal properties and are widely used in photothermal actuators.[109b,116] Hu et al. prepared a RGO-CNT/ PDMS bimorph optical actuator, which can be actuated by sunlight.[83a] Based on this rolling RGO-CNT/PDMS bimorph, the crawler "robot" can be simulated to mimic the movement of the tank quickly, over obstacles and climb the steps. Hu et al. also prepared a CNT/PDMS bilayer composite multistimulus response actuator.[84] The rolling-based CNT/polymer double-layer composite actuator can perform actions such as scrolling and jumping. The natural flowering behavior could be simulated by four CNT bilayers, which can be rolled up under ambient sunlight.

Other Actuators: In addition to the actuation forms described above, there are other actuators that are used for shape actuation. Pneumatic actuators are a common form of wearable actuation that changes the shape of materials through the flow of air pressure. Recently, Cappello et al. reported a textile based pneumatic actuator.[117] Knitted and woven textiles have different strain properties. Knitted textiles, woven textiles and intermediate thin airbags were integrated for the preparation of actuators. When the intermediate balloon was inflated, a series of multiple degrees of freedom motion could be produced, as shown in Figure 5f. Despite the emergence of flexible and stretchable actuators, actuators with sensing capabilities are rare. Yeo et al. proposed a simple method of integrating a flexible pneumatic actuator with a tensile strain sensor to create a sensing actuator glove that demonstrates its potential for use in rehabilitation.[118] Chemically reactive pneumatic actuators have also been fabricated.[74] The fuels of monopropellant are rapidly decomposed into gas upon exposure to the catalyst, and the coupling of the monopropellant fuels and microfluidic logic powered these pneumatic systems.

3.3. Displays

Textile-based displays are poised to revolutionize wearable electronics and fashion industries.[119] Generally, traditional light emitting devices exhibit bulky and rigid structure, which hinder the development of next-generation wearable electronics. Recently, the emergence and blooming research of organic electroluminescent devices, such as organic light emitting diode (OLED) and polymer light-emitting electrochemical cell (PLEC), make wearable textile displays become possible.[120]

Generally, light emitting devices based on fiber substrate show relative poorer performance than the counterparts on planar substrates due to the disproportionate distribution of electron–holes on the fibers. To address this issue, Choi et al. reported a highly efficient 1D fiber OLEDs utilizing a simple, cost-effective and low-temperature solution process.[119e] The obtained state-of-the-art device showed a compatible light emitting efficiency and lifetime to conventional glass-based ones. In addition, this device was demonstrated to be weavable into knitted clothes and withstand tensile strain of up to 4.3% with a radius of 3.5 mm. By optimizing the fabrication process, an OLED device with a very small diameter of 90 μm can be further obtained. This work is compatible with cost-effective roll-to-roll production, and may realize low-cost commercially fiber-based displays.

In addition to the 1D fiber-based configuration, OLEDs with 2D fabric architecture were also intensively investigated. One of the major challenges for the widespread use of the fiber-based light emitting device is their operational stability. To this end, Kim et al. developed an actual fabric-based reliable OLED device.[120b] The surface roughness of the substrates was reduced by applying PU and multilayer barrier films, where moisture and oxygen in the environment was isolated from the OLED device by inserting multilayer barrier and capping films. The resultant double-side encapsulated device can remain a similar performance level even after working for 3500 h in ambient air.

PLECs have a similar structure as OLEDs that comprising of two electrodes connected with a semiconductor. Because of the different mechanisms for ion mobility, PLECs show the merits of high electron conversion and power efficiencies, and low operating voltage as compared with OLEDs. In addition, PLECs can be effectively prepared on rough surfaces, which shows advantage in practical fiber-based wearable applications. Peng et al. developed a color-tunable, weavable PLEC, using scalable and all-solution based processes.[120i] This device displayed a coaxial structure, where a modified metal wire as the cathode, conducting aligned CNT sheet as the anode, and electroluminescent polymer layer sandwiched between them. This lightweight, flexible, and wearable PLEC provides a variety of tunable colors, which show potential in being woven into smart fabrics for wearable applications. Peng et al. also developed a novel device from continuous electroluminescent fibers by one-step extrusion process.[120a] The resultant device is flexible, stretchable, twistable, breathable, conformable to arbitrarily curved skins, and compatible with a series of desired patterns. Furthermore, it could communicate with a computer for smart display application. This work opens up a new direction for the integration of electroluminescent devices with wearable devices, and may provide promising communication platform for future electronic system.

Except for the integration of lighting devices, textile-based displays could also be achieved by introducing materials capable to change color under various external stimulus, such as heat, electrical field and mechanical forces. The color change could be both reversible and irreversible, and we will focus on reversible color changes that are suitable for wearable devices.

Thermochromism: The mechanism of thermochromism is that the color of materials changes from one color to another when heated, and return to the original color when cooled. Materials used for thermochromism mainly include inorganic materials, organic materials, and photonic crystals.

Amongst inorganic materials, vanadium dioxide (VO_2) is widely used in thermochromic applications.[121] When heated above the phase transition temperature, VO_2 is converted from a monoclinic (so-called M1 phase) to a tetragonal rutile (R phase) structure, and its band gap disappears, resulting in sharp changes in optical constants and light absorption.[121b] Guo et al. synthesized highly dispersed M phase VO_2 nanoparticles by hydrothermal method.[121a] A thermochromic flexible film was prepared by combining the VO_2 nanoparticles with polyacrylonitrile, which exhibit a solar modulation efficiency of 12.34% and luminous transmittance of 54.26%. While generally inorganic nanoparticles have a higher phase transition temperature, which is a limitation for their application.

For organic materials, polydiacetylene (PDA) with conjugated polymer chains is a commonly applied for thermochromic applications. Typically, once their ene-yne conjugated backbone is distorted by exposure to a stimulus, the PDA undergoes a blue to red transition.[122] This unique feature has prompted many research efforts to design PDA molecules with the ability to monitor specific stimuli. Kim et al. synthesized a series of diacetylene (DA) monomers with bisamide linkages with different peripheral alkyl chains (n = 6–9; DA1-DA4).[123] They found peripheral alkyl chain length of these DA monomers exhibits an odd/even effect on the top chemical polymerization. And the as-prepared PDA-embedded polyethylene oxide film has excellent thermochromic reversibility and stability between 20 and 100 °C and can be stored for several months without deformation. In addition, a polymer containing a lactone ring is also a commonly used thermochromic material. Its color conversion is based on the change of states of the lactone ring: i) a colored state with an open chain; ii) a colorless state with a closed chain.[124] In weak acidic environment, when the temperature is high, it is favorable for the formation of a closed-loop state, and at a low temperature, it is advantageous for the formation of an open-loop state. Based on this color change mechanism, Chen et al. prepared rewritable paper based on thermochromic dye and photothermal-converting toner. Patterns could be written by an electrothermal pen and erased by chilling or illumination by NIR light. The proposed rewritable paper provides long clear information time (>6 months), excellent reversibility (>100 times) and high resolution.[125]

Photonic crystals (PCs) are regular structures in which materials having different refractive indices are periodically arranged. The color exhibited by the photonic crystal belongs to the structural color, which obeys the Bragg's diffraction law: the color changes with the change in period, or the refractive index of materials or the angle.[126] Banisadr et al. prepared an actuator that can simultaneously change the color and surface morphology under infrared (IR) driving.[127] SWNT-LCE film as the deformation layer and elastomer photonic crystal film as the color change layer were used in this study. Thermal stimulation caused the deformed layer to bend. And the bending caused the periodicity of the photonic crystal to change and produced a color change. Wang et al. reported a new class of reversible thermochromic responses achieved by controlling the refractive index of the environment in a butterfly PC structure.[128]

Photon ethanol-filled nanostructured samples were simply assembled by encapsulating liquid ethanol-filled butterfly wings. The refractive index of the environment was adjusted by the volatility of ethanol. The butterfly wing exhibits a significant discoloration response to the ambient refractive index, which can be controlled by liquefaction and evaporation of ethanol.

Electrochromism: Electrochromism is a phenomenon in which the color, transparency, or other optical properties of a material change in response to charge.[129] It is widely used in a variety of devices, including smart windows,[130] displays,[131] and eyewear.[132] Currently, typical electrochromic devices have multilayer layouts including an electrochromic electrode layer, a counter electrode layer, an electrolyte layer, a transparent conductive layer, and a support substrate.[129] The electrochromic layer is in a bleached state without application of a voltage, and cations (such as H^+ or Li^+) are in the electrolyte and around the counter electrode. When a voltage is applied, the electrochromic layer is oxidized. The cations migrate toward the electrochromic material electrode and change the optical properties of the electrochromic material, by which the electrochromic material turns into a colored state. After applying a reversible voltage, the electrochromic layer returns to the bleached state. The performance of electrochromic devices is largely determined by the selection of electrochromic materials, and transition metal oxides are widely adopted, such as tungsten oxide,[133] nickel oxide,[134] vanadium pentoxide,[135] and other transition metal oxides.[136] Yan et al. used tungsten oxide to prepare a stretchable and wearable electrochromic device. AgNWs embedded PDMS elastomer matrix was applied as the elastic conductor, and a tungsten oxide layer was electrochemically deposited onto the elastic conductor.[137] The device is capable of fast coloring (1 s) and bleaching (4 s) and has good stability under cyclic stretching, twisting, folding and wrinkling. This electrochromic device was successfully implanted onto a cotton textile substrate for potential wearable applications.

In addition, there are also various types of electrochromic polymers (ECP), such as thiophene derivatives,[132,138] aniline derivatives,[139] viologen derivatives,[122] spiropyran derivatives,[140] metal-supramolecular polymers,[141] and PDA/CNT composites.[142] The generally accepted mechanism of discoloration of electrochromic polymers is that under the action of a reversible voltage, the electrochromic material switches between an oxidized state and a reduced state, thereby its optical properties are altered. It is interesting that the discoloration mechanism of PDA/CNT composites is different from pure PDA. When a voltage is applied across the PDA/CNT composite, 3D jumps of electrons along the carbon nanotubes and through the carbon nanotubes are induced. The backbone of PDA is readjusted to support efficient π-π interactions between the sp^2 hybrid orbitals on the MWCNT-PDA interface. As the structure of the PDA main chain changes, the absorption rate of the composite material also changes. Thereafter, the color of the composite changed significant from blue to red.[142a]

Photochromism: Photochromism is a phenomenon in which optical properties change under the stimulation of photons. The photochromic compound undergoes isomerization between at least two forms, with light triggering at least one isomerization process.[143] There are two main mechanisms of photochromism currently studied: one is to change color by open- and closed-ring isomers (such as, naphthopyrans (NPT) diarylethene (DAE)), and the other is to change color by bond angle change (such as, azobenzene (ABS)).[144] Mao et al. developed a stimuli-responsive polymeric dye based on aqueous polyurethane and azobenzene chromophores, which could be coated on a textile to obtain a photoresponsive cellulose fabric.[145] In trans-cis isomerism, the fabric exhibits a color change between yellow and orange after alternative ultraviolet (UV) illumination and darkness. Pinto et al. successfully prepared PVDF fibers doped with naphthopyran functionalized silica nanoparticles (SiO_2@NPT) by dry–jet wet spinning.[146] This fibers could respond to both ultraviolet and sunlight, exhibiting fast coloring kinetics and good optical contrast with a coloring time of less than 1 min. In addition, this fibers were completely bleached in 49 min. Pinto et al. also dispersed SiO_2@NPT particles in aqueous PU-based media.[147] The SiO_2 nanoparticles were successfully incorporated into knitted cotton fabrics by a screen printing process, and all of the textiles exhibited reversible photochromism under solar radiation, resulting in rapid reaction, intense coloration and excellent stability during washing test.

Generally, the photochromic properties of organic dyes are greatly attenuated under long-term exposure to ultraviolet light. And pure inorganic photochromic materials have poor reversibility or no reversible color properties in solid state. The combination of. Polyoxometalates (POMs) and organic proton donors allows to overcome this problem, resulting in materials with enhanced and highly adjustable photochromism. Pinto et al. prepared a photochromic nanocomposite by electrostatically interacting negatively charged phosphomolybdates on positively charged amine-functionalized silica nanoparticles (SiO_2 NPs).[148] A core–sheath type fiber was prepared by melt spinning, and polypropylene (PP) doped with composite nanoparticles was used as a sheath layer and pure PP as the core. The obtained smart composite fiber has good mechanical properties and can be woven into a photoresponsive mesh. The fiber mesh shows UV response properties, good stability in high temperature and color change cycles. Khattab et al. prepared a water-based pigment-binder composite ink containing an inorganic pigment phosphor with good light stability and thermal stability.[149] The water-based pigment-binder composite ink was successfully screen coated onto the cotton fabric and then thermally fixed. The printed fabric exhibited a rapid and reversible photochromic response during UV excitation without fatigue. After UV radiation, the fabric shows good fastness under washing, rubbing, perspiration, sublimation and light exposure.

Humidity-Induced Discoloration: Humidity-induced discoloration is a phenomenon in which color changes with humidity. Humidity in a human living environment is in a state of change, and the body's perspiration to the outside environment can also cause changes in humidity around the skin. Therefore, reflecting changes in humidity through color changes is a more intuitive way to monitor humidity changes. However, as far as the authors are aware, there is currently little research on humidity actuating color-changing materials, probably because the mechanism of color change has not been studied. Like the mechanochromism described above, the integration of different mechanisms can also achieve a good degree of humidity

actuating discoloration. Xuan et al. prepared a humidity sensor by integrating photonic crystals and moisture deformation materials.[150] As the humidity changes, the sensor automatically displays a different color. They first prepared $Fe_3O_4@SiO_2$ core/shell colloidal particles, then dispersed $Fe_3O_4@SiO_2$ into a liquid precursor of poly(ethylene glycol) acrylate, prepared a photonic crystal structure using a magnetic component, and then solidified the structure. When in contact with moist air, the matrix strongly absorbs water and thus expands, causing the lattice constant of the photonic crystal to increase and the color to change from blue-green to red.

Sum-Up: Although significant achievements have been made recently in fiber-based displays, there are still many problems to be solved. For example, most of the reported devices showed short operational lifetimes (less than 100 h because of the exposure to moisture and oxygen), which is still one of the biggest hurdles for the development of practical wearable displays. Furthermore, the preparation techniques of high-resolution full-color LED array, as the input/output terminals in electronic system, still limit. In addition, the integration of fiber-based display devices with other wearable electronic devices is still a challenge.

3.4. Antennas

Antenna is an essential component in wireless communication modules. To fulfill the specific requirements for wearable applications, it requires planar and flexible textile substrates.[151] The performance of a planar microstrip antenna largely depends on the permittivity and thickness of the textile substrate, which directly affect its efficiency and bandwidth.[152] The antenna is required to be thin, lightweight, robust, cheap and easy to be integrated into the flexible circuits. Generally, commercially available textiles exhibit a relatively low dielectric constant (less than 2), which can decrease the surface wave losses to some extent and increase the impedance width of the antenna. Another issue needs to be addressed is that the spatial geometry of the antenna is affected by the movement of the body, which further influences its performance and stability. Thus, the structure of the antenna should be specifically designed, for example with a wide frequency bandwidth, to avoid suffering from the frequency detuning caused by the mechanical deformation. Vandenbosch et al. fabricated a wearable antenna at 2.4 GHz for medical application.[153] The metamaterial structured patch antenna with the dimensions of $46.5 \times 39 \times 3.34$ mm^3 can generate a broadside or an omnidirectional radiation pattern by reconfiguring the dispersion curve. Its bandwidth can cover the industrial, scientific, and medical (ISM) band in all the operating states. However, the bending of this antenna in *y*-direction induces the shift of resonance peak. To eliminate the mismatch and frequency shift caused by the human body movement, Ashyap et al. developed a compact antenna with a novel miniaturized electromagnetic bandgap (EBG) structure.[154] The antenna shows a dimension of $46 \times 46 \times 2.4$ mm^3, and delivers an impedance bandwidth of 27%, exhibiting a gain enhancement of 7.8 dBi. This newly designed structure shows superior advantages in biomedical application. To further lessen the physical size of the patch, Ashyap et al. demonstrated a miniaturized textile antenna for ISM band applications.[152] The size of the E-shaped antenna is only 25% of a conventional one. In addition, its performance can maintain the same under different bending conditions.

Antennas can also be used for energy transfer and harvesting.[155] For instance, Singh et al. designed a modified and efficient antenna to gain efficient power.[155c] The antenna was prepared on a jeans and exhibited triple band features, which gave three different wide bands with gains of 3.353, 4.237, and 5.193 dBi, respectively. It is suitable for different wireless communication systems and promising in power transfer, military use and various welfare applications. Loss et al. fabricated a series of embedded dual-band textile antennas for electromagnetic energy harvesting.[155b] The fully integrated antennas were prepared by printing, lamination and embroidering techniques, successively. They can be operated at global system for mobile communication (GSM) 900 and digital cellular system (DCS) 1800 bands, and showed prospect in the field of IoTs that related to wireless sensor networks (WSN) and radio frequency identification (RFID) systems.

Textile-based wearable antennas will become a central component with the rapidly development of wireless communication system and technology. However, there are still many issues to be resolved, including proximity to human body, and very limited volumes with existing structural design, substrate, material, and fabrication techniques.

3.5. Energy Harvesters

Energy harvesters are one kind of device that can convert the ambient energy ubiquitously presents in the environment (kinetic, thermal, bionic, photovoltaic, and radio-frequency energy) into electricity for continuous, sustainable and portable power supply. Energy storage devices efficiently store the energy generated by energy harvesters and other power sources. Textiles are one of the most suitable substrate materials for future wearable applications due to their high flexibility and wearable property, which can effectively accommodate to mechanical deformations induced by body movement and host various electronic devices and components. It is highly imperative to develop textile-based harvester and storage devices with outstanding performance for future wearable applications.

Energy-harvesting textiles can be achieved by adding active materials as films or coating on the surface of textile, or as yarns that are woven or embroidered into the textiles.[156] Three transduction mechanisms have been employed to convert mechanical energy into electrical energy: electromagnetic, piezoelectric, and triboelectric effect (triboelectrification and electrostatic induction). Thermoelectric and photovoltaic effects are another two common transduction mechanisms to convert thermal and solar energy into electrical energy, respectively. Meanwhile, hybrid generators based on multiple transduction mechanisms have been developed, showing higher conversion efficiency than the generator based on single transduction mechanism. This section discusses the generators based on single transduction mechanism first and then discusses hybrid generators, with the representative performance of textile-based generators listed in **Table 1**.

Table 1. The performance of representative textile-based energy harvesters.

No.	Nanogenerator Type	Materials	Preparation method	Maximum efficiency	Peak voltage	Year
1[158b]	Electromagnetic	Commercial magnet and graphite sheet	Macroscopic assembly	32mW	0.68 V	2014
2[158c]	Electromagnetic	NdFeB, copper and acrylic	Macroscopic assembly	654.38 μW	0.3 V	2015
3[158e]	Electromagnetic	PE filament, PU coated Cu filament	Winding and twisting	N.A.	12 V	2018
4[44]	Piezoelectric	PVDF, $NaNbO_3$, Ag coated polyamide textile	Electrospinning	21.5 mW m^{-2}	3.2 V	2013
5[160]	Piezoelectric	PVDF, Ag coated polyamide textile	Melt spinning	5.1 mW m^{-2}	14 V	2014
6[159b]	Piezoelectric	PVDF, CVD graphene and PET	Electrospinning	1 mW m^{-2}	2.5 V	2016
7[161]	Piezoelectric	PZT, AgNPs, silver ink, and Kapton PI	Screen printing	7.5 mW m^{-2}	17 V	2017
8[162c]	Piezoelectric	$BaTiO_3$, PVC, Cu, PET	Spinning and Knitting	10.02 nW (size data absent)	1.9 V	2015
9[162a]	Piezoelectric	$BaTiO_3$, PDMS, ITO coated PET	Electrospinning and infiltration	154.7 mW m^{-2}	2.67 V	2016
10[54]	Triboelectric	PU, Ag coated nylon, PVDF-TrFE and CNT	Electrospinning and surface coating	N.A.	0.25 V	2016
11[169b]	Triboelectric	Ni, rGO and PE	Electroless deposition	2.42 mW cm^{-2}	40 V	2016
12[169d]	Triboelectric	Polyester, Ni and silicon rubber	Weaving	0.892 mW cm^{-2}	500 V	2017
13[170b]	Triboelectric	Nylon, FEP, Ag	Layer-by-layer assembly	4.65 μW cm^{-2}	22 V	2015
14[171a]	Triboelectric	PE, silicon rubber, stainless steel	knitting	8.5 μW cm^{-2}	1.7 V	2017
15[171b]	Triboelectric	PTFE, silver	knitting	0.6 μW cm^{-3}	23.5 V	2017
16[172]	Triboelectric	Commercial Ag coated textile, PDMS, ZnO	Epitaxial growth, dip coating	1.1 mW (size data absent)	170 V	2015
17[187c]	Thermoelectric	Glass fabric, Bi_2Te_3, Sb_2Te_3, PDMS and Cu	Printing	3.8 mW cm^{-2} ($\Delta T = 50$ K)	0.09 V ($\Delta T = 50$ K)	2014
18[187b]	Thermoelectric	$B_{i0.3}Sb_{1.7}Te_3$, $Bi_2Se_{0.3}Te_{2.7}$, commercial Kryotherm, Cu	Printing and membrane transfer	2.28 μW cm^{-2} ($\Delta T = 50$ K)	0.02 V	2018
19[188g]	Thermoelectric	Sb_2Te_3, PAN, Bi_2Te_3, Au	Electrospinning and deposition	62 μW cm^{-2} ($\Delta T = 55$ K)	0.0452 V	2016
20[188h]	Thermoelectric	CNT, PEI and PDMS	CVD and winding	697 μW g^{-1} ($\Delta T = 40$ K)	1.2 V g^{-1} ($\Delta T = 40$ K)	2017
21[177k]	Thermoelectric	BiTe, SbTe and glass fabric	Screen printing	5.75 μW cm^{-2} ($\Delta T = 50$ K)	0.14 V ($\Delta T = 76$ K)	2016
22[176r]	Thermoelectric	CNT and PEDOT:PSS	Wet spinning	0.43 μW cm^{-2} ($\Delta T = 10$ K)	0.44 V ($\Delta T = 10$ K)	2018
23[191a]	Photovoltaic	CNT, Ti and TiO_2	Anodic oxidation, twisting	6.58%	0.73 V	2014
24[192]	Photovoltaic	Rubber, Ti, TiO_2, CNT, P3HT: PCBM, PEDOT:PSS	Winding and deposition	1.23%	0.51 V	2015
25[194]	Photovoltaic	Ti, TiO_2, CNT and Pt	Anodic oxidation and weaving	10.00%	0.73 V	2018
26[196]	Photovoltaic	PE, AgNW, graphene, Al/LiF PEDOT: PSS, P3HT: PCBM	Weaving, blade coating, deposition	2.27%	0.55 V	2017
27[197]	Photovoltaic	Nylon, P3HT, PAMD and PEI	Scooping	2.90%	0.58 V	2017
28[201]	Photovoltaic	MoOx, ITO, ZnO, PNTz4T,$PC_{71}BM$	Lamination, deposition	7.90%	0.71 V	2017
29[204a]	Hybrid	PVDF, PDMS and MWCNT	Wet spinning and blade coating	222 μW cm^{-2}	161.66 V	2018
30[166a]	Hybrid	PTFE, Cu, Mn, PBT, CuI and ZnO	Weaving	40 μW cm^{-2}	80 V	2016
31[205b]	Hybrid	PE, Ni, Ti, TiO2, Pt, $LiClO_4$ based electrolyte	Screen printing and weaving	320 μW cm^{-2}	3.4 V	2016
32[206]	Hybrid	Al, PTFE, Cu, PVDF, Kapton film	Deposition and pasting	14.62 μW cm^{-2}	0.8 V	2015

Electromagnetic Generators: Electromagnetic generators, converting kinetic energy into electrical energy, have been invented and developed to be the most important technology for power generation since the electromagnetic induction effect was discovered by Michael Faraday in 1831.[157] Small-scale electromagnetic generators also have been developed for wearable applications (**Figure 6**a),[158] harvesting energy from human motions, such as the swinging movement of arm legs,[158e] low- frequency hand shaking,[158a,c,d] walking and slow running,[158a,b] through magnets and coils. Such devices can generate power up to dozens of or hundreds of microwatts. However, conductive coils and magnetic bodies are normally made of heavy materials, which are rarely applied in textile integrated power systems. Therefore, lightweight materials of conductive coils and magnetic bodies are crucial for electromagnetic generators employed in wearable apparitions. If lightweight materials of magnets and conductive coils have been developed, electromagnetic generators and their hybrid generators will be integrated in textile to power microelectronics for wearable applications.

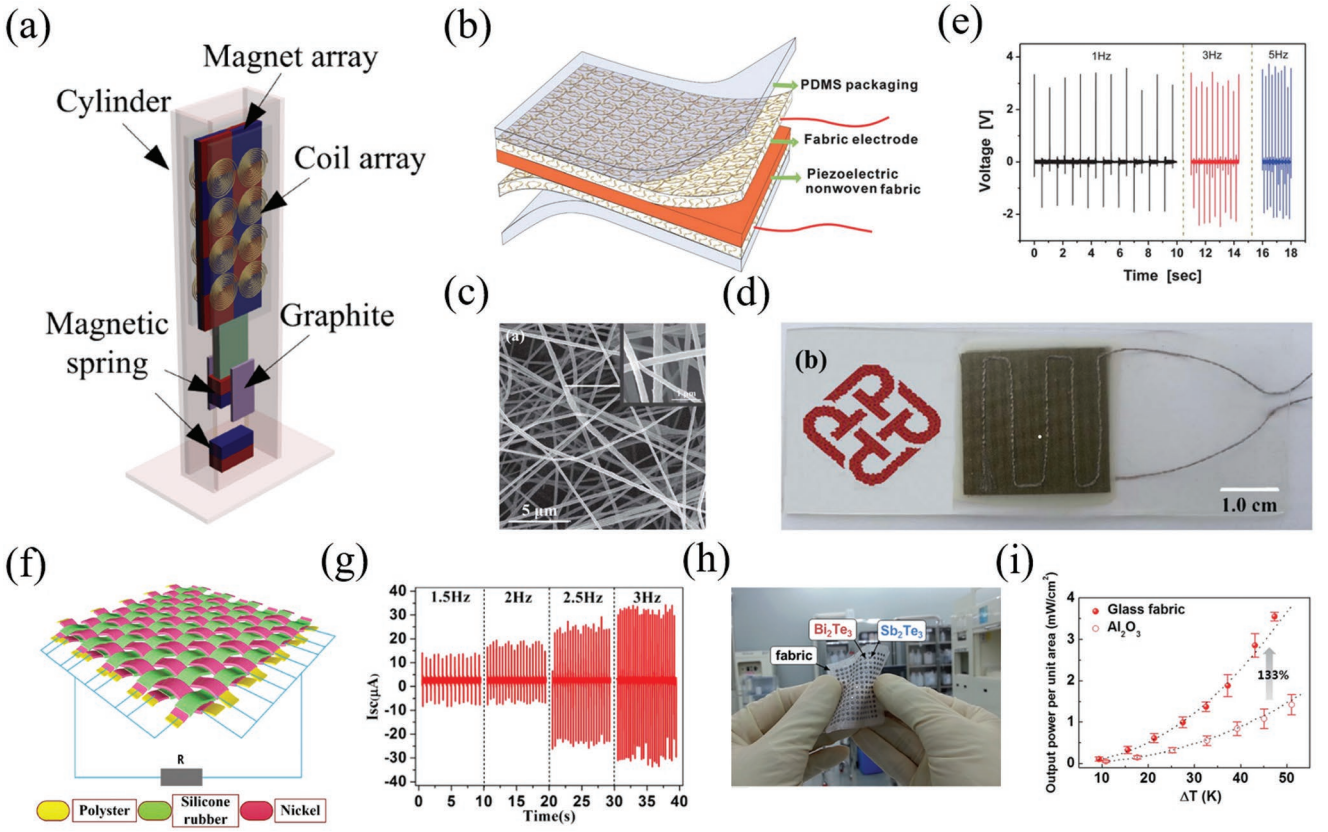

Figure 6. Fiber/textile-based energy harvester. a) Schematic of the electromagnetic energy harvesting spring. Reproduced with permission.[158b] Copyright 2014, AIP Publishing LLC. b) The schematic of a textile-based piezoelectric generator. c) The SEM image of PVDF–$NaNbO_3$ piezoelectric nanofibers. d) The photo of the piezoelectric generator. e) The performance of the piezoelectric generator. b–e) Reproduced with permission.[44] Copyright 2013, RSC. f) Schematic of a triboelectric textile. g) Short current circuit of the triboelectric textile with different frequency. Reproduced with permission.[169d] Copyright 2017, Elsevier. h) Photo of a textile-based thermoelectric generator array. i) output power per unit area for the glass fabric and Al_2O_3-based substrate-based thermoelectric generator. Reproduced with permission.[187c] Copyright 2014, RSC.

Piezoelectric Generators: Piezoelectric generators, converting mechanical energy into electrical energy through piezoelectric effect, hold great potential to power microelectronics for wearable applications. Comparing to piezoelectric generators made of uniform plane-films, textile-based or fiber-based piezoelectric generators normally have higher conversion efficiency in wearable applications, due to high piezoelectric coefficient, flexibility, and ease of stress concentration. PVDF or PVDF composites made by electrospinning technologies are mostly utilized in wearable applications due to the merits of high piezoelectric coefficient, lightweight, and low stiffness (Figure 6b–e).[44,159] "3D spacer" technology was applied in the fabrication of all-fiber piezoelectric fabrics, where the knitted single-structure piezoelectric generator consists of spacers composed of piezoelectric PVDF monofilaments (with 80% β -phase) interconnected with two silver coated polyamide multifilament yarn layers serving as the top and bottom electrodes, can provide an output power density in the range of 1.10–5.10 μW cm^{-2} at applied impact pressures in the range of 0.02–0.10 MPa, showing superior performances over the existing 2D woven and nonwoven piezoelectric textiles.[160] Besides polymer, other lead-free solid materials such as lead zirconate titanate (PZT) particles[161] and $BaTiO_3$ nanofibers,[162] also have been utilized to make flexible piezoelectric nanogenerators, where the generator with $BaTiO_3$ nanofibers aligned vertically in the PDMS matrix achieved piezoelectric energy conversion output of 0.18 μW under a low mechanical stress of 2 kPa,[162a] and the maximum energy density of PZT composites under bending was found to be 14.3 J m^{-3} on a cotton textile.[161] However, the electric output is remarkably affected by the frequency and magnitude of the exerted excitation force, specifically, the output demonstrates a linear relationship with the excitation force.[159a] Thus, textile integrated microelectronic systems by using single piezoelectric effect are normally used for sensors (shown in Section 2.1) not energy harvesters.

Triboelectric Generators: Triboelectric nanogenerators (TENGs), coupling triboelectrification and electrostatic induction, have been demonstrated to harvest mechanical energy from human activities as sustainable self-sufficient micro/nanopower sources. Such generators have been attracted extensive research efforts due to high convert coefficient, low cost, environmental friendless, universal availability, easy of fabrication and a wide range of potential applications,[163] making tremendous processes in boosting output performance,[164] theoretical models,[165] structural design[165f,166] for various of applications since the first proposed triboelectric nanogenerator

at 2012.[167] The development of TENGs based on textile platform have been reviewed recently,[168] including the basic components of fibers, yarns, fabrics made using various weaving and knitting techniques, and the possessing electrical outputs. In these cases, TENGs with various structures have been developed and integrated in textile, such as functional fiber in woven structures (Figure 6f,g),[54,166a,169] layered structures,[170] or knitted structures,[171] and fabric with nanopatterned/nanostructured surfaces,[166b,172] forming textile-based TENGs. Four working modes, including vertical contact mode, single electrode mode, lateral sliding mode and freestanding mode, have been employed in textile-based TENGs,[168a,b] where vertical contact-mode is mostly utilized in textile-based TENGs due to ease of fabrication and possessing higher outputs than others. Though the peak voltage of textile-based TENGs can be up to dozens or hundreds of volts, the generated power of textile-based TENGs has not been enough to meet the continuously consuming power of wearable electronics yet since such electrical pulses are sharp and have low frequency below 10 Hz.[168b] Besides, the study of triboelectric charge for porous and deformable fabric made from polymer fibers indicated that nominal charge density is normally lower than the effective charge density calculated by the actual contact area.[173] Because the effective contact area is smaller than the nominal area due to a structural hierarchy of fabric, though surface area can be large, making much lower outputs than expected. Moreover, the measured charge and the possessing power highly also relies on the applied pressure.[173] Thereby, structure optimization or novel design of textile-based TENGs considering the operation conditions is highly desirable for boosting the generated power.

Thermoelectric Generators: Fiber-based thermoelectric generators (FTEGs), which could harvest scavenged thermal energy from human body, have great potential in wearable applications.[174] Traditional TE materials are usually bulky, rigid and toxic. Therefore, many researchers have endeavored to develop new TE materials which are light-weight, flexible, and environmentally friendly. TE materials for FTEGs can be divided into three primary categories: organic TE materials,[175] TE composites,[176] and inorganic flexible TE materials.[177] Organic TE materials are generally conducting polymers, such as polyacetylene (PA), PEDOT, polypyrrole, polyaniline (PANI), and others.[178] Although they can fulfill the requirement of FTEGs in terms of mechanical properties, their instability in air inhibits their application.[179] TE composites commonly comprise inorganic nanomaterials dispersed in polymer matrix,[180] which combine the advantage of high electrical conductivity and the Seebeck coefficient of inorganic materials, as well as the low thermal conductivity of the polymer. Inorganic flexible TE materials, including CNTs, ceramics, and 2D materials, could be processed into freestanding thin films or deposited on flexible substrates.[181] Among them, graphene attracts much attention recently in the application of FTEGs, due to its good mechanical properties, high electrical conductivity, and high theoretic calculation result of figure-of-merit.[182] However, its low Seebeck coefficient and high thermal conductivity impede the TE application. To improve its TE performance, modification of graphene is adopted, including nanostructuring, doping, introduction of structural defects and boundaries, as well as integrating graphene into a polymer matrix, by which the thermal conductivity is reduced and Seebeck coefficient is increased. Besides, the intrinsically high electrical conductivity of graphene isn't sacrificed. The detailed information can be found in the review article.[183]

The performance of TE materials is characterized by power factor (PF) = $S^2\sigma$, where S and σ represent the Seebeck coefficient and electrical conductivity, respectively. For most TE materials, Seebeck coefficient and power factor fall into −200 to 200 μV K^{-1} and 1–1000 μW m^{-1} K^{-2}, respectively. Notably, one great breakthrough about Cu_2Se-based TE devices has been reported, whose Seebeck coefficient is over ±2 mV K^{-1} and power factor is 2.3 W m^{-1} K^{-2}, respectively.[184]

The operation temperature of wearable FTEGs is around 310 K, Bi-Te alloys are more appropriated than other inorganic TE materials, such as skutterudite compounds, half-Heusler compounds, metal silicide, and Ag-Pb-Sb-Te quaternary systems.[181] However, their application is hampered by their brittleness and high fabrication temperature.[174a] In order to apply Bi-Te alloys, researchers have tried to overcome the drawbacks in several approaches. For instance, half-ring TEGs were fabricated with Bi_2Te_3-based materials for specific tube-like heat source.[185] Although the maximum output power reached 1.62 mW at ΔT = 39 K, this device cannot deform arbitrarily. Except for the half-ring structure, helical structure has been applied to reduce the rigidity of inorganic TE materials, allowing devices to exhibit extremely high stretchability (≈100% strain).[186] A device in helical structure generated an open-circuit voltage of 8.9 mV, when worn as a bracelet at room temperature of around 16 °C.[186b] Another method to overcome the disadvantages of inorganic TE materials is to fix the bulk materials in flexible structures.[187] For example, these materials constituted a wearable device in the appearance of a watch, which can be used to some parts of human body, such as wrists and ankles.[187a] Instead of the insertion into a wristband, eight rigid p- and n-type thermocouples were inserted into glass fabric to compose a device that can apply to heat sources with arbitrary configuration (Figure 6h,i).[187c] This device performed 3.8 mW cm^{-2} and 28 mW g^{-1} at ΔT = 50 K. Besides, bulk Bi-Te thermocouples were fixed in flexible polymer.[187b] This device generated 2.28 μW cm^{-2} at a temperature difference of 0.9 K, when it was applied to an artificial arm under still air condition. Apart from the bottleneck of materials properties, the harsh processing conditions also impede the scalable production of devices based on many TE materials like rGO. In response to this issue, our group has successfully fabricated the TE device by a low-temperature and solution-based method.[182b] A wristband-type TEG was prepared by connecting seven bendable rGO-based grids electrically in series. A volunteer wore this device on the wrist at room temperature of 15 °C, which provided the maximum power of 0.88 μW by the temperature difference between human body and environment.

Except for the appropriate device structure, another method is to fabricate TE materials directly on the surface of flexible substrates.[176l–q,177h–k,188] A bendable device composed of silver chalcogenide nanoparticle films and plastic substrate generated a power density of 106 mW cm^{-2} when the hot and cold side temperature were 100 and 85 °C, respectively.[177j] Despite the outstanding performance, the work temperature was much higher than human body temperature. Additionally, researchers

used 1D and 2D substrate materials like fibers, cables, yarns and fabrics to fabricate FTEGs by printing or sputtering technology. For example, Bi_2Te_3, Sb_2Te_3, and gold (the electrode material) were sputtered on the surface of electrospun PAN nanofiber at regular intervals.[188j] And the fibers could be plain-weaved, knitted and zigzag-stitched into TE textiles. Among them, plain-weave FTEGs exhibited best performance: 0.62 W m^{-2} at ΔT = 55 K. Additionally, CNT yarns were doped with polyethylenimine and $FeCl_3$ (n- and p-type TE materials) at regular intervals.[188h] No metal electrode was used in this FTEG, which avoided the high contact resistance at the interface of CNT and metal electrodes. This was benefit from the CNT yarn having high electrical conductivity, which played the role of electrodes. This FTEGs with 60 pairs of thermocouples showed the maximum power density of 10.85 and 697 μW g^{-1} at ΔT = 5 and 40 K. BiTe-thick films could be printed on various fabrics to fabricate FTEGs.[177k] Among them, the device prepared on glass fiber fabrics exhibited the maximum power of 2.3 μW at ΔT = 20 K. But in order to make the surface of fabrics smooth, a film or waterproof layer was precoated before coating TE materials. Thus, although the flexibility of these devices satisfied the requirement, the precoated layer reduced the permeability of the fabrics.

Additionally, the first wet-spun TE fibers were recently reported, which were directly fabricated with CNT/PEDOT: PSS composite.[176r] The diameter of these TE fibers was around 500–600 μm. A simple FTEG device, which was composed of twelve p- and n-type thermocouples, was fabricated with these fibers. This device generated 0.43 μW at ΔT = 10 K. Since wet spinning is a mature method for industrial production of fibers and filaments, this work could provide a possible approach to the mass production of FTEGs. However, the mechanical properties of these TE fibers may be a crucial issue of postproduction process and application.

Currently, Bi-Te compounds are most widely used materials for FTEG devices because of their outstanding performance at near-room-temperature. However, the maximum output power of FTEGs based on Bi–Te compounds is usually 3–6 orders lower than bulk Bi–Te-based TEGs. Furthermore, the film devices usually sacrifice the permeability and cause uncomfortable feeling when they are worn on human body, which deserves further efforts for structural optimization.

Photovoltaic Cells: The utilization of solar energy has long been regarded as the ultimate solution of energy crisis. Although silicon-based photovoltaic cells have reached a photoconversion efficiency (PCE) of more than 20%,[189] their bulkiness and rigidity hinder the application in wearable devices. Therefore, fiber- and textile-based photovoltaic cells have been developed to overcome this limitation. Although the performance of fiber/textile-based photovoltaic cells has yet to catch up with rigid counterparts, they are flexible, lightweight, and have great potential for everyday harvesting of solar energy.

A fiber-based photovoltaic cell is generally constructed by a photoanode and a counter electrode. The photoanode is usually composed of a conductive fiber coated by a light sensitive layer. And the counter electrode could be another conductive layer deposited outside the photoanode (coaxial structure), or another conductive fiber interlaced with the photoanode (interlaced structure). To minimize the mechanical mismatch between metallic fiber and the photosensitive coating within the photoanode, the TiO_2/Ti system is widely adopted, which is achieved by controlled oxidation of Ti wire[190] or anodic growth of TiO_2 nanotube around the Ti wire.[191] TiO_2 is a good photosensitive material with its band gap of 3.2 eV, within the visible light range. Besides, a seamless chemical bonding between Ti and TiO_2 prevents the possibility of interfacial failure under deformation. The stretchability of the photoanode could be achieved by interwining Ti wire on a polymer fiber like a spring.[192] Although the PCE of 1.23% is not high, the as-prepared cell remains 90% of the PCE after 30% stretching for 1000 times. On the other hand, for the interlaced structure, the gap between interlaced fibers increases the internal resistance of the photovoltaic cell, which could cause the reduction of PCE. In response to this issue, counter electrode fibers based on carbon nanomaterials were developed by Peng et al.[191a,193] The high surface area facilitates both the loading of metal nanoparticles as well as renders a more intimate contact with the photoanode fiber, which dramatically reduces the internal resistance and improves the PCE. Representatively, a MWCNT sheet is half treated with oxygen plasma before rolled into a fiber, which has a hydrophobic core and a hydrophilic sheath. This heterogeneous MWCNT fiber has both high conductivity (undamaged crystalline structure of the inner core) and high loading capacity of Pt nanoparticles, which finally renders a PCE of 10%.[194] Besides, a meterscale photovoltaic textile could be prepared by weaving large amount of photoanode and counter electrode fibers by an industrial loom.[195]

Photovoltaic textiles could be prepared not only by weaving by photovoltaic fibers, but also through the deposition of functional components onto textile substrates. Since the textile surface is not as smooth as planar substrate, the energy conversion performance is usually not as good. Li et al. built a solar textile on polyester textile, with AgNW and graphene serving as the bottom electrode, poly(3-hexylthiophene-2,5-diyl): [6,6]-phenyl-C61-butyric acid methyl ester (P3HT:PCBM) as the light active layer, Al/LiF as the top electrode. The solar textile demonstrates a PCE of 2.27%, which decreases merely by 13% and 23% after curling and folding for 400 times, respectively.[196] Zhen et al. prepared the a layered structure with the light active layer (P3HT:PCBM and PSSNa) and top electrode prepared on a silicon wafer. After wet etching of the silicon wafer, the layered film could be scooped up by a conductive fabric. Compared with common deposition method like sputtering and spin coating, the scooping process ensures a conformal contact between the light active layer and the fabric substrate, thus improves the electrical conductivity and mechanical stability within the photovoltaic textile. As a result, a PCE of 2.90% was achieved, with an open-circuit voltage of 0.58 V and short-circuit current of 12.10 mA cm^{-2}, which outperformed most photovoltaic cells based on unmodified woven textile.[197]

Although the research of fiber/textile-based photovoltaic cells has met great progress, the low PCE still motivates further efforts in this field. Dye-sensitized solar cells[198] and perovskite solar cells[199] are also introduced in fiber/textile system, which benefits the improvement of PCE. While the toxicity of dyes and perovskite materials cannot be overlooked. Except for the enhancement of energy harvesting performance, the integration of photovoltaic fiber/textile with energy storage systems,[200] as

well as endowing the photovoltaic textile with improved stretchability and washability,[201] is also significant for the industrial application of fiber/textile based photovoltaic cells.

Hybrid Generators: Since a generator based on single transduction mechanism has been demonstrated to be insufficient to directly power the wearable microelectronic system due to the limitation of space and convention efficiency as well as application scenarios, hybrid generators, incorporating different transduction mechanisms, also have been attracted extensive research efforts aiming to power the wearable microelectronic systems continuously.

A hybrid generator combining triboelectric and electromagnetic transduction mechanisms has been shown as a highly efficient mechanical energy harvester,[202] where triboelectric units is in form of contact-mode or rotating-mode and electromagnetic units are made of metal coils and magnets. However, such hybrid generator has structures in block[202a,d,e,g–j] or multilayer[202b,c,f] rather than textile because heavy materials are employed.

Electrical energy generated by hybrid generators using electromagnetic and piezoelectric transducer mechanisms, are normally consisted by a piezoelectric cantilever beam and a magnet spring with coils,[203] which greatly relies on the applied force and the vibration velocity of structure. These generators are also made of heavy materials, such as magnets, coils and cantilever beams, thus there has been no such hybrid generators fabricated in textile-based yet.

A hybrid generator, incorporating triboelectric and piezoelectric effect, normally has cascaded piezoelectric and triboelectric units because of facile integration process, short vertical displacement and high energy convention.[165e,204] Among these devices, piezoelectric units were made of PVDF or PVDF composite fibers and the conductive fabric for flexible devices,[165e,204a,d,e] and triboelectric units were fabricated through contact-mode[165e,204a,c,d] or single-electrode,[204b,e] forming hybrid generators as wearable power sources. Since the generated energy from piezoelectric effect greatly relies on the applied force, while the generated energy from electrostatic induction does not, combination of piezoelectric and triboelectric units as hybrid generators can effectively enhance the convention efficiency of energy. Thus, such convention efficiency also greatly relies on the working condition and structural design.[165e,204b]

Hybrid generators, incorporating triboelectric and photovoltaic effect, have been integrated on textile.[166a,205] In these studies, textile based generators were all chosen woven structures, where solar cells fabricated from lightweight polymer fibers were then woven into,[166a,205a] or sewed into a cloth,[205b] and triboelectric units fabricated from composition or conductive fibers were then woven into[166a,205a] or padded on[205b] the clothes. Such generator can enhanced the total amount of energy outputs, such as a hybrid harvester of textile-based TENGs and solar cells with a size of 4 cm by 5 cm can have a stable average output of 0.5 milliwatt under a load resistance from 10 kΩ to 10 MΩ for a human walking,[166a] close to the consuming power of wearable electronics. However, the harvesting circuits are still based on the similar or same rectifier/load without carefully considering the different outputs generated from solar cells and triboelectric units.

Hybrid generators with over two transduction mechanisms, have also been developed, such as triboelectric-pyroelectric-piezoelectric hybrid generators.[206] With the mechanical energy harvesting efficiency of 26.2%, the hybrid generator was able to instantaneously drive an LED with long illumination time and charge a supercapacitor that has a charging rate about twice of that charged merely by a triboelectric generator.[206] Though this hybrid generator was not fabricated on textile platform, it shows lights for developing high performance textile-based harvesters by incorporating more transduction mechanisms simultaneously.

3.6. Energy Storage Devices

There are mainly two kinds of electrochemical energy storage devices, supercapacitors and batteries. Supercapacitors show the merits of high power density, fast charge-discharge rate and long cyclic stability. According to energy storage mechanism, they can be categorized into two groups: the electric double layer capacitors (EDLC), and pseudocapacitors that store energy by fast surface redox reaction occurred at the near surface of active materials. Basically, the electrode materials of EDLC are typically carbon-based ones,[207] such as activated carbon, carbon nanotube, graphene. For pseudocapacitors, the materials are mainly transition metal oxides,[208] hydroxide,[209] conducting polymers,[210] etc. Compared to supercapacitors, batteries show the advantages of high energy density, high working voltage, and low self-discharge properties. They store energy by converting the electrical energy into chemical form. Li-based batteries, including Li–ion,[211] Li–S[212] and Li–air[213] batteries, etc., have been intensely investigated in recent years. In addition, some other ones, such as Al–air,[214] Zn–air,[215] Si–O_2,[216] Ni–Zn,[217] and Zn–MnO_2[218] batteries were investigated recently. A Rageon plot (**Figure 7**) is drawn to illustrate the specific power and energy for supercapacitors,[219] Li-based batteries and Zn-based batteries. We found the supercapacitors show the highest specific power and lowest specific energy, while the Li-based batteries are just the opposite. Besides, both

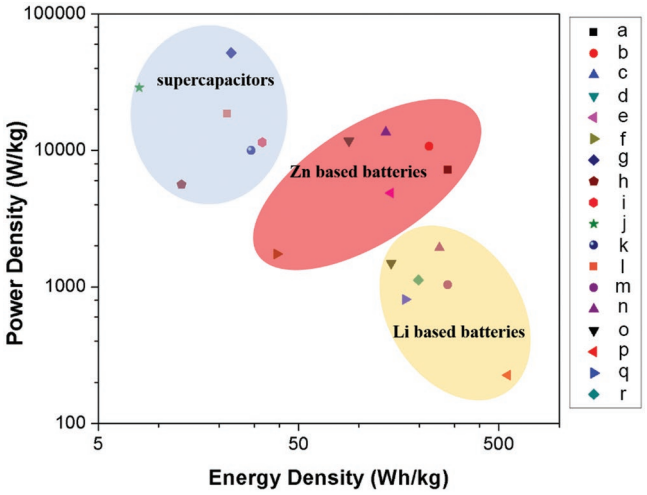

Figure 7. Specific power versus specific energy for supercapacitors and Li-based and Zn-based batteries.[219]

the specific power and specific energy are moderate for Zn-based batteries. According to the Rageon plot, a specific energy storage system could be selected based on its application scenarios.

The textile-based SC and battery are mainly composed of current collectors, electrodes, separators, and electrolyte. Based on the device configuration, they can be classified into 1D fiber/yarn structure and 2D fabric architecture. To realize the integration of these device onto textile substrate, all the components of the energy storage devices are required be mechanically flexible. In addition, conventional textile yarns, metal fiber (Ni, Pt, Au, etc.), and some fibers (CNT, graphene, polymers, etc.) developed by spinning or other techniques, are applied as substrates to fabricate energy storage device. Another route toward the conductive fiber or fabric is to metallize or carbonize conventional insulating fibers or fabrics.

1D Fiber/Yarn Shaped Configuration: For energy storage devices with 1D configuration from fiber/yarn substrates, including supercapacitors and batteries, they can be weaved or knitted into textiles through conventional bottom-up approaches. These industrially adoptable approaches render scalable manufacture of the devices and preserve good porosity of the textiles.

It is a straightforward route to place two electrodes in parallel configuration and form 1D shaped supercapacitor. For instance, Du et al. developed an ultrahigh-strength parallel supercapacitor based on ultrahigh molecular weight polyethylene (UHMWPE) fiber (**Figure 8**a).[210] To "metallize" the UHMWPE substrate (polydopamine), Ag and pseudocapacitive PEDOT:PSS layers were coated on its surface, successively. The asymmetrical supercapacitor exhibits a specific areal capacity as high as 563 mF cm^{-2} at the current density of 0.17 mA cm^{-2} (Figure 8b). For the 1D shaped supercapacitors, one basic challenge is how to avoid the short circuit between the cathode and anode. Liu et al. made an all solid-state flexible hybrid twisted fiber supercapacitor by using gel electrolyte.[220] Wet-spinning method was used to develop the pseudocapacitive V_2O_5-SWCNT cathode and EDL rGO-SWCNT anode. This device shows high specific capacity, superior rate performance and cycling stability, as well as remarkable flexibility to tolerate long-term and repeated bending. To further increase the energy density of the fiber-based supercapacitors, the volume ratio of the nonactive-material (fibers) should be reduced. To this end, Zhang et al. fabricated an ultrafast all-solid-state coaxial asymmetric fiber supercapacitors.[207b] To enhance the conductivity of the substrate, a layer of CoNi alloy was coated onto the CNT fiber. Then, the MnO_x materials doped with Au nanoparticle was coated onto the current collector as the cathode. In addition, a holey graphene paper (HGP) was used as the anode. Owing to the superior electron transport and ion shuttling performance of the electrodes, the supercapacitor delivers an excellent charge/discharge rate performance at up to 10 V s^{-1}.

Li–ion battery possesses the same architectures as the supercapacitors. For example, Feng et al. reported a flexible parallel Li–ion battery based on hybrid fiber electrode developed by

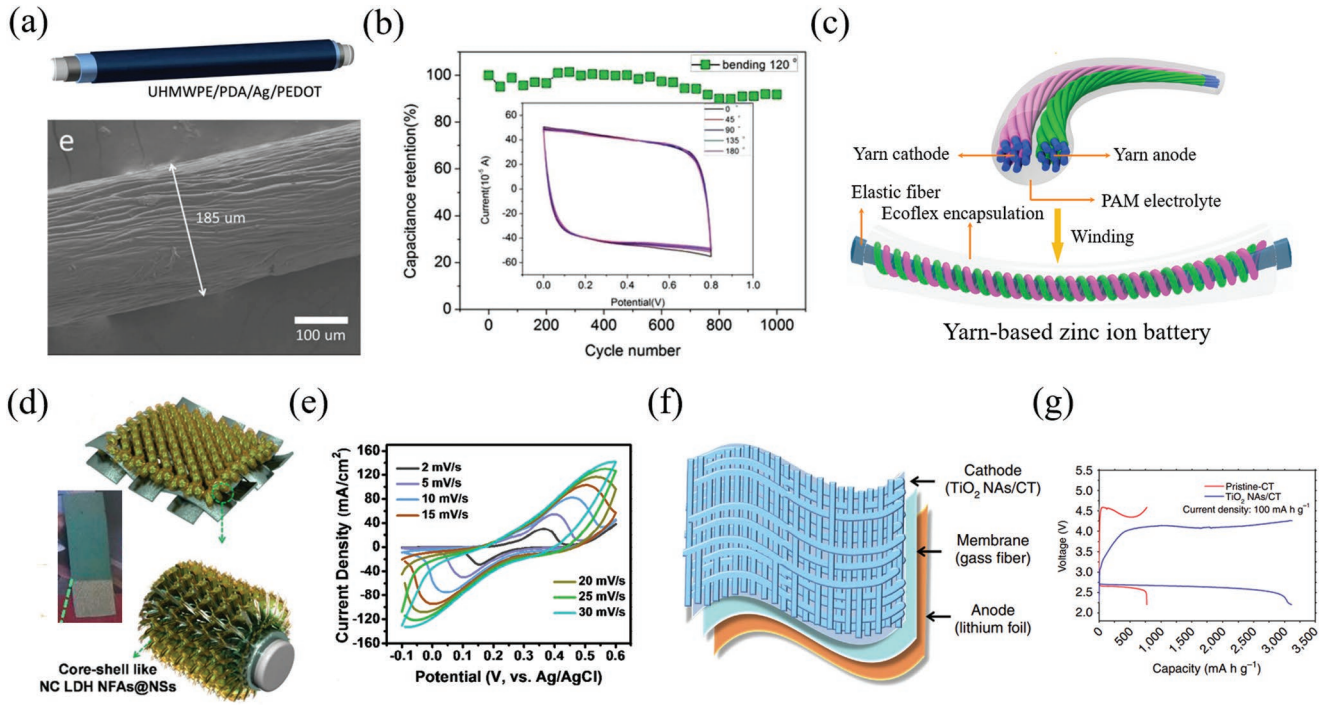

Figure 8. Fiber/textile-based energy storage devices. a) Top: schematic of a UHMWPE/PDA/Ag/PEDOT fiber capacitor. Bottom: SEM image of a UHMWPE/PDA/Ag/PEDOT fiber capacitor. b) Capacitance retention of the fiber-based capacitor during 1000 bending cycles. Inset: CV curves of the fiber-based capacitor in different bending states. Reproduced with permission.[210] Copyright 2018, WILEY-VCH. c) A schematic of a yarn-based zinc-ion battery. Reproduced with permission.[218] Copyright 2018, ACS. d) A schematic of the structure of a fabric-based supercapacitor. Inset: optical image of the supercapacitor. e) The CV curves of the supercapacitor at different scanning rates. Reproduced with permission.[209] Copyright 2017, ACS. f) Schematic of a glass-fiber-based Li–O_2 battery. g) A full-range test of the Li–O_2 battery with a pristine carbon-textile cathode and a TiO_2 nanowire array/carbon-textile cathode. Reproduced with permission.[224] Copyright 2015, Springer Nature.

wet-spinning.[211] Benefiting from the novel material-design paradigm toward fiber electrodes by assembling TiO_2 nanosheets into an ordered RGO macroscopic structure, the battery can exhibit superior electrochemical properties, including energy density, rate capability, and cyclic behaviors. Li–air battery is considered as one of the next-generation energy storage candidates with much higher energy density compared to conventional Li–ion battery. However, it suffers from many problems, including low cycle stability, capacity degradation and rigid bulk architecture that cannot meet the requirement for future flexible electronics. Peng et al. developed a new group of Li–air batteries based on Li fibers, which exhibited high discharge capacity, long cycle stability (100 cycles) and superior flexibility.[213] Other novel batteries beyond Li ones, such as Zn, Mg, Na, and K ion batteries, were also studied in the last decade. Zhi et al. designed a rechargeable parallel Zn-ion battery (ZIB) based on CNT yarn (Figure 8c).[218] The battery consists of double-helix yarn structured MnO_2 cathode, Zn anode, and cross-linked polyacrylamide (PAM) electrolyte with high ionic conductivity. This yarn ZIB delivers a high specific capacity and excellent cycling stability. Furthermore, this battery shows excellent waterproof, stretchable, and tailorable properties and superior knit-ability.

2D Fabric Configuration: For energy storage devices based on fabric substrates, they usually present a 2D configuration consisting of a pair of electrodes isolated by the separator.[221] Nagaraju et al. developed a hybrid supercapacitor using polyester fabrics with layered double hydroxide coaxial nanostructures.[209] The nonconductive fabrics was metallized by in situ electroless deposition of a layer of Ni, which was then coated with another layer of self-branched bimetallic double hydroxide electrode material (Figure 8d). The hierarchical architecture of the electrodes provides ideal pathways for ion diffusion and charge transportation. The flexible supercapacitor can deliver a high areal capacitance of 1147.23 mF cm^{-2} and an energy density of 0.392 mWh cm^{-2} (Figure 8e). In addition to the sandwiched configuration, there are also other different structural prototypes. For example, Pu and co-workers reported an in-plane supercapacitor based on common textile (polyester, nylon, etc.).[222] The interdigitated current collectors were prepared by laser-scribing and then electroless deposition of conformal Ni coatings. The resulting all-solid-state microsupercapacitors exhibited high capacitance, stable cycling performances, decent rate capability, and can be directly incorporated into a fabric garment for possible stylish designs. Furthermore, Yong et al. fabricated an all-in-one solid-state supercapacitor based on one single woven cotton textile.[223] In this work, activated carbon electrode material was spray coated onto both the upper and lower sides of the textile, leaving the middle part as the separator. This all-in-one architecture integrates all the components (including electrodes, separator, and electrolyte) into a single textile substrate, which avoids additional fabrication complexity, such as aligning and bonding in conventional sandwiched structure. In addition, the authors designed scalable fabrication processes, and used nonhazardous and cheap materials, which show great potential for practical wearable applications.

The 2D fabric batteries are investigated using the same approaches as the supercapacitors. For instance, Liu and co-workers reported a flexible $Li–O_2$ battery based on carbon textiles (CT) substrate.[224] In this work, TiO_2 nanowire array was grown onto CT as a free-standing cathode (Figure 8f), which showed excellent recoverability that can extend the battery cycle life. In addition, this battery exhibited superior electrochemical performances even under stringent bending and twisting conditions (Figure 8g). Mei et al. fabricated a hierarchical sulfur composite cathode based on carbonized textile for Li–S battery.[212] By using a facile scalable dip-coating method, the authors successfully coated carbon-based materials, sulfur and titania nanoparticles onto the carbonized textile substrate. The areal capacity of this battery could reach 5.2 mAh cm^{-2} with the sulfur loading of 7.0 mg cm^{-2}. The low cost and high electrochemical performance make it suitable for future flexible application.

This section connects the conventional textile industry with energy storage field, which further extends to the application of emerging flexible and wearable electronics. Remarkable progress has been achieved in the last decade. To cater to the next-generation wearable applications in the future, it requires to improve not only the electrochemical performance of the devices (including capacity, energy and power densities, cycle stability), but also the flexibility, durability, safety, scalability, and device integration issues.

3.7. Flexible Circuit Boards

Circuit boards provide reliable electrical connections of electronic components and mechanical support to the circuits. They have advantages because of employment of the mature packing processes and available machinery. In particular, the circuit boards should be long-lasting, comfortable and deformable in wearable applications. Thus, our review only covers fiber-based and elastomer film-based circuit boards, exclusive of directly embedding conventional electronic devices on fabric. Printing has been used in film-based circuit boards. It has a seamless integration with the existing packing processes. However, the high porosity and surface roughness of fabric require excessive amount of conductive materials to achieve high conductivity. Interlacing conductive fibers in textiles is an alternative method for making fabric circuit boards, which is discussed in Section 2.3. The properties of circuit board based on paper and PDMS are shown in **Table 2**.

A variety of additive methods like screen printing, gravure printing,[235] offset printing,[236] inkjet printing,[237] flexographic printing,[238] Aerosol jet printing,[239] evaporation or vapor deposition[225] have been explored to develop circuits boards using paper and other flexible substrates. All the fabrication methods but inkjet printing and Aerosol jet printing need attach stencil on substrates to form designed circuits. The roughness of flexible substrates affects the conductivity of fabricated circuits because some conductive materials will penetrate fabric and paper. Siegel et al. fabricated circuit boards on paper through evaporation/sputter deposition/spray-deposition with the help of stencil.[225] In this paper, an aerosol-based adhesive was used to fix stencil on paper which determine the finest wire developed having a width of 50 μm. However, the unmatched flexibility of polymer or metal stencil and fabric, paper and elastomer substrates leads to poor adhesion between stencil and substrates, further results in low resolution of circuits.

Table 2. Properties of flexible circuit board.

Substrate	Fabrication method	Conductive Material	Thickness [μm]	Width [mm]	Conductivity	Measured conductivity to initial conductivity; number of folds
Paper	Sputter[225]	Sn	1.5	0.17	0.107 Ω sq^{-1}	20%; 8
Paper	Direct writing[226]	Silver	1000	1	6.8 μΩ cm^{-1}	30%; 5
Paper	Direct writing[227]	Silver	20	0.62	16 Ω cm^{-1}	31%; 10 000
Paper	Transfer writing[228]	graphene	0.364	0.72	400 Ω sq^{-1}	83%; 1000
Paper	Transfer printing[229]	EGaIn	-	1	0.25Ω cm^{-1}	99%; 1
Paper	Mechanically sintering[230]	GaIn	40	500	1.5 Ω cm^{-1}	96%; 10 000
Paper	Stencil printing[231]	EGaIn	–	–	0.1 Ω cm^{-1}	85%; 100
PDMS	Lithography[232]	Cu wire	12	0.2	0.13 Ω cm^{-1}	92%; 50
PDMS	stencil printing[233]	Ag		0.2–2	2 Ω cm^{-1}	9–25%; > 1000
PDMS	Print[22]	Ag flakes	30	0.5	738 S cm^{-1}	25%; 100
PDMS	Lithography[234]	TiW/Au	0.25	0.1	–	99%; > 500 000

A previous review[240] covered conductive materials like PEDOT:PSS, CNTs, graphene, and metals for paper electronics. Recently, liquid metals (LM) were used to fabricate circuit on paper[229,230] due to their both superior electrical conductivity and high fluidity.[241] Guo, e.g., developed a paper-based circuit through one-step LM transfer printing method.[229] The major fabrication process of this method is as follows: First, polymethacrylates (PMA) glue was painted on a hardboard through a brush, eutectic gallium–indium (EGaIn) was brushed on the surface of PMA glue. Then, a ball-point pen prints designed pattern of PMA glue on paper. Lastly, the side of paper printed with PMA pattern was put on the surface of EGaIn on hardboard. After applying a pressure on paper and removing paper from EGaIn layer, the EGaIn circuits could be transferred on paper directly. The finest line width developed through this method will be determined by the size of pen nib.

Stretchable flexible circuits are highly desirable for electronic textiles, because they can keep the natural feeling of the fabric. PDMS is a common elastomer which has been adopted to fabricate flexible devices as it has high chemical and thermal stability as well as low elastic modulus and surface energy.[242] More importantly, it can bond with itself without any adhesive.[243] The PDMS is required to be applied on a temporary carrier such as glass and wax. The conductive layer can be printed Ag,[22] lithographed metals,[234] etched copper and laser-designed copper.[244] After the conductive tracks are developed, the carrier is usually replaced by an elastomer PDMS and transfer these conductive tracks on PDMS substrate.

Lin developed a stretchable circuit on PDMS substrate through depositing metals on it followed by lithography technique.[232] Before antisputtering applying metal on PDMS substrate, O_2 plasma surface treatment was conducted on the PDMS substrate for improving its surface energy. This paper adopted an intermittent deposition process to avoid the occurrence of cracks on copper layer, which sputtering for 1 min and cooling down for 4 min. The resistance of as-prepared metal film only rises by 7.4% under a strain of 30%. Although lithography technique could directly develop circuits on PDMS, the multisteps fabrication methods limits its application. Larmagnac et al. produced an Ag-PDMS based stretchable circuit boards on soft substrate through stencil printing and screen printing.[233] The thin copper stencil used still has the problem to attach well with PDMS substrate. As a result, although the circuit boards could survive under a tensile strain of 40%, cracks emerge after several repeated stretching cycles. For the fabrication of double-sided soft circuit boards, the top and bottom PDMS substrates were bonded together by punching holes through the substrate and filling them with Ag-PDMS paste, which endows a cyclic durability of more than 1000 cycles. Matsuhisa et al. developed a printed stretchable Ag-PDMS based conductor, and fabricated a stretchable organic transistor active matrix connecting with the developed elastic conductor on a PDMS substrate.[22] The printed conductive lines have a conductivity of 182 S cm^{-1} on PDMS substrate even when stretching up to 215% strain. The interconnections can be designed in a straight-line shape because the conductive ink is intrinsically stretchable. A stretchability gradient substrates were introduced to protect organic thin film transistor embedded on rigid polyimide island. Besides, the active matrix could be stretched to 60%. Recently, our research team adopted a multiple layered flexible glass fiber/PDMS as substrate, opened the via holes by a laser scribe technique, and demonstrated monolithically 3D integrated circuits, where all-in-one supercapacitor, resistors, lighting emitting devices, and driving circuit are integrated onto a single substrate.[245] The capacitance retention didn't demonstrate an obvious decrease after more than 12 000 charging–discharging cycles.

The unmatched modulus between PDMS and conductive materials and rigid electronic devices may result in circuits broken. Mechanical failure tests like stretching, bending and folding tests are required to be conducted.

3.8. Memory Devices

Memory is an indispensable part for storing information, which is important to the implementation of complex electronic systems.[246] Based on the basic components of functional fibers, the wearable electronic system can provide applications that

Table 3. Controllers, ADCs, wireless modules, data storage units, and batteries in representative textile-based systems.

Reference	Microcontroller	ADC	Storage/memory	Wireless module	Battery
[248]	Atmega328 processor	Atmega328 processor	Not mentioned	CC2541 BLE	3.7 V Li–Po battery
[249]	Intel Edison	Intel Edison.	Intel Edison	WiFi and Bluetooth.	3.3 V low dropout regulator (LDO)
[250]	CC2541	CC2541 (12-b ADC)	CC2541	CC2541 BLE	3.3-V low-dropout regulator (LDO) (XC6206-3.3)
[251]	MSP430F5418A (Texas Instruments Inc., Dallas, Texas, US).	12-bit ADC channels on chip	Not mentioned	Bluetooth module	170mAh Li–ion battery
[252]	MSP-430	Not mentioned	Not mentioned	Bluetooth module	Not mentioned
[253]	A field-programmable gate array (FPGA)	24-bits ADC	Not mentioned	serial ports (UART-USB)	Not mentioned
[254]	dsPIC33FJ series	multichannel ADC (dsPIC33FJ series)	Not mentioned	Bluetooth (RN-42 module)	800 mAh Li–Po battery
[255]	PIC18f1320 (Microchip Technology Inc.).	Not mentioned	Not mentioned	wireless module (XBee Pro, Digi International Inc.)	Not mentioned
[256]	ICP12-USBSTICK (ICircuit Technologies, Malaysia)	ICP12-USBSTICK	Not mentioned	Not mentioned	9 V battery
[257]	MP150 (Biopac, USA)	MP150	Acknowledge 3.8.1	Not mentioned	Not mentioned

facilitate hand-free access to computing, storage and other devices.

It has been reported that electrochemical deposition and metal coating are useful methods for constructing textile memory devices.[247] Aluminum coating cotton fiber and carbon fiber based on textiles are used to switch the resistance of the random access memory (RRAM) device. Aluminum coating and thin natural Al_2O_3 layer are formed on the cotton fiber, which can be used as a switch, and shows the bipolar resistance switching behavior. At the same time, carbon fiber is used as the electrode. Conductive atomic force microscopy (C-AFM) was carried out to reveal the resistive mechanism and it showed that the resistive switching occurred at the thin native Al_2O_3 layer between the two electrodes through the conducting points.

Logic-in-memory system on textile has been reported. Bae et al. demonstrated that the prepared logic-in-memory arrays can be used to fully realize complicated works similar to logic circuits.[169c] Realizing the logic-in-memory on fabric helps reduce power consumption and extend battery life. This platform shows advantages such as more comfortable than the conventional direct attached commercial devices system. In addition, it still has the potential of further improving the performance and reducing the manufacturing costs at the same time.

Though there are great developments in the past years, the technologies currently face enormous technical challenges such as how to remain the wearing comfort and meanwhile not lower the performances during the manufacturing process.

4. STIMES Architecture and System Integration

The construction of an independent textile-based electronic system must integrate rigid microelectronic components, such as those transmit and process the data for the analysis, display and feedback of the input signal.

4.1. Controller, ADC, and Wireless Module

In order for the conversion from the obtained data to a practical output, the textile-based systems always consist of a data processing system, which contains calculating devices (described in Section 4.2) and controllers. Besides, analog/digital converters (ADC) are needed to bridge the front-end measurement and processors. Wireless communication module is also an important component in e-textile system, by which the output in e-textile systems could be displayed on a friendly user interface, such as the screen of smartphones and computers. Mostly, the controllers, ADC and wireless module in textile-based systems are commercially available products, which are selected based on their performance, size, energy consumption, as well as the compatibility with the IoT modules. Herein, we made a table (**Table 3**) which lists the types of controllers, ADCs, wireless modules, as well as data storage units and batteries in representative textile-based systems, which we believe could provide some guidance in the selection of these components for future design of textile-based systems.

4.2. Computing Devices

Computing units are central devices for processing signals, which is also an essential part in building an entire textile-based functional system. Conventional computing devices are usually manufactured by complementary metal-oxide-semiconductor (CMOS) processing technologies on Si wafer, which are mechanically rigid, brittle, and planar, and are incompatible with the textile processing. It has been a great challenge to construct wearable computing system over a long term.[45,258] Hence, at present, there are mainly two types of routes: directly attaching rigid computing devices onto textiles and functionalizing fibers for the logic devices. At the early stage, most works focus on directly integrating commercial computing components onto fabric, where the computing functions are usually

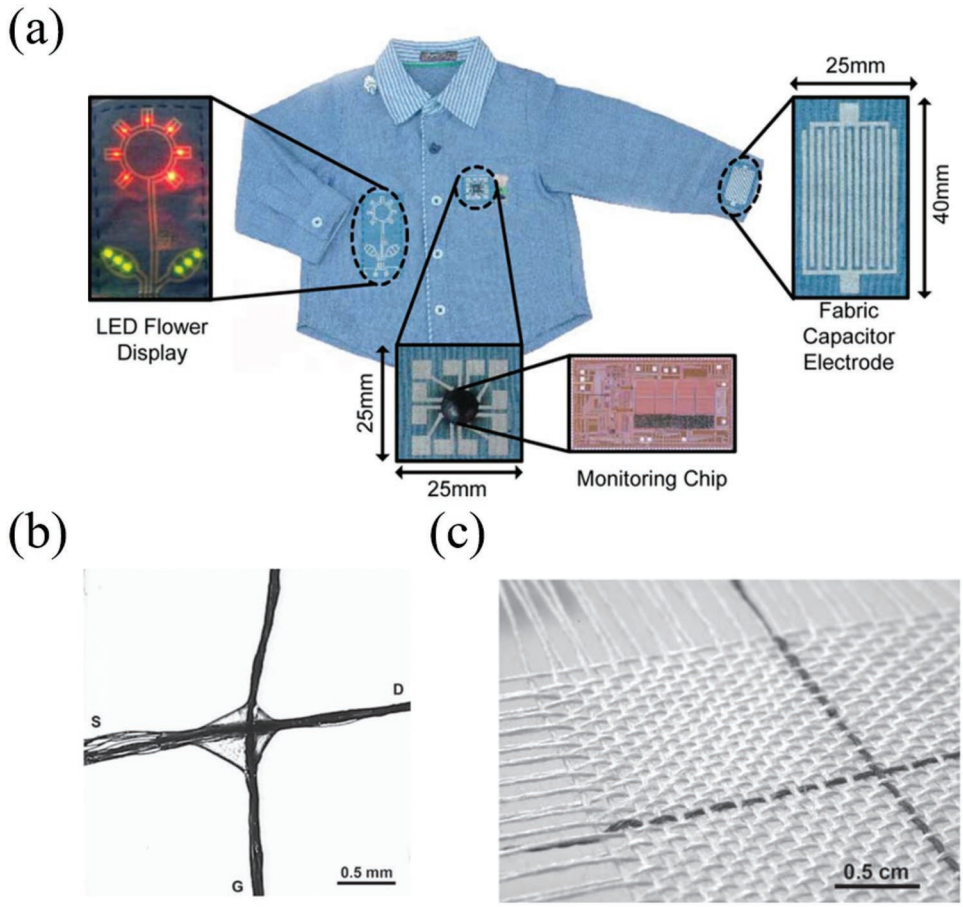

Figure 9. Textile-based computing system. a) Rigid devices integrated directly on clothes. Reproduced with permission.[258d] Copyright 2010, IEEE. b) Silk-fiber-based electrochemical transistor. c) The silk-fiber-based electrochemical transistor woven into a basket-weave fabric. Reproduced with permission.[260c] Copyright 2017, WILEY-VCH.

achieved through traditional CMOS based chips. Recently, functionalized fibers for computing are investigated progressively, including traditional field effect transistors (FETs) and electrochemical transistor (ECTs). Most works focus on the integration of the fabric transistors into the yarn's structure, retaining mechanical properties of textile and showing good performances.

Attached Rigid Computing Components on Textile: There have been many works focusing on attaching commercial computing components on textile fibers.[258d] As a simple example, Kim et al. demonstrated that discrete electronic devices including the controlling chips can be integrated for a complete system for continuous healthcare.[259] The method of manufacturing flexible circuit relies on a standard printed circuit board to temporarily reinforce the process on the flexible substrate. In contrast, the loose nature of textiles brings about difficulty of integrating a few discrete components together. To make such circuits more wearable, the design and integration are important. First, the circuit can be divided into different functional parts to avoid large mechanical stiffness in specific field of the cloth, which can help protect the devices. Second, the proper integration technique can make the textile circuits crumple nondestructively as textile would do. Direct integration of devices outside the textile is shown in **Figure 9**a.[258d] Traditional Si-based computing units ensure the high computing performance. Thus, attaching computing components on textile is a promising way though there are still many drawbacks such as wearing is not comfortable and such integrated clothes cannot be generally washed.

Functionalized Fibers for Computing Device: An alternative way to construct wearable computing units is to functionalize the textile fiber to create electronic circuits, rather than attaching computing components directly to cloth (Figure 8b).[260] Monolithic integration is of the great importance in the advanced integrated computing chips and textiles, which reduces the amount of manufacturing step and improves convenience and comfort. Recently, researchers fabricated electronic devices onto the yarn to maintain mechanical properties and electronic performance. With a few centimeters of bending radius, the fiber can withstand a bending radius of less than 1 mm and a large tensile strain. Transistors are the building blocks of electronic components in the field of textile electronics to obtain computing power for fabrics.[25,258c,261] Among the various available transistors, two monolithic integrated e-textiles have been studied[262]: organic FETs and organic ECTs. Different from the silicon-based devices, organic materials are used as active

transistor channels, providing superior mechanical properties as well as the ability to print directly onto textiles.

4.3. Connection of Heterogeneous Electronic Components

Soldering has been used to connect electronic components. Solder materials that have metallic properties and are resistant to high temperatures of soldering process can be used in this connection method. Buechley et al. tried to create solder joints as connectors on a metallic fabric circuit. In following step, IC sockets or controllers were soldering on developed connectors.[263] However, few fiber- and fabric-based conductive materials could withstand high temperature about 280 °C, which is the lowest melting temperature of soldering.[264] Low temperature solders can decrease bonding temperature significantly and increase flexibility and component reliability.[265] While one single alloy is not a universal solution. Specific electronic components and the properties of fiber-based circuit have to be considered when selecting the best solder alloy. Molla et al. measured the failure types of low-melt solder joints which are the connections between LED packages and the stitched traces on fabric substrate.[266] In this research, they also found that the biggest electronic components have the strongest durability at tumble tests by a slim margin. Out of the total chips testes for different size, the failure rate of 5 mm LED chips was about 21% (63 out of 300), whereas the values of 3 mm and 2 mm LED chips were 21.33% (64 out of 300) and 44% (88 out of 200), respectively. Further, they demonstrated that the wider trace has stronger connection, and the sources of failure include connection between solder joints and the LED chips, connection between solder joints and the threads, connection within the solder joints and connection within the LED package. For integration microelectronics in textile adopting soldering technology, there is still a challenge because the connectors area of miniature chips is very small, for a surface mount LED the solderable area is about 0.05×0.35 mm^2.

Mechanical Gripping: In electronic wearable systems, soldering technology is limited by high solder melting temperature and solder joints interface failure. In conditions where rigid connectors like poppers, standard snap fasteners and electronic module are integrated onto textile, mechanical gripping can be applied to make electronic connections between conductive textile and the rigid connectors or the metallic wires of circuits.[267] Leśnikowski integrated rigid poppers on fabric as electronic connectors to create connection between different textile signal lines.[267b] Li and Tao explored unique structure to wrap the conductive track around a stainless-steel needle with the diameter about 1 mm for forming a circular helix and achieve a helical connection between knitted interconnect and wire.[268] In this paper, the diameter of enameled copper wire is about 50 μm which makes it weak and brittle, thus silver coated nylon yarn was knotted around it to create connection. The flexible properties of this connection enable its stable when the fabricated fabrics were stretched along axial directions. Mechanical gripping could be applied to develop electronic connection for almost all the conductive textile. The main drawback is that the rigid connection cannot keep stability and may break under big deformation.

Conductive Adhesives: Conductive adhesives composing of metal or conductive particles and a polymer adhesive can be adopted to connect electric devices with FCB.[269] Siegel et al. applied a commercially conductive adhesive on the metallic wires on fiber-based substrate using a syringed needle, and bonded electronic devices to the metallic pathways through pressing the electrodes of the electronic devices on the adhesive.[225] The conductive adhesive cured in 15 min at low temperature (65 °C). The main advantage of using conductive adhesive to form electrical connections is its simple fabrication process. While the electrical connection quality of conductive adhesive will be affected by humidity and temperature.[270] Thus, a suitable encapsulation layer is required. Siegel et al. applied a layer of acrylic or a PDMS insulator on the surface of paper-based circuits embedding with electronic chips to achieve electrically insulted properties and water resistance.[225] Kallmayer et al. developed encapsulation layers to incorporate two layers of fabrics, electronic chips and adhesive in a cell.[271]

Traditional epoxy adhesive has high elastic moduli which limited their application in large deformable connectors. Li et al. developed a highly stretchable electrically conductive adhesive by mixing PDMS and silver flakes.[272] The silicone-based adhesive has much less curing shrinkage compared with epoxy-based adhesive. Through adjusting curing process, the optimization of electrical conductivity could be achieved.

Flip Chip Technology: Flip chip bonding could be used to sit unpacked bare die onto a flexible circuit to increase flexibility and reduce volume.[273] Choi and Oh fabricated a Si chip with the help of photoresist patterning, at the same time the Cu lead frame was transferred to a heat-resistant fabric substrate.[274] Then, a commercial anisotropic conductive adhesive was dispensed to the Cu/Sn bumps on the Si chip. Finally, a flip chip bonder was used to bond Cu/Sn bumps to the Cu lead frame on fabric substrate at 160 °C and 100 MPa about 1 min. The total contact resistance of flip chip joints is about 10 mΩ. The performance characteristics such as durability and shear strength of joints are found to strongly depend on the configuration of substrates and bonding materials.[275] Further, Li and his coauthors tried to package silicon die on thin flexible circuits using flip chip technology, and then integrated circuits within yarns for protecting die.[276] Theoretical simulations and experimental analysis of electronic packaging method were reported for minimizing stress of packaged adhesive layer for electronic textiles. The resultant flip chip assemblies are much smaller than traditional carrier-based system. The lack of wires greatly decreases inductance, enabling higher-speed signals as well as better heat conducting. The miniature flip chip assembly allows the integration of chips in textiles, yarns even in the fiber. The different kinds of connection types and methods have been listed in **Table 4** to demonstrate their properties.

5. Wearable Applications of STIMES

5.1. For Human Beings

With sensing units, effectors, as well as data transmission and processing systems combined together, textile-based smart systems could be integrated. In this section, examples of smart

Table 4. Properties of connection types and methods.

Connection type	Method	Structure	Advantages	Disadvantages
Fiber to fiber	Mechanical gripping[268]	Knotted conductive yarn around metal fiber on sensor;	Simple; Flexible connection	Required a conductive fiber on sensor
Fiber to chips	Mechanical gripping[263]	Twisted leads of through-hole LEDs to create LEDs with looped leads;	Simple; Flexible connection	Poor durability
	Soldering[266]	Attached LEDs to trace through solder paste;	Simple	Poor connection quality; Required heat resistance substrate
Chips to board	Flip chip[273b,274]	Connected Si chip to Cu lead frame;	Low contact resistances of flip-chip joints	Poor durability
	Flip chip[276b,a]	Connected die to substrate;	High reliability; Low stress of resultant assembly circuit; Smaller electronic package	Difficulty to replace and manually install
	Mechanical gripping[263]	Stitched socket which used to hold the microcontroller on fabric	Required only IC sockets and conductive thread of socket button technique	Poor durability
	Soldering[263]	Solder IC sockets and controllers to trace on fabric	High conductivity; Robust physical connection	Required substrate withstanding high temperature; Rigid connection
	Conductive adhesive[225]	Bonded chips to metallic trace through conductive adhesive	High conductivity; Strong connection	Can be damaged by humidity and temperature

textile-based systems will be introduced, which are mostly human health-oriented. The smart textile-based systems could work independently and provide feedbacks or displays within the system, which shows great promise in developing home-use products.

Real-time respiration monitoring could not only facilitate the diagnosis and recovery of respiratory diseases, but also provide an in-time warning of a sudden deterioration for unconscious patients. Min and coworkers developed a respiration measurement system based on a textile-integrated capacitive device at the abdomen.[277] A single respiration process could reduce the distance between plates in the capacitive device, by which an analog signal was generated. The analog signal could be then transformed into a digital signal by an MP150 ADC, and counted by a data storage system. In this way the respiration rates could be determined.

Sleep quality is closely related to both physical and mental health of a human being. Samy and coworkers prepared a bed sheet in which a pressure sensing array was embedded (**Figure 10**a).[278] The sleep stages of a patient could be

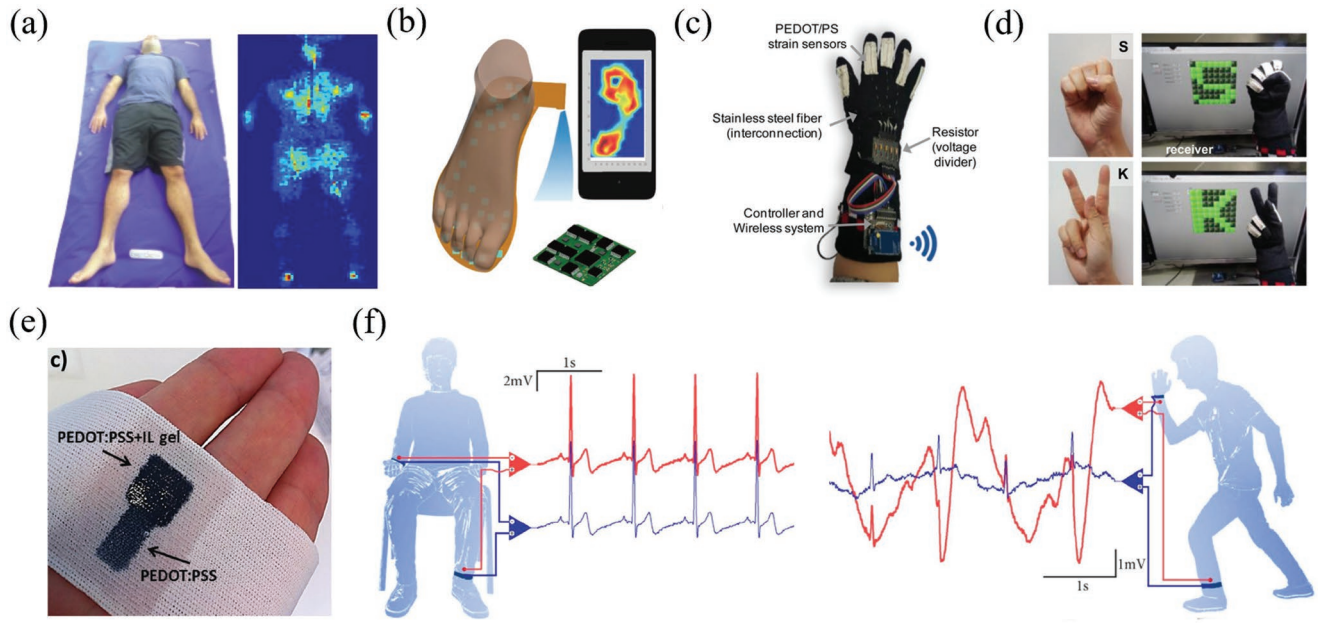

Figure 10. STIMES applied to human beings. a) A smart bed sheet for pressure mapping during sleep. Reproduced with permission.[278] Copyright 2014, IEEE. b) A smart insole integrated with a pressure sensor array for gait analysis. Reproduced with permission.[279a] Copyright 2018, WILEY-VCH Verlag GmbH & Co. KGaA, Weinheim. c) A smart glove with strain sensors, interconnections, resistors, controllers, and a wireless communication system. d) Application of the smart glove for interpreting sign languages. Reproduced with permission.[255] Copyright 2017, ACS. e) Photograph of a textile wristband with a PEDOT:PSS electrode. f) The recorded ECG patterns during resting (left) and exercise (right) of the tester. Reproduced with permission.[280b] Copyright 2015, Springer Nature.

identified. Precision rate of more than 70% was achieved after a complex calculation from both respiration and leg movement data, which could be extracted from pressure mapping results (Figure 10a). Furthermore, the system provides unprecedented unobstructiveness and comfort compared to traditional sleep tracking methodologies.

Gait patterns reflect much of age, injuries, as well as many locomotive and neural diseases. Much efforts have been devoted in a scalable gait analysis. Customized smart insoles could be developed (Figure 10b),[249,279] which obtains gait information from the embedded pressure sensing array, followed by data processing and a wireless data transfer to external display systems. Through the comparison with stored reference data, the gait patterns of the insole wearer could be determined.

Compared with step counters in commercial wristbands and smart watches, textile-based motion sensing systems could map the pressures of the muscles, which could reveal more detailed information of the motion. Besides, with the help of processing units and big data, the textile-based motion sensing systems could even give some analysis and feedbacks about the motions, which benefits the clinical diagnosis and treatment of neurological disorders, such as Parkinson's disease, muscle rigidity and stroke. Zhou and co-authors developed a smart sport band with an 8×16 pressure sensing array which could monitor the shank muscle during daily exercise.[254] The system could not only recognize the type of a sport activity, but also perform the quality evaluation in exercise. Ishac and coworkers developed a smart cushion which could classify the sitting postures based on the pressure mapping of dorsal muscles.[248] 11 postures could be identified with an accuracy of 98.1%, which could promote an upright sitting posture and avoid slouching for the sitting person. Eom and coworkers fabricated a smart glove (Figure 10c), which could interpret sign language from the strain sensors of each finger (Figure 10d).[255] Dong et al. developed a training system for golf striking movement with a triboelectric pressure sensor, through the comparison of the electrical signals with a standard striking.[60a]

Embedded sensors enable electronic textiles to be capable for health monitoring of human beings. Cardiovascular diseases have long been the first cause of death around the world. Tracking the electrocardiogram (ECG) of human beings could provide not only an alert of acute cardiovascular malfunctions, but much information about physical conditions from the ECG waveforms. In e-textile based ECG monitoring system, the working and reference electrodes fabricated on textiles could be separately contacted to the two upper limbs of the wearer (Figure 10e), which could provide ECG recording with high signal-to-noise ratio and long term stability (Figure 10f).[7,280] On the other hand, many ultrasensitive e-textile based mechanical sensors enable the recording of wrist pulses,[51,270] by which the indicators of age, gender as well as some diseases, such as hypertension, could be reflected.

Since e-textiles could contact directly to the wearers' skin, textile based chemical sensors also have the intrinsic advantage for analyzing the sweat chemistries, which provides significant indication in determining the metabolic disorders. Jeerapan et al. embedded a self-powered sensor into a sock for wirelessly detecting the lactate in sweat. Notably, a rise in lactate concentration is observed when the wearer started cycling exercise.[21] In the work by Parrilla et al. A printed circuit on fabric could be modified to selectively bond the sodium and potassium ions, which could determine the concentration of the ions for further investigation of the dehydration status of the wearers.[20a] Wang et al. weaved together Na^+, K^+, Ca^{2+}, pH and glucose sensing fiber into a single textile, which renders a more comprehensive analysis of the sweat metabolities.[71] Except for sweat analysis, the respiration process could also be monitored in terms of frequency, as well as the humidity and chemical components of the exhaled air by e-textile based masks,[282] which is significant for analyzing respiratory disorders.

Many e-textile based actuators are designed for building an active feedback system. Electromechanical mechanism is the most widely principle in designing the actuators. Chen et al. fabricated an artificial wing by attaching a highly twisted MWCNT fiber onto a paper piece, which could simulate the flapping process of birds when electrical current is passed.[283] Maziz et al. fabricated textile-based actuators by weaving or knitting the PPy coated cellulose yarns. The as-prepared actuators demonstrated the capability to move a LEGO lever arm, which have great promise in assistive movements.[284] Han et al. prepared a electrospun PEDOT:PSS/MWCNT coated carbon fiber mat which could bend upon multiple external stimulus, including humidity increase, light exposure, and electrical heating.[285] Up to now, the mechanical outputs of state-of-art textile-based actuators are far from enough for practical behavioral rehabilitation process, which necessitate further innovation in materials and structural layouts.

5.2. For Nonhuman Applications

Although most e-textile applications are human-oriented, there are still attempts for broadening the application of e-textiles in nonhuman scenarios. Similar to the health monitoring application for human beings, the behavioral characteristics of animals could also be monitored with e-textiles. In practice, sensors were usually embedded in collars worn by investigated animals (**Figure 11**a).[286] In this way, the daily activities could be real-time monitored by the culturists (Figure 11b). GPS devices could also be embedded in e-collars to provide the positional information of animals, which greatly facilitate the management in large-scale stock farming.

Textiles are traditionally applied as structural materials for architectures, such as tents and Yurt. In recent decades, electrical components are introduced into the structural fabrics to enable a variety of functions. For illuminating the spaces within the building, light emitting diodes could be embedded into the textiles. Directly mounting optical fibers into the structural textiles is also an interesting approach in controlled illumination and color changing, which could have dramatic aesthetic significance in architecture design. Photovoltaic and piezoelectric textiles could also be introduced in buildings, which could utilize the solar and wind energy to provide power for the indoor electrical devices, without needing the external electrical power supply.

Structural health monitoring is a concerned issue all around the world. The catastrophic failure of architectures usually originates from small cracks, which should be real-time monitored.

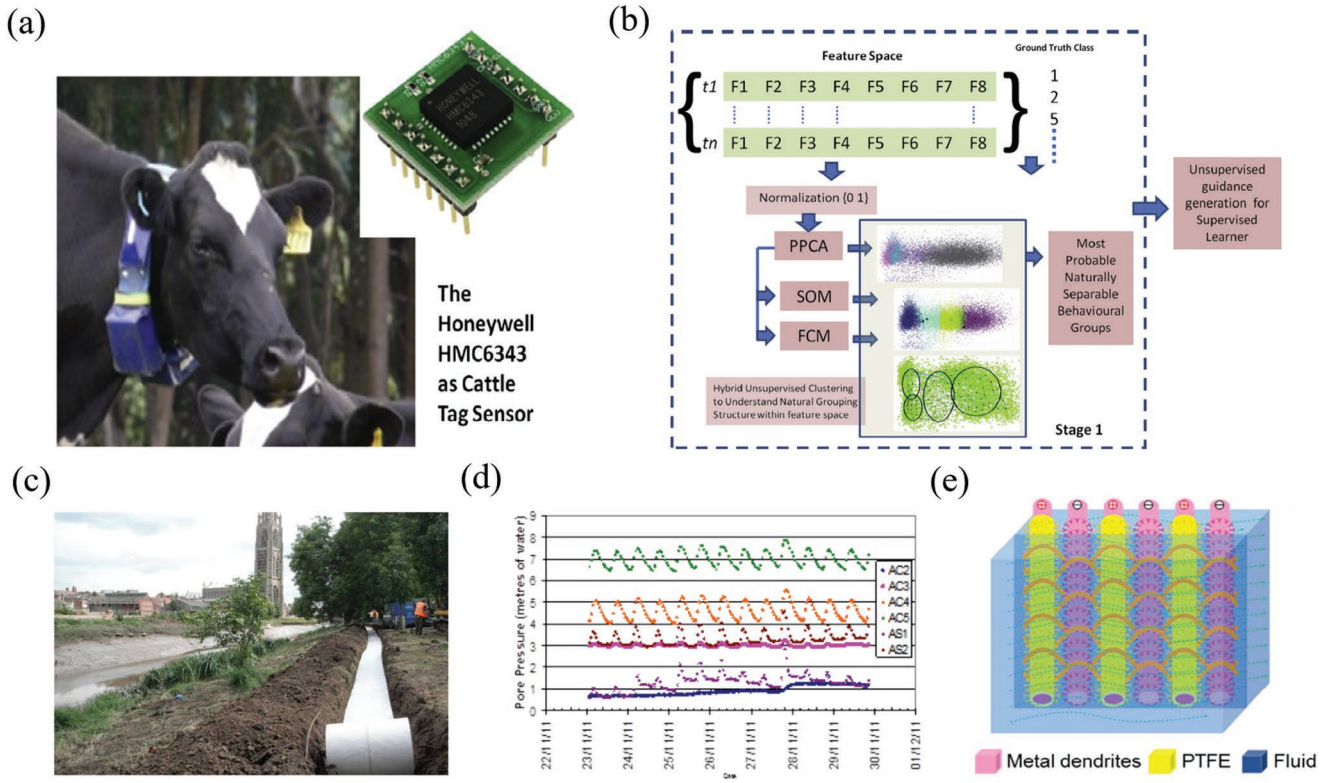

Figure 11. Nonhuman applications of STIMES. a) collar sensor system worn on a cow. b) A procedure for the behavioral analysis of a cattle using collar sensor system. Reproduced with permission.[286a] Copyright 2015, Elsevier. c) A photo of a piezometer-integrated geo-textile embedded underground. d) piezometer response over a week. Reproduced with permission.[287b] Copyright 2013, Taylor & Francis. e) A schematic of a sensor textile in fluid. Reproduced with permission.[290] Copyright 2018, ACS.

Geotextiles, which could be applied for liquid-solid separation and structural reinforcement, have been recently integrated with various sensors for the detection of cracks. Dams play an important role in protecting people and properties from bloods, which are also vulnerable from the mechanical hitting and chemical corrosion of the water. Several attempts using sensor-embedded geotextiles for the monitoring of dams have been reported. Strain and pressure sensor arrays could directly detect local stress concentration and displacement within the dam, which are most widely adopted (Figure 11c,d).[286] Besides, embedded temperature sensors could provide additional information about cracks through capturing the temperature drop by water infusion into the dam.[287] Chemical sensors monitoring the pH could also be introduced in geotextile systems, which could warn the initiation of dam corrosion. Sensor-embedded geotextiles for road and railway monitoring have also been reported.[289]

The usage of e-textiles could also facilitate the pipeline transportation process. Zhang et al. embedded polytetrafluoroethylene (PTFE) coated metal dendrites into a cotton textile. The flowing of fluids nearby the textile could induce charge generation at the liquid/solid interface (Figure 11e). The induced voltage was influenced by the velocity, acceleration, as well as the chemistry of the flowing liquid, which enabled the textile to be applied for the monitoring of the pipeline leakage and blockage.[290] Ainda et al. integrated an e-textile "valve" into a paper-based microfluidic system. At the resting stage, the hydrophobic e-textile precluded the passing of liquids through the microfluidic system. When a voltage of 100–1000 volts was applied, a quick transition from hydrophobicity to hydrophilicity occurs for the e-textile, which turned on the valve and allowed the liquid to penetrate the microfluidic system.[291] Since textiles are flexible, air/water permeable and biocompatible substrates, future progress is envisaged for a wider application of e-textiles in Internet of Things (IoT).

6. Safety and Security of STIMES

6.1. Safety

With the development of e-textiles, the safety issue has been increasingly concerned, especially for their application in daily use. The safety concern of e-textiles mainly lies in the following aspects. First, the electrical components of e-textiles are mostly nanomaterials, which usually require a comprehensive assessment of their effect on the human body and environment. For example, CNTs could be internalized into the cell, which increase the residue oxidative stress of the cell, cause inflammation and granuloma, and finally lead to cell apoptosis.[292] Graphene oxide platelets could aggregate at the lungs after intravenous injection and induce pulmonary thromboembolism.[293] Second, for energy conversion and storage, electrolyte is often introduced in e-textile system. The organometallic

compound in the electrolyte could cause harm to the wearers if the electrolyte is leaked. Third, the electrical leakage should be considered, since the salient sweat could erode the protection coating layer and let the skin directly contact the electrical components of the e-textile. Fourth, the ohmic heating during the operation of e-textiles could cause the scald of the skin, especially for the use of infants. Last but not least, the dyes used in traditional textile industry, which cause severe water and air pollution, could also lead to environmental problems in e-textile production. All these issues should be considered and minimized in the mass production and application of e-textiles.

6.2. Security

Wearable devices embedded with sensors could collect, process, and transfer the information of the users. More and more researchers focused on the security and privacy concerns of these wearable technologies.[294]

Privacy and Security Risks of Data: From the perspective of data analysts, the sensitivity and the importance of wearable devices makes them face a variety of privacy and security threats. The collected information can be physiological data, environment data and living habits. The leakage of these information may lead to harmful usage, fraud and a series of social problems.

Different data source faces different privacy and security risks. Physiological data may face the leakage of health data. The attacker can analyze the target user's heart rate, blood sugar, ECG, electroencephalogram (EEG) and other health related data. The leaked health information may lead to discriminations against the users. The physical data like user trajectory may be tracked by attacker and which is very harmful to subjects. Environment and navigation data will be illegally used to analyze group privacy information. The user interactive data mainly embodies the characteristics of input data which will be peeped, eavesdropped, etc. Attacker can illegally acquire target text generated by users through touch screen, keyboard, microphone and camera. The data source in device mainly includes application logs, communication logs and users which may suffer from IP information leakage, user identity attack.

Protection Technique in Wearable Devices: Wearable devices and some third-party smart devices cannot store the massive sensor data collected in real time, also they cannot be used to run computer task requiring high energy consumption. Cloud computing technology that can greatly facilitate the computational tasks of wearable device. To enhance the privacy protection quality of wearable applications, researches on cloud-assisted secure protocols mechanism are emerging.[295] Shen et al. developed a cloud-aided wireless body area networks (WBANs), wearable device which can provide stronger security protection for private information compared with existing scheme.[296] The proposed protocol ensure that user's real identity cannot be achieved by anyone except for the people who registers in advance. They also conducted the security analysis experiment of designed protocol and demonstrated the security proof according to the developed security model. Besides secure protocols, hardware-based protection have also been developed by researchers and industry. ARM TrustZone is an industry millstone in offering a foundation of trust for various applications,[297] like secure payment, enterprise and web-based services and digital rights management (DRM). TrustZone technology enables a designer who can perform specific functions in a security environment. Intel presented the concept of enclaves which consists of software code, data and a stack which are protected by hardware enforced access control policies.[298] Recently, Mohanty proposed a hardware system for a secure digital camera integrated with secure better portable graphics (SBPG) compression algorithm.[298b] The presented SBPG architecture provides two layers of protection containing concurrent encryption and watermarking, which can solve all issues related security, privacy and DRM in the smart healthcare of the IoT.

Security and privacy protection are key issues in wearable devices applications because they have volume big data related with health, location and context information. Technical hacking and social engineering security threats are the main types of security attack. Just using hardware and software is impossible to eliminate attack. Future work should focus on not only developing security information on the technique side, but also exploring efficient security mechanisms to protect data of wearable devices from social engineering attacks.

7. Conclusions

In this article, we have reviewed the recent developments of smart textile integrated microelectronic systems for wearable applications. It is evident that there has been a rapid increase in research activities and published work around the world. Many promising applications in health, IoT, smart city, robotics, etc., have explored and demonstrated. This article covers several main aspects of STIMES: the functional materials, three major fabrication processes of smart textile components, functional devices, system architectures and heterogeneous integration, wearable applications in human-related and nonhuman categories, as well as safety and security of STIMES. In particular, major types of textile integrated nonconventional functional devices are discussed in detail. They are mechanical, chemical and environmental sensors; shape actuators based on electrochemical, thermomechanical and other mechanisms, displays from additive and subtractive processes, antennas, mechanical, thermal, radiative energy harvesters and their hybrids, energy storage devices like battery and supercapacitors, circuit boards, and memory devices. An important aspect, that is, safety and security of STIMES, has been added for the first time. The wearable applications of STIMES have shown great promises in health, sports, protection and other related fields.

Acknowledgements

J.D.S. and S.L. contributed equally to this work. This work was supported by Ministry of Science and Technology of the People's Republic of China, National Key R&D Program of China (No. 2018YFC2000900) and Research Grants Council, Hong Kong (Grant Nos. 15215214E, 15204715E, 1521016E, and 15200917E). The authors thank Dr. Wei Zeng for helpful discussions. The authors also thank Xujiao Ding for drawing Figure 1.

Conflict of Interest

The authors declare no conflict of interest.

Keywords

actuators, energy harvesting, sensors, smart textiles, wearable electronics

Received: March 28, 2019
Revised: May 2, 2019
Published online: July 5, 2019

[1] X. Tao, *Smart Fibers, Fabrics and Clothing: Fundamentals and Applications*, Woodhead Publishing, Cambridge, UK **2001**.
[2] X. Tao, *Handbook of Smart Textiles*, Springer, Singapore **2015**.
[3] a) C. G. Núñez, L. Manjakkal, R. Dahiya, *npj Flexible Electron.* **2019**, *3*, 1; b) D. Son, J. Kang, O. Vardoulis, Y. Kim, N. Matsuhisa, J. Y. Oh, J. W. To, J. Mun, T. Katsumata, Y. Liu, A. F. McGuire, M. Krason, F. Molina-Lopez, J. Ham, U. Craft, Y. Lee, Y. Yun, J. B.-H Tok, Z. Bao, *Nat. Nanotechnol.* **2018**, *13*, 1057; c) Z. Zou, C. Zhu, Y. Li, X. Lei, W. Zhang, J. Xiao, *Sci. Adv.* **2018**, *4*, eaaq0508.
[4] W. Zeng, L. Shu, Q. Li, S. Chen, F. Wang, X. Tao, *Adv. Mater.* **2014**, *26*, 5310.
[5] W. S. Hummers Jr., R. E. Offeman, *J. Am. Chem. Soc.* **1958**, *80*, 1339.
[6] a) X. Li, T. Hua, B. Xu, *Carbon* **2017**, *118*, 686; b) Y. J. Yun, W. G. Hong, N.-J. Choi, B. H. Kim, Y. Jun, H.-K. Lee, *Sci. Rep.* **2015**, *5*, 10904.
[7] N. Karim, S. Afroj, A. Malandraki, S. Butterworth, C. Beach, M. Rigout, K. S. Novoselov, A. J. Casson, S. G. Yeates, *J. Mater. Chem. C* **2017**, *5*, 11640.
[8] a) Y. Li, Y. Li, M. Su, W. Li, Y. Li, H. Li, X. Qian, X. Zhang, F. Li, Y. Song, *Adv. Electron. Mater.* **2017**, *3*, 1700253; b) M. Park, J. Im, M. Shin, Y. Min, J. Park, H. Cho, S. Park, M.-B. Shim, S. Jeon, D.-Y. Chung, J. Bae, J. Park, U. Jeong, K. Kim, *Nat. Nanotechnol.* **2012**, *7*, 803; c) J. Lee, H. Kwon, J. Seo, S. Shin, J. H. Koo, C. Pang, S. Son, J. H. Kim, Y. H. Jang, D. E. Kim, T. Lee, *Adv. Mater.* **2015**, *27*, 2433.
[9] a) Z. Wang, Y. Huang, J. Sun, Y. Huang, H. Hu, R. Jiang, W. Gai, G. Li, C. Zhi, *ACS Appl. Mater. Interfaces* **2016**, *8*, 24837; b) S. L. Gao, R. C. Zhuang, J. Zhang, J. W. Liu, E. Mäder, *Adv. Funct. Mater.* **2010**, *20*, 1885.
[10] a) J. Eom, J.-S. Heo, M. Kim, J. H. Lee, S. K. Park, Y.-H. Kim, *RSC Adv.* **2017**, *7*, 53373; b) L. Lu, X. Wei, Y. Zhang, G. Zheng, K. Dai, C. Liu, C. Shen, *J. Mater. Chem. C* **2017**, *5*, 7035.
[11] a) C. Niu, *MRS Bull.* **2011**, *36*, 766; b) D. Langley, G. Langley, C. Mayousse, C. Celle, D. Bellet, J. Simonato, *Nanotechnology* **2013**, *24*, 452001.
[12] K. D. Ausman, R. Piner, O. Lourie, R. S. Ruoff, *J. Phys. Chem. B* **2000**, *104*, 8911.
[13] a) V. C. Moore, M. S. Strano, E. H. Haroz, R. H. Hauge, R. E. Smalley, *Nano Lett.* **2003**, *3*, 1379; b) J. Lee, I. Lee, T. Kim, J. Lee, *Small* **2013**, *9*, 2887.
[14] J. Lee, S. T. Connor, Y. Cui, P. Peumans, *Nano Lett.* **2008**, *8*, 689.
[15] a) M. K. Smith, K. A. Mirica, *J. Am. Chem. Soc.* **2017**, *139*, 16759; b) M. A. Squillaci, L. Ferlauto, Y. Zagranyarski, S. Milita, K. Müllen, P. Samorì, *Adv. Mater.* **2015**, *27*, 3170.
[16] a) N. K. Noel, S. N. Habisreutinger, B. Wenger, M. T. Klug, M. T. Hörantner, M. B. Johnston, R. J. Nicholas, D. T. Moore, H. J. Snaith, *Energy Environ. Sci.* **2017**, *10*, 145; b) C. Glynn, C. O'Dwyer, *Adv. Mater. Interfaces* **2017**, *4*, 1600610.
[17] a) W. Yi, Y. Wang, G. Wang, X. Tao, *Polym. Test.* **2012**, *31*, 677; b) Y. Wang, T. Hua, B. Zhu, Q. Li, W. Yi, X. Tao, *Smart Mater. Struct.* **2011**, *20*, 065015; c) W.-J. Yi, X.-M. Tao, G.-F. Wang, Y.-Y. Wang, *J. Xi'an Polytech. Univ.* **2009**, *23*, 75.
[18] Y. Guo, M. T. Otley, M. Li, X. Zhang, S. K. Sinha, G. M. Treich, G. A. Sotzing, *ACS Appl. Mater. Interfaces* **2016**, *8*, 26998.
[19] A. Frutiger, J. T. Muth, D. M. Vogt, Y. Mengüç, A. Campo, A. D. Valentine, C. J. Walsh, J. A. Lewis, *Adv. Mater.* **2015**, *27*, 2440.
[20] a) M. Parrilla, R. Cánovas, I. Jeerapan, F. J. Andrade, J. Wang, *Adv. Healthcare Mater.* **2016**, *5*, 996; b) R. K. Mishra, A. Martin, T. Nakagawa, A. Barfidokht, X. Lu, J. R. Sempionatto, K. M. Lyu, A. Karajic, M. M. Musameh, I. L. Kyratzis, J. Wang, *Biosens. Bioelectron.* **2018**, *101*, 227.
[21] I. Jeerapan, J. R. Sempionatto, A. Pavinatto, J.-M. You, J. Wang, *J. Mater. Chem. A* **2016**, *4*, 18342.
[22] N. Matsuhisa, M. Kaltenbrunner, T. Yokota, H. Jinno, K. Kuribara, T. Sekitani, T. Someya, *Nat. Commun.* **2015**, *6*, 7461.
[23] a) X. Li, T. Zhao, K. Wang, Y. Yang, J. Wei, F. Kang, D. Wu, H. Zhu, *Langmuir* **2011**, *27*, 12164; b) X. Li, T. Zhao, Q. Chen, P. Li, K. Wang, M. Zhong, J. Wei, D. Wu, B. Wei, H. Zhu, *Phys. Chem. Chem. Phys.* **2013**, *15*, 17752; c) J. A. Lee, A. E. Aliev, J. S. Bykova, M. J. de Andrade, D. Kim, H. J. Sim, X. Lepró, A. A. Zakhidov, J. Lee, G. M. Spinks, S. Roth, S. J. Kim, R. H. Baughman, *Adv. Mater.* **2016**, *28*, 5038; d) P. Xue, J. Wang, X. Tao, *High Perform. Polym.* **2014**, *26*, 364.
[24] X. Wang, Y. Qiu, W. Cao, P. Hu, *Chem. Mater.* **2015**, *27*, 6969.
[25] S. S. Yoon, K. E. Lee, H.-J. Cha, D. G. Seong, M.-K. Um, J.-H. Byun, Y. Oh, J. H. Oh, W. Lee, J. U. Lee, *Sci. Rep.* **2015**, *5*, 16366.
[26] C. S. Yeo, H. Kim, T. Lim, H. J. Kim, S. Cho, K. R. Cho, Y. S. Kim, M. K. Shin, J. Yoo, S. Ju, S. Y. Park, *J. Mater. Chem. C* **2017**, *5*, 12825.
[27] S. J. Choi, H. Yu, J. S. Jang, M. H. Kim, S. J. Kim, H. S. Jeong, I. D. Kim, *Small* **2018**, *14*, 1703934.
[28] J. Sun, Y. Li, Q. Peng, S. Hou, D. Zou, Y. Shang, Y. Li, P. Li, Q. Du, Z. Wang, Y. Xia, L. Xia, X. Li, A. Cao, *ACS Nano* **2013**, *7*, 10225.
[29] S. Ling, Q. Wang, D. Zhang, Y. Zhang, X. Mu, D. L. Kaplan, M. J. Buehler, *Adv. Funct. Mater.* **2018**, *28*, 1705291.
[30] J. Yun, H.-I. Kim, Y.-S. Lee, *J. Mater. Sci.* **2013**, *48*, 8320.
[31] a) J. Fang, X. Wang, T. Lin, *J. Mater. Chem.* **2011**, *21*, 11088; b) J. Fang, H. Niu, H. Wang, X. Wang, T. Lin, *Energy Environ. Sci.* **2013**, *6*, 2196; c) E. Yang, Z. Xu, L. K. Chur, A. Behroozfar, M. Baniasadi, S. Moreno, J. Huang, J. Gilligan, M. Minary-Jolandan, *ACS Appl. Mater. Interfaces* **2017**, *9*, 24220.
[32] L. Persano, C. Dagdeviren, Y. Su, Y. Zhang, S. Girardo, D. Pisignano, Y. Huang, J. A. Rogers, *Nat. Commun.* **2013**, *4*, 1633.
[33] M.-F. Lin, J. Xiong, J. Wang, K. Parida, P. S. Lee, *Nano Energy* **2018**, *44*, 248.
[34] W. Yan, A. Page, T. Nguyen-Dang, Y. Qu, F. Sordo, L. Wei, F. Sorin, *Adv. Mater.* **2019**, *31*, 1802348.
[35] M. Bayindir, F. Sorin, A. F. Abouraddy, J. Viens, S. D. Hart, J. D. Joannopoulos, Y. Fink, *Nature* **2004**, *431*, 826.
[36] S. Egusa, Z. Wang, N. Chocat, Z. Ruff, A. Stolyarov, D. Shemuly, F. Sorin, P. Rakich, J. Joannopoulos, Y. Fink, *Nat. Mater.* **2010**, *9*, 643.
[37] S. Danto, F. Sorin, N. D. Orf, Z. Wang, S. A. Speakman, J. D. Joannopoulos, Y. Fink, *Adv. Mater.* **2010**, *22*, 4162.
[38] X. Lu, H. Qu, M. Skorobogatiy, *Sci. Rep.* **2017**, *7*, 2907.
[39] J. Shi, Y. Fang, *Adv. Mater.* **2018**, 1804895.
[40] a) S. Park, Y. Guo, X. Jia, H. K. Choe, B. Grena, J. Kang, J. Park, C. Lu, A. Canales, R. Chen, Y. S. Yim, G. B. Choi, Y. Fink, P. Anikeeva, *Nat. Neurosci.* **2017**, *20*, 612; b) A. Canales, X. Jia, U. P. Froriep, R. A. Koppes, C. Tringides, J. Selvidge, C. Lu, C. Hou, L. Wei, Y. Fink, P. Anikeeva, *Nat. Biotechnol.* **2015**, *33*, 277.
[41] Q. Li, H. Chen, Z.-Y. Ran, L.-N. Zhang, R.-F. Xiang, X. Wang, X.-M. Tao, X. Ding, *Smart Mater. Struct.* **2018**, *27*, 105017.

[42] J. Xie, H. Long, M. Miao, *Smart Mater. Struct.* **2016**, *25*, 105008.
[43] Q. Li, X. Tao, *Text. Res. J.* **2011**, *81*, 1171.
[44] W. Zeng, X.-M. Tao, S. Chen, S. Shang, H. L. W. Chan, S. H. Choy, *Energy Environ. Sci.* **2013**, *6*, 2631.
[45] E. R. Post, M. Orth, P. Russo, N. Gershenfeld, *IBM Syst. J.* **2000**, *39*, 840.
[46] M. D. Irwin, D. A. Roberson, R. I. Olivas, R. B. Wicker, E. Macdonald, *Fibers Polym.* **2011**, *12*, 904.
[47] J. Roh, *Text. Res. J.* **2017**, *87*, 1445.
[48] F. Wang, S. Liu, L. Shu, X.-M. Tao, *Carbon* **2017**, *121*, 353.
[49] X. Wang, X. Tao, R. C. So, L. Shu, B. Yang, Y. Li, *Smart Mater. Struct.* **2016**, *25*, 125022.
[50] S. Seyedin, J. M. Razal, P. C. Innis, A. Jeiranikhameneh, S. Beirne, G. G. Wallace, *ACS Appl. Mater. Interfaces* **2015**, *7*, 21150.
[51] J. Zhou, X. Xu, Y. Xin, G. Lubineau, *Adv. Funct. Mater.* **2018**, *28*, 1705591.
[52] C. Wang, X. Li, E. Gao, M. Jian, K. Xia, Q. Wang, Z. Xu, T. Ren, Y. Zhang, *Adv. Mater.* **2016**, *28*, 6640.
[53] M. Zhang, C. Wang, H. Wang, M. Jian, X. Hao, Y. Zhang, *Adv. Funct. Mater.* **2017**, *27*, 1604795.
[54] H. J. Sim, C. Choi, S. H. Kim, K. M. Kim, C. J. Lee, Y. T. Kim, X. Lepro, R. H. Baughman, S. J. Kim, *Sci. Rep.* **2016**, *6*, 35153.
[55] Y. Liu, L.-Q. Tao, D.-Y. Wang, T.-Y. Zhang, Y. Yang, T.-L. Ren, *Appl. Phys. Lett.* **2017**, *110*, 123508.
[56] M. Liu, X. Pu, C. Jiang, T. Liu, X. Huang, L. Chen, C. Du, J. Sun, W. Hu, Z. L. Wang, *Adv. Mater.* **2017**, *29*, 1703700.
[57] a) L. Viry, A. Levi, M. Totaro, A. Mondini, V. Mattoli, B. Mazzolai, L. Beccai, *Adv. Mater.* **2014**, *26*, 2659; b) R. Li, Y. Si, Z. Zhu, Y. Guo, Y. Zhang, N. Pan, G. Sun, T. Pan, *Adv. Mater.* **2017**, *29*, 1700253.
[58] C. B. Cooper, K. Arutselvan, Y. Liu, D. Armstrong, Y. Lin, M. R. Khan, J. Genzer, M. D. Dickey, *Adv. Funct. Mater.* **2017**, *27*, 1605630.
[59] Y. Cheng, R. Wang, H. Zhai, J. Sun, *Nanoscale* **2017**, *9*, 3834.
[60] a) K. Dong, J. Deng, W. Ding, A. C. Wang, P. Wang, C. Cheng, Y. C. Wang, L. Jin, B. Gu, B. Sun, Z. L. Wang, *Adv. Energy Mater.* **2018**, *8*, 1801114; b) Z. Zhao, C. Yan, Z. Liu, X. Fu, L. M. Peng, Y. Hu, Z. Zheng, *Adv. Mater.* **2016**, *28*, 10267; c) Z. Lin, J. Yang, X. Li, Y. Wu, W. Wei, J. Liu, J. Chen, J. Yang, *Adv. Funct. Mater.* **2018**, *28*, 1704112.
[61] H. Qi, J. Liu, Y. Deng, S. Gao, E. Mäder, *J. Mater. Chem. A* **2014**, *2*, 5541.
[62] G. Zhou, J.-H. Byun, Y. Oh, B.-M. Jung, H.-J. Cha, D.-G. Seong, M.-K. Um, S. Hyun, T.-W. Chou, *ACS Appl. Mater. Interfaces* **2017**, *9*, 4788.
[63] G. Rosace, V. Trovato, C. Colleoni, M. Caldara, V. Re, M. Brucale, E. Piperopoulos, E. Mastronardo, C. Milone, G. De Luca, M. R. Plutino, *Sens. Actuators, B* **2017**, *252*, 428.
[64] Q. Wu, S. Zou, F. P. Gosselin, D. Therriault, M.-C. Heuzey, *J. Mater. Chem. C* **2018**, *6*, 12180.
[65] Q. Li, L. N. Zhang, X. M. Tao, X. Ding, *Adv. Healthcare Mater.* **2017**, *6*, 1601371.
[66] a) M. D. Husain, R. Kennon, *Fibers* **2013**, *1*, 2; b) M. D. Husain, R. Kennon, T. Dias, *J. Ind. Text.* **2014**, *44*, 398.
[67] Y. He, Q. Gui, S. Liao, H. Jia, Y. Wang, *Adv. Mater. Technol.* **2016**, *1*, 1600170.
[68] M. Tessarolo, I. Gualandi, B. Fraboni, *Adv. Mater. Technol.* **2018**, *3*, 1700310.
[69] K. Low, C. B. Horner, C. Li, G. Ico, W. Bosze, N. V. Myung, J. Nam, *Sens. Actuators, B* **2015**, *207*, 235.
[70] a) N. Coppedè, G. Tarabella, M. Villani, D. Calestani, S. Iannotta, A. Zappettini, *J. Mater. Chem. B* **2014**, *2*, 5620; b) I. Gualandi, M. Marzocchi, A. Achilli, D. Cavedale, A. Bonfiglio, B. Fraboni, *Sci. Rep.* **2016**, *6*, 33637.
[71] L. Wang, L. Wang, Y. Zhang, J. Pan, S. Li, X. Sun, B. Zhang, H. Peng, *Adv. Funct. Mater.* **2018**, *28*, 1804456.
[72] H. Qi, B. Schulz, T. Vad, J. Liu, E. Mäder, G. Seide, T. Gries, *ACS Appl. Mater. Interfaces* **2015**, *7*, 22404.
[73] a) S. M. Mirvakili, I. W. Hunter, *Adv. Mater.* **2018**, *30*, 1704407; b) G. V. Stoychev, L. Ionov, *ACS Appl. Mater. Interfaces* **2016**, *8*, 24281; c) L. Kong, W. Chen, *Adv. Mater.* **2014**, *26*, 1025.
[74] M. Wehner, R. L. Truby, D. J. Fitzgerald, B. Mosadegh, G. M. Whitesides, J. A. Lewis, R. J. Wood, *Nature* **2016**, *536*, 451.
[75] H. Arazoe, D. Miyajima, K. Akaike, F. Araoka, E. Sato, T. Hikima, M. Kawamoto, T. Aida, *Nat. Mater.* **2016**, *15*, 1084.
[76] C. Lu, L. Zhao, Y. Hu, W. Chen, *Chem. Commun.* **2018**, *54*, 8733.
[77] a) J. Gong, H. Lin, J. W. Dunlop, J. Yuan, *Adv. Mater.* **2017**, *29*, 1605103; b) H. Cheng, Y. Hu, F. Zhao, Z. Dong, Y. Wang, N. Chen, Z. Zhang, L. Qu, *Adv. Mater.* **2014**, *26*, 2909.
[78] C. S. Haines, M. D. Lima, N. Li, G. M. Spinks, J. Foroughi, J. D. Madden, S. H. Kim, S. Fang, M. J. de Andrade, F. Göktepe, Ö. Göktepe, S. M. Mirvakili, S. Naficy, J. Oh, M. E. Kozlov, S. J. Kim, X. Xu, B. J. Swedlove, G. G. Wallace, R. H. Baughman, *Science* **2014**, *343*, 868.
[79] a) S. Jiang, F. Liu, A. Lerch, L. Ionov, S. Agarwal, *Adv. Mater.* **2015**, *27*, 4865; b) H. Kim, J. H. Moon, T. J. Mun, T. G. Park, G. M. Spinks, G. G. Wallace, S. J. Kim, *ACS Appl. Mater. Interfaces* **2018**, *10*, 32760.
[80] a) C. Lu, Y. Yang, J. Wang, R. Fu, X. Zhao, L. Zhao, Y. Ming, Y. Hu, H. Lin, X. Tao, *Nat. Commun.* **2018**, *9*, 752; b) C. Yang, Z. Suo, *Nat. Rev. Mater.* **2018**, *3*, 125.
[81] a) P. Chen, Y. Xu, S. He, X. Sun, S. Pan, J. Deng, D. Chen, H. Peng, *Nat. Nanotechnol.* **2015**, *10*, 1077; b) X. Yang, W. Wang, M. Miao, *ACS Appl. Mater. Interfaces* **2018**, *10*, 32256.
[82] a) A. H. Gelebart, D. J. J. Mulder, M. Varga, A. Konya, G. Vantomme, E. W. Meijer, R. Selinger, D. J. Broer, *Nature* **2017**, *546*, 632; b) Y. Hu, Z. Li, T. Lan, W. Chen, *Adv. Mater.* **2016**, *28*, 10548.
[83] a) Y. Hu, G. Wu, T. Lan, J. Zhao, Y. Liu, W. Chen, *Adv. Mater.* **2015**, *27*, 7867; b) Y. Hu, W. Chen, L. Lu, J. Liu, C. Chang, *ACS Nano* **2010**, *4*, 3498.
[84] Y. Hu, J. Liu, L. Chang, L. Yang, A. Xu, K. Qi, P. Lu, G. Wu, W. Chen, Y. Wu, *Adv. Funct. Mater.* **2017**, *27*, 1704388.
[85] S. M. Mirvakili, I. W. Hunter, *Adv. Mater.* **2017**, *29*, 1604734.
[86] J. Foroughi, G. M. Spinks, S. Aziz, A. Mirabedini, A. Jeiranikhameneh, G. G. Wallace, M. E. Kozlov, R. H. Baughman, *ACS Nano* **2016**, *10*, 9129.
[87] J. E. Huber, N. A. Fleck, M. F. Ashby, *Proc. R. Soc. London, Ser. A* **1997**, *453*, 2185.
[88] J. A. Lee, N. Li, C. S. Haines, K. J. Kim, X. Lepró, R. OvalleRobles, S. J. Kim, R. H. Baughman, *Adv. Mater.* **2017**, *29*, 1700870.
[89] D. Copic, A. J. Hart, *ACS Appl. Mater. Interfaces* **2015**, *7*, 8218.
[90] K. Y. Chun, S. H. Kim, M. K. Shin, C. H. Kwon, J. Park, Y. T. Kim, G. M. Spinks, M. D. Lima, C. S. Haines, R. H. Baughman, S. J. Kim, *Nat. Commun.* **2014**, *5*, 3322.
[91] L. Ionov, G. Stoychev, D. Jehnichen, J. U. Sommer, *ACS Appl. Mater. Interfaces* **2017**, *9*, 4881.
[92] a) L. Chen, M. Weng, P. Zhou, L. Zhang, Z. Huang, W. Zhang, *Nanoscale* **2017**, *9*, 9825; b) W. Wang, C. Xiang, Q. Zhu, W. Zhong, M. Li, K. Yan, D. Wang, *ACS Appl. Mater. Interfaces* **2018**, *10*, 27215.
[93] a) G. Wu, Y. Hu, J. Zhao, T. Lan, D. Wang, Y. Liu, W. Chen, *Small* **2016**, *12*, 4986; b) N. Terasawa, K. Asaka, *Langmuir* **2016**, *32*, 7210.
[94] J. Torop, A. Aabloo, E. Jager, *Carbon* **2014**, *80*, 387.
[95] G. Wu, Y. Hu, Y. Liu, J. Zhao, X. Chen, V. Whoehling, C. Plesse, G. T. M. Nguyen, F. Vidal, W. Chen, *Nat. Commun.* **2015**, *6*, 7258.
[96] K. Asaka, M. Hashimoto, *Sens. Actuators, B* **2018**, *273*, 1246.
[97] K. Uh, B. Yoon, C. W. Lee, J. M. Kim, *ACS Appl. Mater. Interfaces* **2016**, *8*, 1289.
[98] L. Lu, J. Liu, Y. Hu, W. Chen, *Chem. Commun.* **2012**, *48*, 3978.
[99] a) J. Shi, X. Li, H. Cheng, Z. Liu, L. Zhao, T. Yang, Z. Dai, Z. Cheng, E. Shi, L. Yang, Z. Zhang, A. Cao, H. Zhu, Y. Fang, *Adv. Funct.*

Mater. **2016**, *26*, 2078; b) J. Shi, J. Hu, Z. Dai, W. Zhao, P. Liu, L. Zhao, Y. Guo, T. Yang, L. Zou, K. Jiang, H. Li, Y. Fang, *Carbon* **2017**, *123*, 786.

[100] L. Lu, J. Liu, Y. Hu, Y. Zhang, H. Randriamahazaka, W. Chen, *Adv. Mater.* **2012**, *24*, 4317.

[101] L. Lu, J. Liu, Y. Hu, Y. Zhang, W. Chen, *Adv. Mater.* **2013**, *25*, 1270.

[102] C. S. Haines, N. Li, G. M. Spinks, A. E. Aliev, J. Di, R. H. Baughman, *Proc. Natl. Acad. Sci. USA* **2016**, *113*, 11709.

[103] S. He, P. Chen, L. Qiu, B. Wang, X. Sun, Y. Xu, H. Peng, *Angew. Chem.* **2015**, *127*, 15093.

[104] S. H. Kim, C. H. Kwon, K. Park, T. J. Mun, X. Lepro, R. H. Baughman, G. M. Spinks, S. J. Kim, *Sci. Rep.* **2016**, *6*, 23016.

[105] a) D. Han, Y. Zhang, Y. Liu, Y. Liu, H. Jiang, B. Han, X. Fu, H. Ding, H. Xu, H. Sun, *Adv. Funct. Mater.* **2015**, *25*, 4548; b) Y. Huang, H. Cheng, C. Yang, P. Zhang, Q. Liao, H. Yao, G. Shi, L. Qu, *Nat. Commun.* **2018**, *9*, 4166; c) H. Cheng, F. Zhao, J. Xue, G. Shi, L. Jiang, L. Qu, *ACS Nano* **2016**, *10*, 9535; d) D. Han, Y. Zhang, H. Jiang, H. Xia, J. Feng, Q. Chen, H. Xu, H. Sun, *Adv. Mater.* **2015**, *27*, 332.

[106] S. Taccola, F. Greco, E. Sinibaldi, A. Mondini, B. Mazzolai, V. Mattoli, *Adv. Mater.* **2015**, *27*, 1668.

[107] M. Beregoi, N. Preda, A. Evanghelidis, A. Costas, I. Enculescu, *ACS Sustainable Chem. Eng.* **2018**, *6*, 10173.

[108] B. Li, T. Du, B. Yu, J. V. Der Gucht, F. Zhou, *Small* **2015**, *11*, 3494.

[109] a) M. Ji, N. Jiang, J. Chang, J. Sun, *Adv. Funct. Mater.* **2014**, *24*, 5412; b) B. Han, Y. Zhang, Q. Chen, H. Sun, *Adv. Funct. Mater.* **2018**, *28*, 1802235.

[110] D. Han, Y. Zhang, J. Ma, Y. Liu, B. Han, H. Sun, *Adv. Mater.* **2016**, *28*, 8328.

[111] a) S. J. Kim, O. Kim, M. J. Park, *Adv. Mater.* **2018**, *30*, 1706547; b) Q. Yu, X. Yang, Y. Chen, K. Yu, J. Gao, Z. Liu, P. Cheng, Z. Zhang, B. Aguila, S. Ma, *Angew. Chem.* **2018**, *130*, 10349.

[112] S. Iamsaard, S. Asshoff, B. Matt, T. Kudernac, J. J. L. M. Cornelissen, S. P. Fletcher, N. Katsonis, *Nat. Chem.* **2014**, *6*, 229.

[113] T. Lan, W. Chen, *Angew. Chem.* **2013**, *125*, 6624.

[114] T. Lan, Y. Hu, G. Wu, X. Tao, W. Chen, *J. Mater. Chem. C* **2015**, *3*, 1888.

[115] B. Han, Y. Zhang, L. Zhu, Y. Li, Z. Ma, Y. Liu, X. X. Zhang, X. Cao, Q. Chen, C. Qiu, H. Sun, *Adv. Mater.* **2018**, *31*, 1806386.

[116] X. Yu, H. Cheng, M. Zhang, Y. Zhao, L. Qu, G. Shi, *Nat. Rev. Mater.* **2017**, *2*, 17046.

[117] L. Cappello, K. C. Galloway, S. Sanan, D. A. Wagner, R. Granberry, S. Engelhardt, F. L. Haufe, J. D. Peisner, C. J. Walsh, *Soft Rob.* **2018**, *5*, 662.

[118] J. C. Yeo, H. K. Yap, W. Xi, Z. Wang, C. Yeow, C. T. Lim, *Adv. Mater. Technol.* **2016**, *1*, 1600018.

[119] a) Y. Liu, M. An, Y. Bi, D. Yin, J. Feng, H. Sun, *IEEE Photonics J.* **2017**, *9*, 1; b) M. K. Choi, J. Yang, K. Kang, D. C. Kim, C. Choi, C. Park, S. J. Kim, S. I. Chae, T. Kim, J. Kim, T. Hyeon, D. Kim, *Nat. Commun.* **2015**, *6*, 7149; c) M. Rein, V. D. Favrod, C. Hou, T. Khudiyev, A. M. Stolyarov, J. Cox, C. Chung, C. Chhav, M. Ellis, J. Joannopoulos, Y. Fink, *Nature* **2018**, *560*, 214; d) E. Orti, H. J. Bolink, *Nat. Photonics* **2015**, *9*, 211; e) S. Choi, S. Kwon, H. Kim, W. Kim, J. H. Kwon, M. S. Lim, H. S. Lee, K. C. Choi, *Sci. Rep.* **2017**, *7*, 6424; f) K. Ok, J. Kim, S. Park, Y. Kim, C. Lee, S. Hong, M. Kwak, N. Kim, C. J. Han, J. Kim, *Sci. Rep.* **2015**, *5*, 9464.

[120] a) Z. Zhang, L. Cui, X. Q. Shi, X. Tian, D. Wang, C. Gu, E. Y. Chen, X. Cheng, Y. Xu, Y. Hu, J. Zhang, L. Zhou, H. H. Fong, P. Ma, G. Jiang, X. Sun, B. Zhang, H. Peng, *Adv. Mater.* **2018**, *30*, 1800323; b) W. Kim, S. Kwon, Y. C. Han, E. Kim, K. C. Choi, S. Kang, B. Park, *Adv. Electron. Mater.* **2016**, *2*, 1600220; c) S. Kwon, W. Kim, H. Kim, S. Choi, B. Park, S. Kang, K. C. Choi, *Adv. Electron. Mater.* **2015**, *1*, 1500103; d) Y. Lim, O. E. Kwon, S. Kang, H. Cho, J. Lee, Y. Park, N. S. Cho, W. Jin, J. Lee, H. Lee, J. Kang, S. Yoo, J. Moon, B. Bae, *Adv. Funct. Mater.* **2018**, *28*, 1802944; e) Z. Zhang, X. Shi, H. Lou, Y. Xu, J. Zhang, Y. Li, X. Cheng, H. Peng, *J. Mater. Chem. C* **2017**, *5*, 4139; f) Z. Zhang, Q. Zhang, K. Guo, Y. Li, X. Li, L. Wang, Y. Luo, H. Li, Y. Zhang, G. Guan, B. Wei, X. Zhu, H. Peng, *J. Mater. Chem. C* **2015**, *3*, 5621; g) H. E. Lee, D. Lee, T. Lee, J. H. Shin, G. Choi, C. Kim, S. H. Lee, J. H. Lee, Y. H. Kim, S. Kang, S. H. Park, I. Kang, T. Kim, B. Bae, K. J. Lee, *Nano Energy* **2019**, *55*, 454; h) S. Kwon, H. Kim, S. Choi, E. G. Jeong, D. Kim, S. Lee, H. S. Lee, Y. C. Seo, K. C. Choi, *Nano Lett.* **2018**, *18*, 347; i) Z. Zhang, K. Guo, Y. Li, X. Li, G. Guan, H. Li, Y. Luo, F. Zhao, Q. Zhang, B. Wei, Q. Pei, H. Peng, *Nat. Photonics* **2015**, *9*, 233.

[121] a) D. Guo, C. Ling, C. Wang, D. Wang, J. Li, Z. Zhao, Z. Wang, Y. Zhao, J. Zhang, H. Jin, *ACS Appl. Mater. Interfaces* **2018**, *10*, 28627; b) K. Liu, S. Lee, S. Yang, O. Delaire, J. Wu, *Mater. Today* **2018**, *21*, 875.

[122] O. Mapazi, K. P. Matabola, R. M. Moutloali, C. J. Ngila, *Polymer* **2018**, *149*, 106.

[123] M. J. Kim, S. Angupillai, K. Min, M. Ramalingam, Y. Son, *ACS Appl. Mater. Interfaces* **2018**, *10*, 24767.

[124] S. Cho, G. Kim, S. Lee, J. W. Park, W. Shim, *Adv. Opt. Mater.* **2017**, *5*, 1700627.

[125] L. Chen, M. Weng, F. Huang, W. Zhang, *ACS Appl. Mater. Interfaces* **2018**, *10*, 40149.

[126] J. Ge, Y. Yin, *Angew. Chem., Int. Ed.* **2011**, *50*, 1492.

[127] S. Banisadr, J. Chen, *Sci. Rep.* **2017**, *7*, 17521.

[128] W. Wang, G. P. Wang, W. Zhang, D. Zhang, *Nanophotonics* **2018**, *7*, 217.

[129] E. L. Runnerstrom, A. Llordes, S. D. Lounis, D. J. Milliron, *Chem. Commun.* **2014**, *50*, 10555.

[130] Z. Wang, M. Zhu, S. Gou, Z. Pang, Y. Wang, Y. Su, Y. Huang, Q. Weng, O. G. Schmidt, J. Xu, *ACS Appl. Mater. Interfaces* **2018**, *10*, 31697.

[131] H. C. Moon, T. P. Lodge, C. D. Frisbie, *Chem. Mater.* **2015**, *27*, 1420.

[132] A. M. Osterholm, D. E. Shen, J. A. Kerszulis, R. H. Bulloch, M. Kuepfert, A. L. Dyer, J. R. Reynolds, *ACS Appl. Mater. Interfaces* **2015**, *7*, 1413.

[133] a) R. Wen, C. Granqvist, G. A. Niklasson, *Nat. Mater.* **2015**, *14*, 996; b) Z. Huang, J. Song, L. Pan, X. Zhang, L. Wang, J. Zou, *Adv. Mater.* **2015**, *27*, 5309; c) K. R. Reyesgil, Z. D. Stephens, V. Stavila, D. Robinson, *ACS Appl. Mater. Interfaces* **2015**, *7*, 2202; d) L. Shen, L. Du, S. Tan, Z. Zang, C. Zhao, W. Mai, *Chem. Commun.* **2016**, *52*, 6296.

[134] a) G. Cai, X. Wang, M. Cui, P. Darmawan, J. Wang, A. L. Eh, P. S. Lee, *Nano Energy* **2015**, *12*, 258; b) R. Wen, C. Granqvist, G. A. Niklasson, *Adv. Funct. Mater.* **2015**, *25*, 3359.

[135] Z. Tong, H. Lv, X. Zhang, H. Yang, Y. Tian, N. Li, J. Zhao, Y. Li, *Sci. Rep.* **2015**, *5*, 16864.

[136] Y. Wang, J. Kim, Z. Gao, O. Zandi, S. Heo, P. Banerjee, D. J. Milliron, *Chem. Mater.* **2016**, *28*, 7198.

[137] C. Yan, W. Kang, J. Wang, M. Cui, X. Wang, C. Y. Foo, K. J. Chee, P. S. Lee, *ACS Nano* **2014**, *8*, 316.

[138] a) R. Brooke, E. Mitraka, S. Sardar, M. Sandberg, A. Sawatdee, M. Berggren, X. Crispin, M. P. Jonsson, *J. Mater. Chem. C* **2017**, *5*, 5824; b) Y. Dong, F. Luo, L. Chen, F. Yuan, Y. Hou, W. Li, S. Yan, Y. Dai, M. Ouyang, C. Zhang, *Phys. Chem. Chem. Phys.* **2018**, *20*, 12923.

[139] T. Kuno, Y. Matsumura, K. Nakabayashi, M. Atobe, *Angew. Chem.* **2016**, *128*, 2549.

[140] Z. Li, Y. Zhou, L. Peng, D. Yan, M. Wei, *Chem. Commun.* **2017**, *53*, 8862.

[141] C.-Y. Hsu, J. Zhang, T. Sato, S. Moriyama, M. Higuchi, *ACS Appl. Mater. Interfaces* **2015**, *7*, 18266.

[142] a) R. V. Hansen, M. Huang, Z. Zhan, G. Sun, J. Yang, L. Zheng, *Carbon* **2015**, *90*, 222; b) R. V. Hansen, L. Zhong, K. A. Khor,

L. Zheng, J. Yang, *Carbon* **2016**, *106*, 110; c) R. V. Hansen, J. Yang, L. Zheng, *Adv. Colloid Interface Sci.* **2018**, *258*, 21.
[143] A. Fihey, A. Perrier, W. R. Browne, D. Jacquemin, *Chem. Soc. Rev.* **2015**, *44*, 3719.
[144] D. Bleger, S. Hecht, *Angew. Chem., Int. Ed.* **2015**, *54*, 11338.
[145] H. Mao, L. Lin, Z. Ma, C. Wang, *Sens. Actuators, B* **2018**, *266*, 195.
[146] T. V. Pinto, N. Cardoso, P. Costa, C. M. Sousa, N. F. Duraes, C. J. Silva, P. J. Coelho, C. Pereira, C. Freire, *Appl. Surf. Sci.* **2019**, *470*, 951.
[147] T. V. Pinto, P. Costa, C. M. Sousa, C. Sousa, C. Pereira, C. S. M. Silva, M. F. R. Pereira, P. J. Coelho, C. Freire, *ACS Appl. Mater. Interfaces* **2016**, *8*, 28935.
[148] T. V. Pinto, D. M. Fernandes, A. Guedes, N. Cardoso, N. F. Duraes, C. J. Silva, C. Pereira, C. Freire, *Chem. Eng. J.* **2018**, *350*, 856.
[149] T. A. Khattab, M. Rehan, T. Hamouda, *Carbohydr. Polym.* **2018**, *195*, 143.
[150] R. Xuan, Q. Wu, Y. Yin, J. Ge, *J. Mater. Chem.* **2011**, *21*, 3672.
[151] a) X. Y. Zhang, H. Wong, T. Mo, Y. F. Cao, *IEEE Trans. Biomed. Circuits Syst.* **2017**, *11*, 933; b) S. J. Chen, T. Kaufmann, D. C. Ranasinghe, C. Fumeaux, *IEEE Trans. Antennas Propag.* **2016**, *64*, 894; c) L. A. Y. Poffelie, P. J. Soh, S. Yan, G. A. E. Vandenbosch, *IEEE Trans. Antennas Propag.* **2016**, *64*, 757.
[152] A. Y. I. Ashyap, Z. Z. Abidin, S. H. Dahlan, H. A. Majid, A. M. A. Waddah, M. R. Kamarudin, G. A. Oguntala, R. A. Abdalhameed, J. M. Noras, *IEEE Access* **2018**, *6*, 35214.
[153] S. Yan, G. A. E. Vandenbosch, *IEEE Antennas Wireless Propag. Lett.* **2016**, *15*, 1715.
[154] A. Y. I. Ashyap, Z. Z. Abidin, S. H. Dahlan, H. A. Majid, S. M. Shah, M. R. Kamarudin, A. Alomainy, *IEEE Antennas Wireless Propag. Lett.* **2017**, *16*, 2550.
[155] a) E. Heo, K. Choi, J. Kim, J. Park, H. Lee, *Text. Res. J.* **2018**, *88*, 913; b) C. Loss, R. Goncalves, C. Lopes, P. Pinho, R. Salvado, *Sensors* **2016**, *16*, 938; c) N. Singh, V. K. Singh, B. Naresh, *Procedia Comput. Sci.* **2016**, *85*, 856.
[156] R. Torah, J. Lawrieashton, Y. Li, S. Arumugam, H. A. Sodano, S. P. Beeby, *MRS Bull.* **2018**, *43*, 214.
[157] M. Faraday, *Philos. Trans. R. Soc. London* **1831**, *121*, 299.
[158] a) M. A. Halim, H. Cho, M. Salauddin, J. Y. Park, *Sens. Actuators, A* **2016**, *249*, 23; b) Q. Zhang, Y. Wang, E. S. Kim, *J. Appl. Phys.* **2014**, *115*, 064908; c) H. Liu, S. Gudla, F. A. Hassani, C. Heng, Y. Lian, C. Lee, *IEEE Sens. J.* **2015**, *15*, 2356; d) H. Liu, Z. Ji, T. Chen, L. Sun, S. C. Menon, C. Lee, *IEEE Sens. J.* **2015**, *15*, 4782; e) H. Lee, J. Roh, *Text. Res. J.* **2018**, https://doi.org/10.1177/0040517518797349.
[159] a) B. Li, F. Zhang, S. Guan, J. Zheng, C. Xu, *J. Mater. Chem. C* **2016**, *4*, 6988; b) Y. Fuh, C. C. Kuo, Z. M. Huang, S. C. Li, E. R. Liu, *Small* **2016**, *12*, 1875; c) H. J. Sim, C. Choi, C. J. Lee, Y. T. Kim, G. M. Spinks, M. D. Lima, R. H. Baughman, S. J. Kim, *Adv. Eng. Mater.* **2015**, *17*, 1270.
[160] N. Soin, T. Shah, S. C. Anand, J. Geng, W. Pornwannachai, P. Mandal, D. G. Reid, S. Sharma, R. L. Hadimani, D. V. Bayramol, E. Siores, *Energy Environ. Sci.* **2014**, *7*, 1670.
[161] A. Almusallam, Z. Luo, A. Komolafe, K. Yang, A. F. Robinson, R. Torah, S. P. Beeby, *Nano Energy* **2017**, *33*, 146.
[162] a) J. Yan, Y. G. Jeong, *ACS Appl. Mater. Interfaces* **2016**, *8*, 15700; b) M. Zhang, T. Gao, J. Wang, J. Liao, Y. Qiu, Q. Yang, H. Xue, Z. Shi, Y. Zhao, Z. Xiong, L. Chen, *Nano Energy* **2015**, *13*, 298; c) M. Zhang, T. Gao, J. Wang, J. Liao, Y. Qiu, H. Xue, Z. Shi, Z. Xiong, L. Chen, *Nano Energy* **2015**, *11*, 510.
[163] Z. L. Wang, L. Lin, J. Chen, S. Niu, Y. Zi, *Triboelectric Nanogenerators*, Springer, Berlin, Germany **2016**.
[164] a) J. Wang, C. Wu, Y. Dai, Z. Zhao, A. Wang, T. Zhang, Z. L. Wang, *Nat. Commun.* **2017**, *8*, 88; b) Y. Zi, C. Wu, W. Ding, Z. L. Wang, *Adv. Funct. Mater.* **2017**, *27*, 1700049; c) S. Wang, Y. Xie, S. Niu, L. Lin, C. Liu, Y. S. Zhou, Z. L. Wang, *Adv. Mater.* **2014**, *26*, 6720.
[165] a) B. Yang, W. Zeng, Z. Peng, S. Liu, K. Chen, X. Tao, *Adv. Energy Mater.* **2016**, *6*, 1600505; b) S. Niu, Y. Liu, Y. S. Zhou, S. Wang, L. Lin, Z. L. Wang, *IEEE Trans. Electron Devices* **2015**, *62*, 641; c) S. Niu, S. Wang, L. Lin, Y. Liu, Y. S. Zhou, Y. Hu, Z. L. Wang, *Energy Environ. Sci.* **2013**, *6*, 3576; d) S. Niu, Z. L. Wang, *Nano Energy* **2015**, *14*, 161; e) S. Chen, X. Tao, W. Zeng, B. Yang, S. Shang, *Adv. Energy Mater.* **2017**, *7*, 1601569; f) S. Niu, Y. Liu, S. Wang, L. Lin, Y. S. Zhou, Y. Hu, Z. L. Wang, *Adv. Funct. Mater.* **2014**, *24*, 3332; g) S. Niu, S. Wang, Y. Liu, Y. S. Zhou, L. Lin, Y. Hu, K. C. Pradel, Z. L. Wang, *Energy Environ. Sci.* **2014**, *7*, 2339; h) T. Jiang, X. Chen, C. B. Han, W. Tang, Z. L. Wang, *Adv. Funct. Mater.* **2015**, *25*, 2928; i) S. Niu, Y. Liu, X. Chen, S. Wang, Y. S. Zhou, L. Lin, Y. Xie, Z. L. Wang, *Nano Energy* **2015**, *12*, 760; j) Z. L. Wang, *Mater. Today* **2017**, *20*, 74; k) H. Chen, Y. Xu, J. Zhang, W. Wu, G. Song, *Nanoscale Res. Lett.* **2018**, *13*, 346; l) M. Willatzen, Z. L. Wang, *Nano Energy* **2018**, *52*, 517; m) B. Yang, X. Tao, Z. Peng, *Nano Energy* **2019**, *57*, 66.
[166] a) J. Chen, Y. Huang, N. Zhang, H. Zou, R. Liu, C. Tao, X. Fan, Z. L. Wang, *Nat. Energy* **2016**, *1*, 16138; b) S. Lee, W. Ko, Y. Oh, J. Lee, G. Baek, Y. Lee, J. Sohn, S. Cha, J. M. Kim, J. Park, J. Hong, *Nano Energy* **2015**, *12*, 410; c) H. Wang, F. Li, B. Zhu, L. Guo, Y. Yang, R. Hao, H. Wang, Y. Liu, W. Wang, X. Guo, X. Chen, *Adv. Funct. Mater.* **2016**, *26*, 3472; d) K. Dong, J. Deng, Y. Zi, Y. Wang, C. Xu, H. Zou, W. Ding, Y. Dai, B. Gu, B. Sun, Z. L. Wang, *Adv. Mater.* **2017**, *29*, 1702648; e) W. He, H. Van Ngoc, Y. T. Qian, J. S. Hwang, Y. P. Yan, H. Choi, D. J. Kang, *Appl. Surf. Sci.* **2017**, *392*, 1055; f) N. Cui, L. Gu, Y. Lei, J. Liu, Y. Qin, X. Ma, Y. Hao, Z. L. Wang, *ACS Nano* **2016**, *10*, 6131.
[167] F. Fan, Z. Tian, Z. L. Wang, *Nano Energy* **2012**, *1*, 328.
[168] a) W. Paosangthong, R. Torah, S. P. Beeby, *Nano Energy* **2019**, *55*, 401; b) S. S. Kwak, H.-J. Yoon, S.-W. Kim, *Adv. Funct. Mater.* **2019**, *29*, 1804533; c) Y. Hu, Z. Zheng, *Nano Energy* **2019**, *56*, 16.
[169] a) T. Zhou, C. Zhang, C. B. Han, F. R. Fan, W. Tang, Z. L. Wang, *ACS Appl. Mater. Interfaces* **2014**, *6*, 14695; b) X. Pu, L. L. Li, M. Liu, C. Jiang, C. Du, Z. Zhao, W. Hu, Z. L. Wang, *Adv. Mater.* **2016**, *28*, 98; c) H. Bae, B. C. Jang, H. Park, S. Jung, H. M. Lee, J. Park, S. Jeon, G. Son, I. Tcho, K. Yu, S. G. Im, S. Choi, Y. Choi, *Nano Lett.* **2017**, *17*, 6443; d) Z. Tian, J. He, X. Chen, Z. Zhang, T. Wen, C. Zhai, J. Han, J. Mu, X. Hou, X. Chou, C. Xue, *Nano Energy* **2017**, *39*, 562; e) A. Y. Choi, C. J. Lee, J. Park, D. Kim, Y. T. Kim, *Sci. Rep.* **2017**, *7*, 45583.
[170] a) N. Cui, J. Liu, L. Gu, S. Bai, X. Chen, Y. Qin, *ACS Appl. Mater. Interfaces* **2015**, *7*, 18225; b) S. Li, Q. Zhong, J. Zhong, X. Cheng, B. Wang, B. Hu, J. Zhou, *ACS Appl. Mater. Interfaces* **2015**, *7*, 14912.
[171] a) K. Dong, Y. Wang, J. Deng, Y. Dai, S. L. Zhang, H. Zou, B. Gu, B. Sun, Z. L. Wang, *ACS Nano* **2017**, *11*, 9490; b) S. S. Kwak, H. Kim, W. Seung, J. Kim, R. Hinchet, S. Kim, *ACS Nano* **2017**, *11*, 10733.
[172] W. Seung, M. K. Gupta, K. Y. Lee, K. S. Shin, J. Lee, T. Y. Kim, S. Kim, J. Lin, J. H. Kim, S. Kim, *ACS Nano* **2015**, *9*, 3501.
[173] S. Liu, W. Zheng, B. Yang, X. Tao, *Nano Energy* **2018**, *53*, 383.
[174] a) L. Zhang, S. Lin, T. Hua, B. Huang, S. Liu, X. Tao, *Adv. Energy Mater.* **2018**, *8*, 1700524; b) A. R. M. Siddique, S. Mahmud, B. J. Van Heyst, *Renewable Sustainable Energy Rev.* **2017**, *73*, 730.
[175] a) O. Bubnova, Z. U. Khan, A. Malti, S. Braun, M. Fahlman, M. Berggren, X. Crispin, *Nat. Mater.* **2011**, *10*, 429; b) G. Kim, L. Shao, K. Zhang, K. P. Pipe, *Nat. Mater.* **2013**, *12*, 719; c) Z. Fan, D. Du, Z. Yu, P. Li, Y. Xia, J. Ouyang, *ACS Appl. Mater. Interfaces* **2016**, *8*, 23204; d) G. Zuo, O. Andersson, H. Abdalla, M. M. Kemerink, *Appl. Phys. Lett.* **2018**, *112*, 083303; e) B. Russ, M. J. Robb, F. G. Brunetti, P. L. Miller, E. E. Perry, S. N. Patel, V. Ho, W. B. Chang, J. J. Urban, M. L. Chabinyc, C. J. Hawker, R. A. Segalman, *Adv. Mater.* **2014**, *26*, 3473; f) K. Shi, F. Zhang, C. Di, T. Yan, Y. Zou, X. Zhou, D. Zhu, J. Wang, J. Pei, *J. Am. Chem.*

Soc. **2015**, *137*, 6979; g) G. Zuo, Z. Li, E. Wang, M. M. Kemerink, *Adv. Electron. Mater.* **2018**, *4*, 1700501; h) Y. Sun, L. Qiu, L. Tang, H. Geng, H. Wang, F. Zhang, D. Huang, W. Xu, P. Yue, Y. Guan, F. Jiao, Y. Sun, D. Tang, C. Di, Y. Yi, D. Zhu, *Adv. Mater.* **2016**, *28*, 3351.

[176] a) H. Ju, J. Kim, *ACS Nano* **2016**, *10*, 5730; b) Y. Wang, J. Yang, L. Wang, K. Du, Q. Yin, Q. Yin, *ACS Appl. Mater. Interfaces* **2017**, *9*, 20124; c) H. Wang, J. Hsu, S. Yi, S. L. Kim, K. Choi, G. Yang, C. Yu, *Adv. Mater.* **2015**, *27*, 6855; d) C. Wan, X. Gu, F. Dang, T. Itoh, Y. Wang, H. Sasaki, M. Kondo, K. Koga, K. Yabuki, G. J. Snyder, R. Yang, K. Koumoto, *Nat. Mater.* **2015**, *14*, 622; e) R. Tian, C. Wan, Y. Wang, Q. Wei, T. Ishida, A. Yamamoto, A. Tsuruta, W. Shin, S. Li, K. Koumoto, *J. Mater. Chem. A* **2017**, *5*, 564; f) C. Wan, R. Tian, M. Kondou, R. Yang, P. Zong, K. Koumoto, *Nat. Commun.* **2017**, *8*, 1024; g) A. J. Karttunen, L. Sarnes, R. Townsend, J. Mikkonen, M. Karppinen, *Adv. Electron. Mater.* **2017**, *3*, 1600459; h) C. Zhou, C. Dun, Q. Wang, K. Wang, Z. Shi, D. L. Carroll, G. Liu, G. Qiao, *ACS Appl. Mater. Interfaces* **2015**, *7*, 21015; i) H. Ju, D. Park, J. Kim, *J. Mater. Chem. A* **2018**, *6*, 5627; j) Y. Chen, M. He, B. Liu, G. C. Bazan, J. Zhou, Z. Liang, *Adv. Mater.* **2017**, *29*, 1604752; k) Y. Du, J. Chen, X. Liu, C. Lu, J. Xu, B. Paul, P. Eklund, *Coatings* **2018**, *8*, 25; l) D. Madan, Z. Wang, P. K. Wright, J. W. Evans, *Appl. Energy* **2015**, *156*, 587; m) C. J. An, Y. H. Kang, A. Lee, K. Jang, Y. Jeong, S. Y. Cho, *ACS Appl. Mater. Interfaces* **2016**, *8*, 22142; n) H. Song, Y. Qiu, Y. Wang, K. Cai, D. Li, Y. Deng, J. He, *Compos. Sci. Technol.* **2017**, *153*, 71; o) Y. Lu, Y. Qiu, Q. Jiang, K. Cai, Y. Du, H. Song, M. Gao, C. Huang, J. He, D. Hu, *ACS Appl. Mater. Interfaces* **2018**, *10*, 42310; p) D. S. Montgomery, C. A. Hewitt, R. Barbalace, T. Jones, D. L. Carroll, *Carbon* **2016**, *96*, 778; q) K. T. Park, J. Choi, B. Lee, Y. Ko, K. Jo, Y. M. Lee, J. A. Lim, C. R. Park, H. Kim, *J. Mater. Chem. A* **2018**, *6*, 19727; r) J.-Y. Kim, W. Lee, Y. H. Kang, S. Y. Cho, K.-S. Jang, *Carbon* **2018**, *133*, 293.

[177] a) S. Yang, K. Cho, J. Yun, J. Choi, S. Kim, *Thin Solid Films* **2017**, *641*, 65; b) S. Shen, W. Zhu, Y. Deng, H. Zhao, Y. Peng, C. Wang, *Appl. Surf. Sci.* **2017**, *414*, 197; c) J. Gao, C. Liu, L. Miao, X. Wang, Y. Peng, Y. Chen, *RSC Adv.* **2016**, *6*, 31580; d) C. Yang, D. Souchay, M. Kneis, M. Bogner, H. Wei, M. Lorenz, O. Oeckler, G. Benstetter, Y. Q. Fu, M. Grundmann, *Nat. Commun.* **2017**, *8*, 16076; e) B. Paul, E. M. Björk, A. Kumar, J. Lu, P. Eklund, *ACS Appl. Energy Mater.* **2018**, *1*, 2261; f) S. Feng, T. Yao, Y. Lu, Z. Hao, S. Lin, *Nano Energy* **2019**, *58*, 63; g) P. Nuthongkum, R. Sakdanuphab, M. Horprathum, A. Sakulkalavek, *J. Electron. Mater.* **2017**, *46*, 6444; h) J. Y. Oh, J. H. Lee, S. W. Han, S. S. Chae, E. J. Bae, Y. H. Kang, W. J. Choi, S. Y. Cho, J. O. Lee, H. K. Baik, T. I. Lee, *Energy Environ. Sci.* **2016**, *9*, 1696; i) J. Choi, K. Cho, S. Kim, *Adv. Energy Mater.* **2017**, *7*, 1602138; j) S. Yang, K. Cho, Y. Park, S. Kim, *Nano Energy* **2018**, *49*, 333; k) Z. Cao, M. J. Tudor, R. N. Torah, S. P. Beeby, *IEEE Trans. Electron Devices* **2016**, *63*, 4024.

[178] Z. Fan, J. Ouyang, *Adv. Electron. Mater.* **2019**, 1800769.

[179] Y. Du, J. Xu, B. Paul, P. Eklund, *Appl. Mater. Today* **2018**, *12*, 366.

[180] a) H. Yao, Z. Fan, H. Cheng, X. Guan, C. Wang, K. Sun, J. Ouyang, *Macromol. Rapid Commun.* **2018**, *39*, 1700727; b) C. Gao, G. Chen, *Compos. Sci. Technol.* **2016**, *124*, 52; c) H. Song, Q. Meng, Y. Lu, K. Cai, *Adv. Electron. Mater.* **2019**, 1800822.

[181] H. Mamur, M. R. A. Bhuiyan, F. Korkmaz, M. Nil, *Renewable Sustainable Energy Rev.* **2018**, *82*, 4159.

[182] a) S. Deng, X. Cai, Y. Zhang, L. Li, *Carbon* **2019**, *145*, 622; b) W. Zeng, X. M. Tao, S. Lin, C. Lee, D. Shi, K. H. Lam, B. Huang, Q. Wang, Y. Zhao, *Nano Energy* **2018**, *54*, 163.

[183] T. A. Amollo, G. T. Mola, M. S. K. Kirui, V. O. Nyamori, *Crit. Rev. Solid State Mater. Sci.* **2018**, *43*, 133.

[184] D. Byeon, R. Sobota, K. Delimecodrin, S. Choi, K. Hirata, M. Adachi, M. Kiyama, T. Matsuura, Y. Yamamoto, M. Matsunami, T. Takeuchi, *Nat. Commun.* **2019**, *10*, 72.

[185] F. Kim, B. Kwon, Y. Eom, J. E. Lee, S. Park, S. Jo, S. H. Park, B.-S. Kim, H. J. Im, M. H. Lee, T. S. Min, K. T. Kim, H. G. Chae, W. P. King, J. S. Son, *Nat. Energy* **2018**, *3*, 301.

[186] a) J. P. Rojas, D. Singh, D. Conchouso, A. Arevalo, I. G. Foulds, M. M. Hussain, *Nano Energy* **2016**, *30*, 691; b) X. Xu, Y. Zuo, S. Cai, X. Tao, Z. Zhang, X. Zhou, S. He, X. Fang, H. Peng, *J. Mater. Chem. C* **2018**, *6*, 4866.

[187] a) F. Suarez, A. Nozariasbmarz, D. Vashaee, M. C. Ozturk, *Energy Environ. Sci.* **2016**, *9*, 2099; b) C. S. Kim, G. S. Lee, H. Choi, Y. Kim, H. M. Yang, S. H. Lim, S. Lee, B. J. Cho, *Appl. Energy* **2018**, *214*, 131; c) S. J. Kim, J. H. We, B. J. Cho, *Energy Environ. Sci.* **2014**, *7*, 1959; d) Z. Lu, H. Zhang, C. Mao, C. M. Li, *Appl. Energy* **2016**, *164*, 57; e) S. H. Jeong, F. J. Cruz, S. Chen, L. Gravier, J. Liu, Z. Wu, K. Hjort, S. L. Zhang, Z. Zhang, *ACS Appl. Mater. Interfaces* **2017**, *9*, 15791; f) F. Deng, H. Qiu, J. Chen, L. Wang, B. Wang, *IEEE Trans. Ind. Electron.* **2017**, *64*, 1477.

[188] a) H. Choi, Y. Kim, C. S. Kim, H. M. Yang, M. Oh, B. J. Cho, *Nano Energy* **2018**, *46*, 39; b) Y. S. Jung, D. H. Jeong, S. B. Kang, F. Kim, M. H. Jeong, K. Lee, J. S. Son, J. M. Baik, J. Kim, K. J. Choi, *Nano Energy* **2017**, *40*, 663; c) Y. Guo, J. Mu, C. Hou, H. Wang, Q. Zhang, Y. Li, *Carbon* **2016**, *107*, 146; d) S. J. Kim, H. E. Lee, H. Choi, Y. Kim, J. H. We, J. S. Shin, K. J. Lee, B. J. Cho, *ACS Nano* **2016**, *10*, 10851; e) S. J. Kim, H. Choi, Y. Kim, J. H. We, J. S. Shin, H. E. Lee, M.-W. Oh, K. J. Lee, B. J. Cho, *Nano Energy* **2017**, *31*, 258; f) Y. Wang, Y. Shi, D. Mei, Z. Chen, *Appl. Energy* **2018**, *215*, 690; g) J. Choi, Y. Jung, S. J. Yang, J. Y. Oh, J. Oh, K. Jo, J. G. Son, S. E. Moon, C. R. Park, H. Kim, *ACS Nano* **2017**, *11*, 7608.

[189] a) K. Yoshikawa, H. Kawasaki, W. Yoshida, T. Irie, K. Konishi, K. Nakano, T. Uto, D. Adachi, M. Kanematsu, H. Uzu, K. Yamamoto, *Nat. Energy* **2017**, *2*, 17032; b) K. Masuko, M. Shigematsu, T. Hashiguchi, D. Fujishima, M. Kai, N. Yoshimura, T. Yamaguchi, Y. Ichihashi, T. Mishima, N. Matsubara, T. Yamanishi, T. Takahama, M. Taguchi, E. Maruyama, S. Okamoto, *IEEE J. Photovoltaics* **2014**, *4*, 1433.

[190] H. Li, Z. Yang, L. Qiu, X. Fang, H. Sun, P. Chen, S. Pan, H. Peng, *J. Mater. Chem. A* **2014**, *2*, 3841.

[191] a) H. Sun, X. You, J. Deng, X. Chen, Z. Yang, P. Chen, X. Fang, H. Peng, *Angew. Chem., Int. Ed.* **2014**, *53*, 6664; b) T. Chen, L. Qiu, Z. Yang, Z. Cai, J. Ren, H. Li, H. Lin, X. Sun, H. Peng, *Angew. Chem., Int. Ed.* **2012**, *51*, 11977.

[192] Z. Zhang, Z. Yang, J. Deng, Y. Zhang, G. Guan, H. Peng, *Small* **2015**, *11*, 675.

[193] H. Sun, X. You, J. Deng, X. Chen, Z. Yang, J. Ren, H. Peng, *Adv. Mater.* **2014**, *26*, 2868.

[194] X. Fu, H. Sun, S. Xie, J. Zhang, Z. Pan, M. Liao, L. Xu, Z. Li, B. Wang, X. Sun, H. Peng, *J. Mater. Chem. A* **2018**, *6*, 45.

[195] P. Liu, Z. Gao, L. Xu, X. Shi, X. Fu, K. Li, B. Zhang, X. Sun, H. Peng, *J. Mater. Chem. A* **2018**, *6*, 19947.

[196] C. Wu, T. W. Kim, T. Guo, F. Li, *Nano Energy* **2017**, *32*, 367.

[197] H. Zhen, K. Li, C. Chen, Y. Yu, Z. Zheng, Q. Ling, *J. Mater. Chem. A* **2017**, *5*, 782.

[198] M. J. Yun, Y. H. Sim, S. I. Cha, S. H. Seo, D. Y. Lee, *Sci. Rep.* **2019**, *9*, 2322.

[199] a) R. Li, X. Xiang, X. Tong, J. Zou, Q. Li, *Adv. Mater.* **2015**, *27*, 3831; b) L. Qiu, S. He, J. Yang, J. Deng, H. Peng, *Small* **2016**, *12*, 2419.

[200] a) Z. Yang, J. Deng, H. Sun, J. Ren, S. Pan, H. Peng, *Adv. Mater.* **2014**, *26*, 7038; b) Z. Chai, N. Zhang, P. Sun, Y. Huang, C. Zhao, H. J. Fan, X. Fan, W. Mai, *ACS Nano* **2016**, *10*, 9201.

[201] H. Jinno, K. Fukuda, X. Xu, S. Park, Y. Suzuki, M. Koizumi, T. Yokota, I. Osaka, K. Takimiya, T. Someya, *Nat. Energy* **2017**, *2*, 780.

[202] a) M.-L. Seol, S.-B. Jeon, J.-W. Han, Y.-K. Choi, *Nano Energy* **2017**, *31*, 233; b) X. Ren, H. Fan, C. Wang, J. Ma, S. Lei, Y. Zhao, H. Li, N. Zhao, *Nano Energy* **2017**, *35*, 233; c) K. Zhang, Z. L. Wang, Y. Yang, *ACS Nano* **2016**, *10*, 4728; d) B. Zhang, J. Chen, L. Jin,

W. Deng, L. Zhang, H. Zhang, M. Zhu, W. Yang, Z. L. Wang, *ACS Nano* **2016**, *10*, 6241; e) T. Quan, Y. Yang, *Nano Res.* **2016**, *9*, 2226; f) L. Jin, J. Chen, B. Zhang, W. Deng, L. Zhang, H. Zhang, X. Huang, M. Zhu, W. Yang, Z. L. Wang, *ACS Nano* **2016**, *10*, 7874; g) X. Zhong, Y. Yang, X. Wang, Z. L. Wang, *Nano Energy* **2015**, *13*, 771; h) K. Zhang, X. Wang, Y. Yang, Z. L. Wang, *ACS Nano* **2015**, *9*, 3521; i) T. Quan, X. Wang, Z. L. Wang, Y. Yang, *ACS Nano* **2015**, *9*, 12301; j) Y. Hu, J. Yang, S. Niu, W. Wu, Z. L. Wang, *ACS Nano* **2014**, *8*, 7442.

[203] a) H. Yu, J. Zhou, X. Yi, H. Wu, W. Wang, *Microelectron. Eng.* **2015**, *131*, 36; b) X. Yang, Y. Wang, Y. Cao, S. Liu, Z. Zhao, G. Dong, *IEEE Trans. Appl. Supercond.* **2014**, *24*, 1.

[204] a) J. Song, B. Yang, W. Zeng, Z. Peng, S. Lin, J. Li, X. Tao, *Adv. Mater. Technol.* **2018**, *3*, 1800016; b) X. Chen, Y. Song, Z. Su, H. Chen, X. Cheng, J. Zhang, M. Han, H. Zhang, *Nano Energy* **2017**, *38*, 43; c) W. S. Jung, M. G. Kang, H. G. Moon, S. H. Baek, S. J. Yoon, Z. L. Wang, S. Kim, C. Kang, *Sci. Rep.* **2015**, *5*, 9309; d) T. Huang, C. Wang, H. Yu, H. Wang, Q. Zhang, M. Zhu, *Nano Energy* **2015**, *14*, 226; e) X. Li, Z. Lin, G. Cheng, X. Wen, Y. Liu, S. Niu, Z. L. Wang, *ACS Nano* **2014**, *8*, 10674.

[205] a) Z. Wen, M. Yeh, H. Guo, J. Wang, Y. Zi, W. Xu, J. Deng, L. Zhu, X. Wang, C. Hu, L. Zhu, X. Sun, Z. L. Wang, *Sci. Adv.* **2016**, *2*, e1600097; b) X. Pu, W. Song, M. Liu, C. Sun, C. Du, C. Jiang, X. Huang, D. Zou, W. Hu, Z. L. Wang, *Adv. Energy Mater.* **2016**, *6*, 1601048.

[206] Y. Zi, L. Lin, J. Wang, S. Wang, J. Chen, X. Fan, P. Yang, F. Yi, Z. L. Wang, *Adv. Mater.* **2015**, *27*, 2340.

[207] a) C. Shen, Y. Xie, M. Sanghadasa, Y. Tang, L. Lu, L. Lin, *ACS Appl. Mater. Interfaces* **2017**, *9*, 39391; b) Z. Pan, J. Zhong, Q. Zhang, J. Yang, Y. Qiu, X. Ding, K. Nie, H. Yuan, K. Feng, X. Wang, G. Xu, W. Li, Y. Yao, Q. Li, M. Liu, Y. Zhang, *Adv. Energy Mater.* **2018**, *8*, 1702946.

[208] Y. Wang, S. Su, L. Cai, B. Qiu, C. Yang, X. Tao, Y. Chai, *Energy Storage Mater.* **2018**, https://doi.org/10.1016/j.ensm.2018.11.018.

[209] G. Nagaraju, S. C. Sekhar, L. K. Bharat, J. S. Yu, *ACS Nano* **2017**, *11*, 10860.

[210] J. Du, Z. Wang, J. Yu, S. Ullah, B. Yang, C. Li, N. Zhao, B. Fei, C. Zhu, J. Xu, *Adv. Funct. Mater.* **2018**, *28*, 1707351.

[211] T. Hoshide, Y. Zheng, J. G. Hou, Z. Wang, Q. Li, Z. Zhao, R. Ma, T. Sasaki, F. Geng, *Nano Lett.* **2017**, *17*, 3543.

[212] P. Gao, S. Xu, Z. Chen, X. Huang, Z. Bao, C. Lao, G. Wu, Y. Mei, *ACS Appl. Mater. Interfaces* **2018**, *10*, 3938.

[213] Y. Zhang, L. Wang, Z. Guo, Y. Xu, Y. Wang, H. Peng, *Angew. Chem., Int. Ed.* **2016**, *55*, 4487.

[214] Y. Xu, Y. Zhao, J. Ren, Y. Zhang, H. Peng, *Angew. Chem., Int. Ed.* **2016**, *55*, 7979.

[215] Y. Xu, Y. Zhang, Z. Guo, J. Ren, Y. Wang, H. Peng, *Angew. Chem.* **2015**, *127*, 15610.

[216] Y. Zhang, Y. Jiao, L. Lu, L. Wang, T. Chen, H. Peng, *Angew. Chem., Int. Ed.* **2017**, *56*, 13741.

[217] Y. Zeng, Y. Meng, Z. Lai, X. Zhang, M. Yu, P. Fang, M. Wu, Y. Tong, X. Lu, *Adv. Mater.* **2017**, *29*, 1702698.

[218] H. Li, Z. Liu, G. Liang, Y. Huang, Y. Huang, M. Zhu, Z. Pei, Q. Xue, Z. Tang, Y. Wang, B. Li, C. Zhi, *ACS Nano* **2018**, *12*, 3140.

[219] a) N. Zhang, Y. Dong, M. Jia, X. Bian, Y. Wang, M. Qiu, J. Xu, Y. Liu, L. Jiao, F. Cheng, *ACS Energy Lett.* **2018**, *3*, 1366; b) M. Yan, P. He, Y. Chen, S. Wang, Q. Wei, K. Zhao, X. Xu, Q. An, Y. Shuang, Y. Shao, K. T. Mueller, L. Mai, J. Liu, J. Yang, *Adv. Mater.* **2018**, *30*, 1703725; c) N. Zhang, F. Cheng, J. Liu, L. Wang, X. Long, X. Liu, F. Li, J. Chen, *Nat. Commun.* **2017**, *8*, 405; d) H. Pan, Y. Shao, P. Yan, Y. Cheng, K. S. Han, Z. Nie, C. Wang, J. Yang, X. Li, P. Bhattacharya, K. T. Mueller, J. Liu, *Nat. Energy* **2016**, *1*, 16039; e) D. Kundu, B. D. Adams, V. Duffort, S. H. Vajargah, L. F. Nazar, *Nat. Energy* **2016**, *1*, 16119; f) M. H. Alfaruqi, J. Gim, S. Kim, J. Song, D. T. Pham, J. Jo, Z. Xiu, V. Mathew, J. Kim, *Electrochem. Commun.* **2015**, *60*, 121; g) Y. Li, J. Xu, T. Feng, Q. Yao, J. Xie, H. Xia, *Adv. Funct. Mater.* **2017**, *27*, 1606728; h) C. Zhou, Y. Zhang, Y. Li, J. Liu, *Nano Lett.* **2013**, *13*, 2078; i) D. Sarkar, S. Pal, S. Mandal, A. Shukla, D. D. Sarma, *J. Electrochem. Soc.* **2017**, *164*, A2707; j) S. Zhu, L. Li, J. Liu, H. Wang, T. Wang, Y. Zhang, L. Zhang, R. S. Ruoff, F. Dong, *ACS Nano* **2018**, *12*, 1033; k) B. Y. Guan, A. Kushima, L. Yu, S. Li, J. Li, X. W. Lou, *Adv. Mater.* **2017**, *29*, 1605902; l) L. Shen, L. Yu, H. B. Wu, X. Yu, X. Zhang, X. W. Lou, *Nat. Commun.* **2015**, *6*, 6694; m) Z. Wang, Y. Dong, H. Li, Z. Zhao, H. B. Wu, C. Hao, S. Liu, J. Qiu, X. W. Lou, *Nat. Commun.* **2014**, *5*, 5002; n) C. Huang, J. Xiao, Y. Shao, J. Zheng, W. D. Bennett, D. Lu, L. V. Saraf, M. Engelhard, L. Ji, J. Zhang, X. Li, G. L. Graff, J. Liu, *Nat. Commun.* **2014**, *5*, 3015; o) M. Zhao, Q. Zhang, J. Huang, G. Tian, J. Nie, H. Peng, F. Wei, *Nat. Commun.* **2014**, *5*, 3410; p) M. Zhao, H. Peng, G. Tian, Q. Zhang, J. Huang, X. Cheng, C. Tang, F. Wei, *Adv. Mater.* **2014**, *26*, 7051; q) H. Kim, J. Lee, H. Ahn, O. Kim, M. J. Park, *Nat. Commun.* **2015**, *6*, 7278; r) M. Song, Y. Zhang, E. J. Cairns, *Nano Lett.* **2013**, *13*, 5891.

[220] H. Li, J. He, X. Cao, L. Kang, X. He, H. Xu, F. Shi, R. Jiang, Z. Lei, Z. Liu, *J. Power Sources* **2017**, *371*, 18.

[221] a) Y. Xie, Y. Liu, Y. Zhao, Y. H. Tsang, S. P. Lau, H. Huang, Y. Chai, *J. Mater. Chem. A* **2014**, *2*, 9142; b) R. Song, H. Jin, X. Li, L. Fei, Y. Zhao, H. Huang, H. L. Chan, Y. Wang, Y. Chai, *J. Mater. Chem. A* **2015**, *3*, 14963.

[222] X. Pu, M. Liu, L. L. Li, S. Han, X. Li, C. Jiang, C. Du, J. Luo, W. Hu, Z. L. Wang, *Adv. Energy Mater.* **2016**, *6*, 1601254.

[223] S. Yong, J. Owen, S. P. Beeby, *Adv. Eng. Mater.* **2018**, *20*, 1700860.

[224] Q.-C. Liu, J.-J. Xu, D. Xu, X.-B. Zhang, *Nat. Commun.* **2015**, *6*, 7892.

[225] A. C. Siegel, S. T. Phillips, M. D. Dickey, N. Lu, Z. Suo, G. M. Whitesides, *Adv. Funct. Mater.* **2010**, *20*, 28.

[226] Y. Tai, Z. Yang, *J. Mater. Chem.* **2011**, *21*, 5938.

[227] A. Russo, B. Y. Ahn, J. J. Adams, E. B. Duoss, J. T. Bernhard, J. A. Lewis, *Adv. Mater.* **2011**, *23*, 3426.

[228] W. J. Hyun, O. O. Park, B. D. Chin, *Adv. Mater.* **2013**, *25*, 4729.

[229] R. Guo, J. Tang, S. Dong, J. Lin, H. Wang, J. Liu, W. Rao, *Adv. Mater. Technol.* **2018**, *3*, 1800265.

[230] F. Li, Q. Qin, Y. Zhou, Y. Wu, W. Xue, S. Gao, J. Shang, Y. Liu, R. Li, *Adv. Mater. Technol.* **2018**, *3*, 1800131.

[231] H. Chang, R. Guo, Z. Sun, H. Wang, Y. Hou, Q. Wang, W. Rao, J. Liu, *Adv. Mater. Interfaces* **2018**, *5*, 1800571.

[232] S. Lin, J. Xu, X. Zhi, D. Chen, J. Miao, P. B. Shull, D. Cui, *IEEE Electron Device Lett.* **2017**, *38*, 399.

[233] A. Larmagnac, S. Eggenberger, H. Janossy, J. Voros, *Sci. Rep.* **2015**, *4*, 7254.

[234] R. Verplancke, F. Bossuyt, D. Cuypers, J. Vanfleteren, *J. Micromech. Microeng.* **2012**, *22*, 015002.

[235] M. Hambsch, K. Reuter, M. Stanel, G. Schmidt, H. Kempa, U. Fugmann, U. Hahn, A. C. Hubler, *Mater. Sci. Eng., B* **2010**, *170*, 93.

[236] A. C. Huebler, F. Doetz, H. Kempa, H. E. Katz, M. Bartzsch, N. Brandt, I. Hennig, U. Fuegmann, S. Vaidyanathan, J. Granstrom, S. Liu, A. Sydorenko, T. Zillger, G. Schmidt, K. Preissler, E. Reichmanis, P. Eckerle, F. Richter, T. Fischer, U. Hahn, *Org. Electron.* **2007**, *8*, 480.

[237] Y. Wang, H. Guo, J. Chen, E. Sowade, Y. Wang, K. Liang, K. Marcus, R. R. Baumann, Z. Feng, *ACS Appl. Mater. Interfaces* **2016**, *8*, 26112.

[238] H. Yan, Z. Chen, Y. Zheng, C. R. Newman, J. Quinn, F. Dotz, M. Kastler, A. Facchetti, *Nature* **2009**, *457*, 679.

[239] E. Jabari, E. Toyserkani, *Mater. Lett.* **2016**, *174*, 40.

[240] D. Tobjörk, R. Österbacka, *Adv. Mater.* **2011**, *23*, 1935.

[241] Q. Wang, Y. Yu, J. Yang, J. Liu, *Adv. Mater.* **2015**, *27*, 7109.

[242] a) B. Lee, J. Kim, H. Kim, C. Kim, S. Lee, *Sens. Actuators, A* **2016**, *240*, 103; b) H. Shin, J. Ryu, C. Majidi, Y. Park, *J. Micromech. Microeng.* **2016**, *26*, 025011.

[243] C. M. Boutry, A. K. Nguyen, Q. O. Lawal, A. Chortos, S. Rondeaugagne, Z. Bao, *Adv. Mater.* **2015**, *27*, 6954.
[244] S. De Mulatier, M. Nasreldin, R. Delattre, M. Ramuz, T. Djenizian, *Adv. Mater. Technol.* **2018**, *3*, 1700320.
[245] Y. Wang, S. Su, L. Cai, B. Qiu, N. Wang, J. Xiong, C. Yang, X. Tao, Y. Chai, *Adv. Energy Mater.* **2019**, *9*, 1900037.
[246] a) H. E. Lee, J. H. Park, T. J. Kim, D. Im, J. H. Shin, D. H. Kim, B. Mohammad, I. Kang, K. J. Lee, *Adv. Funct. Mater.* **2018**, *28*, 1801690; b) Y. Kim, A. Chortos, W. Xu, Y. Liu, J. Y. Oh, D. Son, J. Kang, A. M. Foudeh, C. Zhu, Y. Lee, S. Niu, J. Liu, R. Pfattner, Z. Bao, T. Lee, *Science* **2018**, *360*, 998; c) K. Rajan, E. Garofalo, A. Chiolerio, *Sensors* **2018**, *18*, 367.
[247] a) Y. Park, M. Park, J. Lee, *Adv. Funct. Mater.* **2018**, *28*, 1804123; b) A. Jo, Y. Seo, M. Ko, C. Kim, H. Kim, S. Nam, H. Choi, C. S. Hwang, M. J. Lee, *Adv. Funct. Mater.* **2017**, *27*, 1605593.
[248] K. Ishac, K. Suzuki, *Sensors* **2018**, *18*, 2261.
[249] D. Chen, Y. Cai, M.-C. Huang, *IEEE Sens. J.* **2018**, *18*, 6337.
[250] F. Lin, A. Wang, Y. Zhuang, M. R. Tomita, W. Xu, *IEEE Trans. Ind. Inf.* **2016**, *12*, 2281.
[251] L. Shu, X. Tao, D. D. Feng, *IEEE Sens. J.* **2015**, *15*, 442.
[252] A. Nelson, G. Singh, R. Robucci, C. Patel, N. Banerjee, *IEEE Trans. Multi-Scale Comput. Syst.* **2015**, *1*, 62.
[253] J. Cheng, M. Sundholm, B. Zhou, M. Hirsch, P. Lukowicz, *Pervasive and Mobile Comput.* **2016**, *30*, 97.
[254] B. Zhou, M. Sundholm, J. Cheng, H. Cruz, P. Lukowicz, *Pervasive and Mobile Comput.* **2017**, *38*, 331.
[255] J. Eom, R. Jaisutti, H. Lee, W. Lee, J.-S. Heo, J.-Y. Lee, S. K. Park, Y.-H. Kim, *ACS Appl. Mater. Interfaces* **2017**, *9*, 10190.
[256] A. C. Yuen, A. A. Bakir, N. N. Z. M. Rajdi, C. L. Lam, S. M. Saleh, D. H. Wicaksono, *IEEE Sens. J.* **2014**, *14*, 2872.
[257] G. Paul, R. Torah, S. Beeby, J. Tudor, *Sens. Actuators, A* **2014**, *206*, 35.
[258] a) J. Mikkonen, E. Pouta, presented at Int. Symp. on Wearable Computers, Osaka, Japan, September **2015**; b) S. Wang, J. Xu, W. Wang, G. N. Wang, R. Rastak, F. Molinalopez, J. W. Chung, S. Niu, V. R. Feig, J. Lopez, T. Lei, S. Kwon, Y. Kim, A. M. Foudeh, A. Ehrlich, A. Gasperini, Y. Yun, B. Murmann, J. B.-H. Tok, Z. Bao, *Nature* **2018**, *555*, 83; c) M. Stoppa, A. Chiolerio, *Sensors* **2014**, *14*, 11957; d) Y. Kim, H. Kim, H.-J. Yoo, *IEEE Trans. Adv. Packag.* **2010**, *33*, 857.
[259] H. Kim, Y. Kim, Y. Kwon, H. Yoo, presented at 2008 IEEE Int. Solid-State Circuits Conf.-Digest of Technical Papers, San Francisco, CA, USA, February **2008**.
[260] a) M. Hamedi, L. Herlogsson, X. Crispin, R. Marcilla, M. Berggren, O. Inganas, *Adv. Mater.* **2009**, *21*, 573; b) J. S. Heo, T. H. Kim, S. Ban, D. Kim, J. H. Lee, J. S. Jur, M. Kim, Y. Kim, Y. Hong, S. K. Park, *Adv. Mater.* **2017**, *29*, 1701822; c) C. Müller, M. Hamedi, R. Karlsson, R. Jansson, R. Marcilla, M. Hedhammar, O. Inganäs, *Adv. Mater.* **2011**, *23*, 898.
[261] a) D. Wang, Y. Zhang, X. Lu, Z. Ma, C. Xie, Z. Zheng, *Chem. Soc. Rev.* **2018**, *47*, 4611; b) J. B. Lee, V. Subramanian, *IEEE Trans. Electron Devices* **2005**, *52*, 269; c) J. Jang, S. Nam, J. Hwang, J. Park, J. Im, C. E. Park, J. M. Kim, *J. Mater. Chem.* **2012**, *22*, 1054.
[262] a) H. Seo, H. Kim, J. Lee, M. Park, S. Jeong, Y. Kim, S. Kwon, T. H. Han, S. Yoo, T. Lee, *Adv. Mater.* **2017**, *29*, 1605587; b) A. Yang, Y. Li, C. Yang, Y. Fu, N. Wang, L. Li, F. Yan, *Adv. Mater.* **2018**, *30*, 1800051; c) H. M. Kim, H. W. Kang, D. K. Hwang, H. S. Lim, B. K. Ju, J. A. Lim, *Adv. Funct. Mater.* **2016**, *26*, 2706; d) M. Maccioni, E. Orgiu, P. Cosseddu, S. Locci, A. Bonfiglio, *Appl. Phys. Lett.* **2006**, *89*, 143515; e) X. Tao, V. Koncar, C. Dufour, *J. Electrochem. Soc.* **2011**, *158*, H572.
[263] L. Buechley, M. Eisenberg, *Pers. Ubiquitous Comput.* **2009**, *13*, 133.
[264] Z. Fang, X. Mao, J. Yang, F. Yang, *J. Micromech. Microeng.* **2013**, *23*, 095008.
[265] Z. Mei, H. A. Holder, H. A. Vander Plas, *Hewlett-Packard J.* **1996**, *47*, 91.
[266] M. T. I. Molla, S. Goodman, N. Schleif, M. E. Berglund, C. Zacharias, C. Compton, L. E. Dunne, presented at Proc. 2017 ACM Int. Symp. on Wearable Computers, Maui, USA, September **2017**.
[267] a) I. G. Trindade, F. Martins, R. Miguel, M. S. Silva, *Sens. Transducers* **2014**, *183*, 42; b) J. Leśnikowski, *Autex Res. J.* **2016**, *16*, 228; c) T. Linz, R. Vieroth, C. Dils, M. Koch, T. Braun, K. Becker, C. Kallmayer, S. M. Hong, *Adv. Sci. Technol.* **2008**, *60*, 85.
[268] Q. Li, X. M. Tao, *Proc. R. Soc. A* **2014**, *470*, 20140472.
[269] a) J. E. Morris, J. Lee, J. Liu, presented at Int. Conf. on Polymers and Adhesives in Microelectronics and Photonics, Warsaw, Poland, February **2005**; b) Y. C. Lin, X. Chen, J. Zhang, *Polym. Test.* **2011**, *30*, 8.
[270] H. Cui, D. Li, Q. Fan, *Polym. Adv. Technol.* **2013**, *24*, 114.
[271] C. Kallmayer, R. Pisarek, A. Neudeck, S. Cichos, S. Gimpel, R. Aschenbrenner, H. Reichlt, presented at Electronic Components and Technology Conf., New Orleans, Louisiana, USA, May **2003**.
[272] Z. Li, K. Hansen, Y. Yao, Y. Ma, K. Moon, C. Wong, *J. Mater. Chem. C* **2013**, *1*, 4368.
[273] a) C. Zysset, T. Kinkeldei, N. Munzenrieder, K. H. Cherenack, G. Troster, *IEEE Trans. Compon., Packag., Manuf. Technol.* **2012**, *2*, 1107; b) J. Choi, T. Oh, *J. Electron. Mater.* **2014**, *43*, 4464.
[274] J. Choi, T. Oh, *Mater. Trans.* **2015**, *56*, 1711.
[275] D. Nowak, A. Dziedzic, Z. Żaluk, H. Roguszczak, M. Weglarski, *Soldering Surf. Mount Technol.* **2016**, *28*, 27.
[276] a) M. Li, J. Tudor, R. Torah, S. P. Beeby, *IEEE Trans. Compon., Packag., Manuf. Technol.* **2018**, *8*, 186; b) M. Li, J. Tudor, J. Liu, R. Torah, A. Komolafe, S. P. Beeby, *IEEE Trans. Compon., Packag., Manuf. Technol.* **2019**, *9*, 216.
[277] S. D. Min, Y. Yun, H. Shin, *IEEE Sens. J.* **2014**, *14*, 3245.
[278] L. Samy, M.-C. Huang, J. J. Liu, W. Xu, M. Sarrafzadeh, *IEEE Sens. J.* **2014**, *14*, 2092.
[279] a) C. Deng, W. Tang, L. Liu, B. Chen, M. Li, Z. L. Wang, *Adv. Funct. Mater.* **2018**, *28*, 1801606; b) Y.-T. Jao, P.-K. Yang, C.-M. Chiu, Y.-J. Lin, S.-W. Chen, D. Choi, Z.-H. Lin, *Nano Energy* **2018**, *50*, 513.
[280] a) M. K. Yapici, T. Alkhidir, Y. A. Samad, K. Liao, *Sens. Actuators, B* **2015**, *221*, 1469; b) S. Takamatsu, T. Lonjaret, D. Crisp, J.-M. Badier, G. G. Malliaras, E. Ismailova, *Sci. Rep.* **2015**, *5*, 15003.
[281] N. Luo, J. Zhang, X. Ding, Z. Zhou, Q. Zhang, Y. T. Zhang, S. C. Chen, J. L. Hu, N. Zhao, *Adv. Mater. Technol.* **2018**, *3*, 1700222.
[282] a) B. Li, G. Xiao, F. Liu, Y. Qiao, C. M. Li, Z. Lu, *J. Mater. Chem. C* **2018**, *6*, 4549; b) F. Güder, A. Ainla, J. Redston, B. Mosadegh, A. Glavan, T. Martin, G. M. Whitesides, *Angew. Chem., Int. Ed.* **2016**, *55*, 5727.
[283] P. Chen, Y. Xu, S. He, X. Sun, W. Guo, Z. Zhang, L. Qiu, J. Li, D. Chen, H. Peng, *Adv. Mater.* **2015**, *27*, 1042.
[284] A. Maziz, A. Concas, A. Khaldi, J. Stålhand, N.-K. Persson, E. W. Jager, *Sci. Adv.* **2017**, *3*, e1600327.
[285] L. Han, J. Xu, S. Wang, N. Yuan, J. Ding, *RSC Adv.* **2018**, *8*, 10302.
[286] a) R. Dutta, D. Smith, R. Rawnsley, G. Bishop-Hurley, J. Hills, G. Timms, D. Henry, *Comput. Electron. Agric.* **2015**, *111*, 18; b) C. Umstätter, A. Waterhouse, J. Holland, *Comput. Electron. Agric.* **2008**, *64*, 19; c) L. Nóbrega, A. Tavares, A. Cardoso, P. Gonçalves, presented at 2018 IoT Vertical and Topical Summit on Agriculture-Tuscany (IOT Tuscany), Tuscany, Italy, May **2018**.
[287] a) K. Kuang, C. Tan, S. Chew, S. Quek, *Sens. Actuators, A* **2011**, *167*, 338; b) J. Simm, D. Jordan, A. Topple, I. Mokhov, A. Pyayt, T. Abdoun, V. Bennett, J. Broekhuijsen, R. Meijer, presented at 2nd European Conf. on FLOODrisk Management: Science, Policy and Practice: Closing the Gap, Rotterdam, Netherlands, November **2012**.
[288] O. Artières, G. Dortland, presented at Fourth European Workshop on Optical Fibre Sensors, Porto, Portugal, September **2010**.

[289] W. R. Habel, K. Krebber, *Photonic Sens.* **2011**, *1*, 268.
[290] L. Zhang, N. Zhang, Y. Yang, S. Xiang, C. Tao, S. Yang, X. Fan, *ACS Appl. Mater. Interfaces* **2018**, *10*, 30819.
[291] A. Ainla, M. M. Hamedi, F. Güder, G. M. Whitesides, *Adv. Mater.* **2017**, *29*, 1702894.
[292] a) K. Pulskamp, S. Diabaté, H. F. Krug, *Toxicol. Lett.* **2007**, *168*, 58; b) J. Muller, F. Huaux, A. Fonseca, J. B. Nagy, N. Moreau, M. Delos, E. Raymundo-Piñero, F. Béguin, M. Kirsch-Volders, I. Fenoglio, B. Fubini, D. Lison, *Chem. Res. Toxicol.* **2008**, *21*, 1698.
[293] a) S. K. Singh, M. K. Singh, P. P. Kulkarni, V. K. Sonkar, J. J. Grácio, D. Dash, *ACS Nano* **2012**, *6*, 2731; b) J. Shi, Y. Fang, in *Graphene* (Eds: H. Zhu, Z. Xu, D. Xie, Y. Fang) Elsevier Inc., London, UK **2018**, Ch. 9, pp. 215–232.
[294] a) S. Wang, R. Bie, F. Zhao, N. Zhang, X. Cheng, H. Choi, *IEEE Network* **2016**, *30*, 61; b) M. Wazid, S. Zeadally, A. K. Das, V. Odelu, *J. Med. Syst.* **2016**, *40*, 1; c) N. Vithanwattana, G. Mapp, C. George, presented at 2016 12th Int. Conf. on Intelligent Environments (IE), London, UK, September **2016**.
[295] a) P. Mvelase, Z. Dlamini, A. Dludla, H. Sithole, presented at Echallenges Conf., Vilnius, Lithuania, November **2015**; b) J. Zhou, Z. Cao, X. Dong, X. Lin, *IEEE Wireless Commun.* **2015**, *22*, 136; c) P. K. Gupta, B. T. Maharaj, R. Malekian, *Multimedia Tools Appl.* **2017**, *76*, 18489; d) T. Ueda, Y. Ikeda, presented at 2017 ITU Kaleidoscope: Challenges for a Data-Driven Society (ITUK), Nanjing, China, November **2017**.
[296] J. Shen, Z. Gui, S. Ji, J. Shen, H. Tan, Y. Tang, *J. Network Comput. Appl.* **2018**, *106*, 117.
[297] *ARM Security Technology Building a Secure System Using Trustzone Technology*, Cambridge, UK **2009**.
[298] a) I. Anati, S. Gueron, S. Johnson, V. Scarlata, presented at Proc. 2nd Int. Workshop on Hardware and Architectural Support for Security and Privacy, ACM, Tel-Aviv, Israel, June **2013**; b) F. McKeen, I. Alexandrovich, A. Berenzon, C. V. Rozas, H. Shafi, V. Shanbhogue, U. R. Savagaonkar, in *Proc. 2nd Int. Workshop on Hardware and Architectural Support for Security and Privacy*, ACM, Tel-Aviv, Israel, June **2013**.